Deutsche Geophysikalische Gesellschaft e.V.

Inhalt

MITTEILUNGEN

Symposium in Memoriam of Prof. Gerhard Müller

Neustadt an der Weinstraße

16 – 17 January 2003

Sonderband I/2004
ISSN-Nr. 0934-6554

Herausgeber:
J. Schweitzer, im Auftrag der Deutschen Geophysikalischen Gesellschaft e.V.

IMPRESSUM

Herausgeber im Auftrag der Deutschen Geophysikalischen Gesellschaft:

J. Schweitzer, NORSAR, Instituttveien 25, P.O. Box 51, 2027 Kjeller, Norwegen
E-Mail: johannes.schweitzer@norsar.no

Die Sonderbände der Mitteilungen der Deutschen Geophysikalischen Gesellschaft werden in unregelmäßiger Folge herausgegeben. In den letzten 5 Jahren sind folgende Bände erschienen:

Sonderband I/2000	Rundtischgespräch zum Thema "Georadar - Erfahrungen und Perspektiven"
Sonderband II/2000	DGG - Kolloquium "Die Magnetik in der Geophysik"
Sonderband III/2000	5.Workshop "Bohrlochgeophysik und Gesteinsphysik"
Sonderband IV/2000	2. Merapi-Galeras Workshop
Sonderband V/2000	6. DGG-Seminar "Ingenieur- und Umweltgeophysik"
Sonderband VI/2000	100 Jahre seismologische Forschung in Jena
Sonderband I/2001	50 Jahre Geophysikalische Dienste aus Leipzig, GGD
Sonderband I/2002	DGG Kolloquium "Neue Aspekte der Explorations-und Produktionsgeophysik"
Sonderband I/2003	DGG Kolloquium "Interdisziplinärer Einsatz geophysikalischer Methoden"
Sonderband I/2004	Prof. Gerhard Müller Symposium

Vorstand der Deutschen Geophysikalischen Gesellschaft e.V.:

Professor Gerhard Müller
(1940 – 2002)

Editorial

On 16 – 17 January 2003, a symposium was held in memoriam of the late Professor Gerhard Müller in Neustadt an der Weinstraße, Germany. This symposium was organized by the Institute for Meteorology and Geophysics of the Johann Wolfgang Goethe-University in Frankfurt am Main where Gerhard Müller had worked and lectured for more than 20 years. It was supported by the Deutsche Geophysikalische Gesellschaft (DGG).

The first day of the symposium was dedicated to scientific results of Gerhard Müller and his group, and the second day allowed for presentations of newer research results, often in many ways influenced by Gerhard Müller.

Obituaries of Gerhard Müller by Brian L. N. Kennett and Walter Zürn have been published elsewhere (Kennett, 2002; Zürn, 2002) and Harro Schmeling has published a German language summary report on the symposium (Schmeling, 2002). This volume now contains in English manuscripts or extended abstracts of all contributions given during the symposium. It therefore gives a much more detailed view of the methods used by Gerhard Müller and also of the continuing scientific relevance of his work. It is hoped that it reaches a broad international audience.

The order of contributions in this volume follows the program of the symposium. In addition, a bibliography of Gerhard Müller's publications as author or co-author is included. This bibliography was compiled by Ingrid H. Hörnchen and Walter Zürn and has been homogenized and completed by the editor. Since many items in the bibliography have been cited many times by the different authors, all citations of publications included in the bibliography were removed from the individual contributions.

May this collection help to remember Gerhard Müller as he was: an internationally respected, excellent scientist, an exceptional teacher in Geophysics at the Universities of Karlsruhe and Frankfurt, and a good friend to many of us.

NORSAR, 29 October 2003

Johannes Schweitzer

References

Kennett, B. L. N., 2002. Prof. Gerhard Müller 1940 – 2002. Astronomy & Geophysics **43, No 6**, 6.35.

Schmeling, H., 2003. Gerhard-Müller-Kolloquium im Herz-Jesu-Kloster in Neustadt/Weinstraße 16. + 17. Januar 2003. Deutsche Geophysikalische Gesellschaft e.V., Mitteilungen **1/2003**, 29-37.

Zürn, W., 2002. Nachruf auf Professor Dr. Gerhard Müller. Deutsche Geophysikalische Gesellschaft e.V., Mitteilungen **3/2002**, 23-26.

Retrospect on First Applications of the S-Reflectivity Method

Rainer Kind, GFZ Potsdam

I first met Gerhard Müller when I came to Karlsruhe in 1972. The reflectivity method (Fuchs, 1968; Fuchs & Müller, 1971) was at the beginning of its breakthrough. It was developed originally for controlled source studies of the crust and uppermost mantle. Gerhard had extended the method at that time to the spherical Earth by applying an Earth flattening approximation to the spherical Earth model (Müller, 1971a; 1973c; 1977b). He had recognized the potential of the method for studies of the mantle and core. The first application to the deep interior of the Earth was a study of reflections from the inner core to estimate the density jump there (Müller, 1973b). He planned to extend these studies to the structure of the outer core using SKS. The DFG accepted his proposal and he asked me to cooperate with him. I had been working with Karl Fuchs on long-range profiles and used this occasion to switch to global seismology. Our first task was to extend the method to the reflected SV wave field of double couple sources (Kind & Müller, 1975). We tested the newly developed extension using crustal models and we were surprised by the multiplicity of the phases, which appeared in the computed sections (Figs. 1 and 2). This was typical for reflectivity results, which sometimes needed as much effort for their interpretation as real data. The reflectivity method at that time did not yet allow for a free surface on top of the model. The uppermost layer in the Earth was a halfspace in the model. A sedimentary halfspace on top of the model, however, caused effects similar to those of a free surface (Fig. 2).

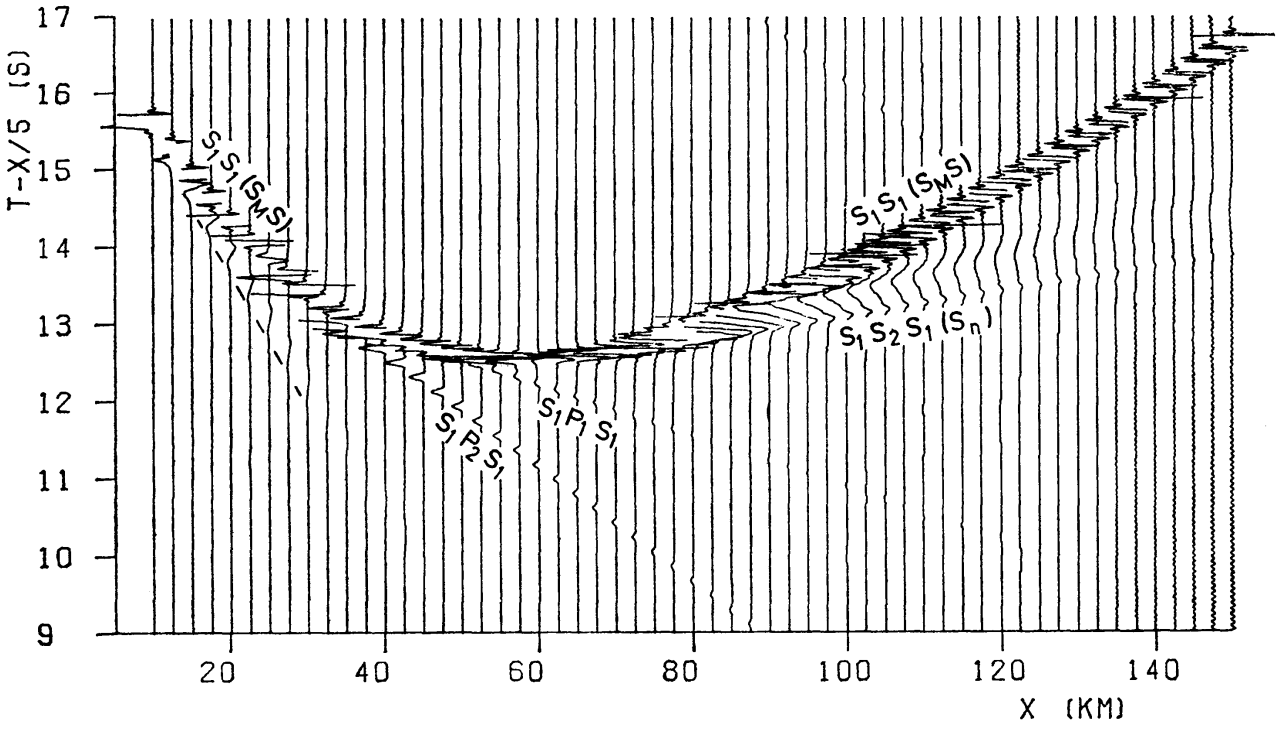

Figure 1: Computed SV wavefield reflected from the crust-mantle boundary. Head waves traveling with the P velocities of the mantle and the crust, and with the S velocity of the mantle are also visible, as are pseudo Rayleigh waves in the mantle (Kind & Müller, 1975).

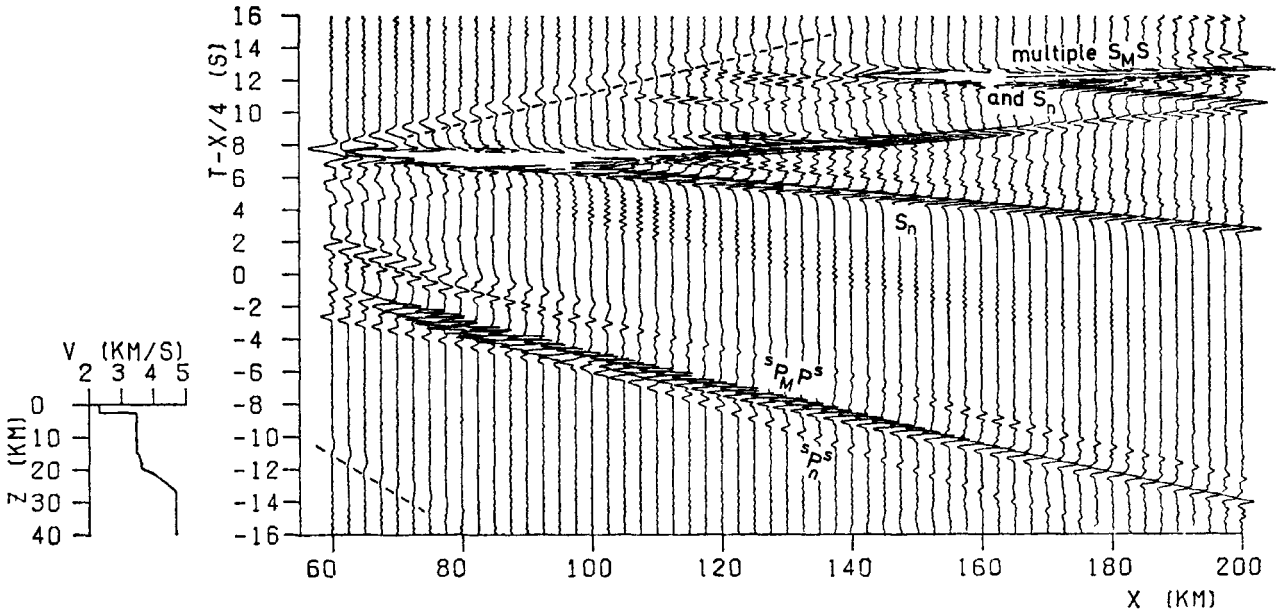

Figure 2: Reflected SV wavefield from the model on the lower left. The source is in the sedimentary layer. The strong contrast between sediments and basement causes many complications in the wavefield (Kind & Müller, 1975).

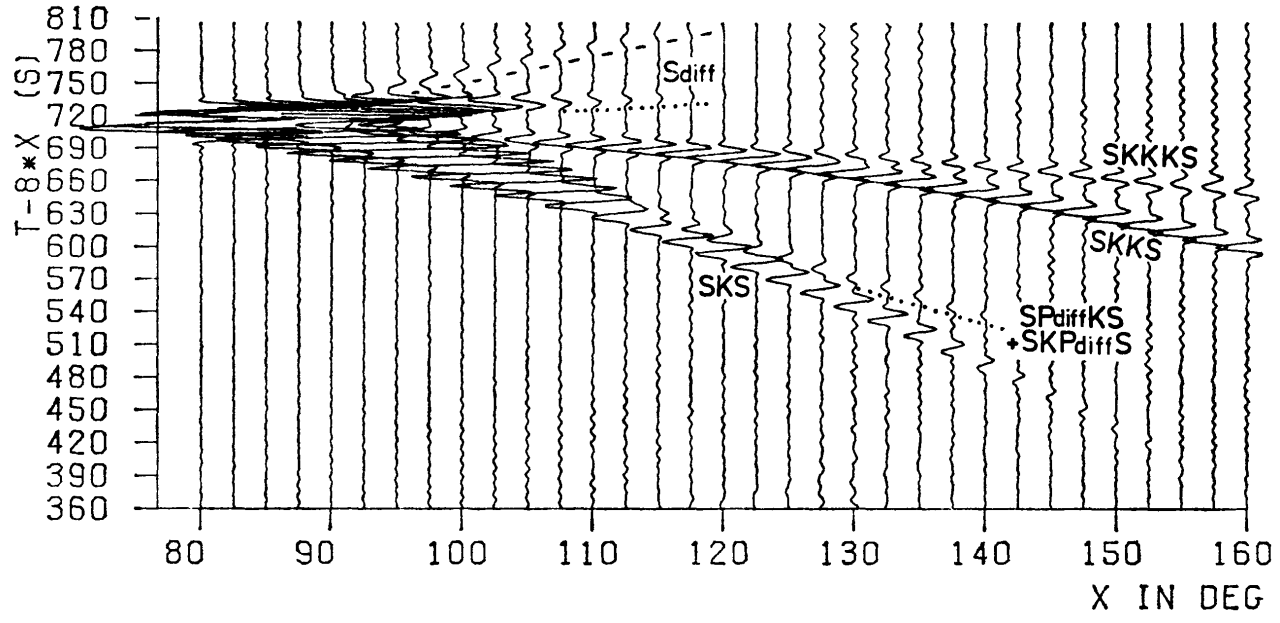

Figure 3: First reflectivity computations of SKS and related phases with the, at that time unknown phases SPdiffKS and SKPdiffS (Kind & Müller, 1975).

The next step was the computation of core phases with the new version of the reflectivity method. Fig. 3 shows the first reflectivity computations of SKS and related phases. There was another surprise in these computations. An unknown phase showed up, which was identified as SKPdiffS or SPdiffKS. This is a diffracted phase traveling along the core-mantle boundary with the P velocity of the lowermost mantle. It is generated by an S phase incident from the top side, or by a core phase incident from below. At that time this phase was not yet observed. Today, however, it is frequently used for studies of the lowermost mantle. We selected a number of useful events for our planned SKS study and digitized from film chips longperiod WWSSN (World Wide Standardized Seismograph Network) and CSN (Canadian Seismic Network) data. The comparison of these data with synthetic seismograms for the 1066B global model (Gilbert & Dziewonski,

1975) revealed differences in the SKKS/SKS amplitude ratios. We thought the anomaly would be located most likely where the ray paths of the two phases have their greatest differences, which was in the outer core in a radially symmetric Earth (Kind & Müller, 1977). Therefore our study resulted in an outer core model, which departed significantly from 1066B. Schweitzer & Müller (1986), however, found that the SKKS/SKS anomaly does not exist globally. Its cause is still unknown, but it could perhaps be related to D" along the ray path from Fiji-Tonga to North America, where most of our data originated.

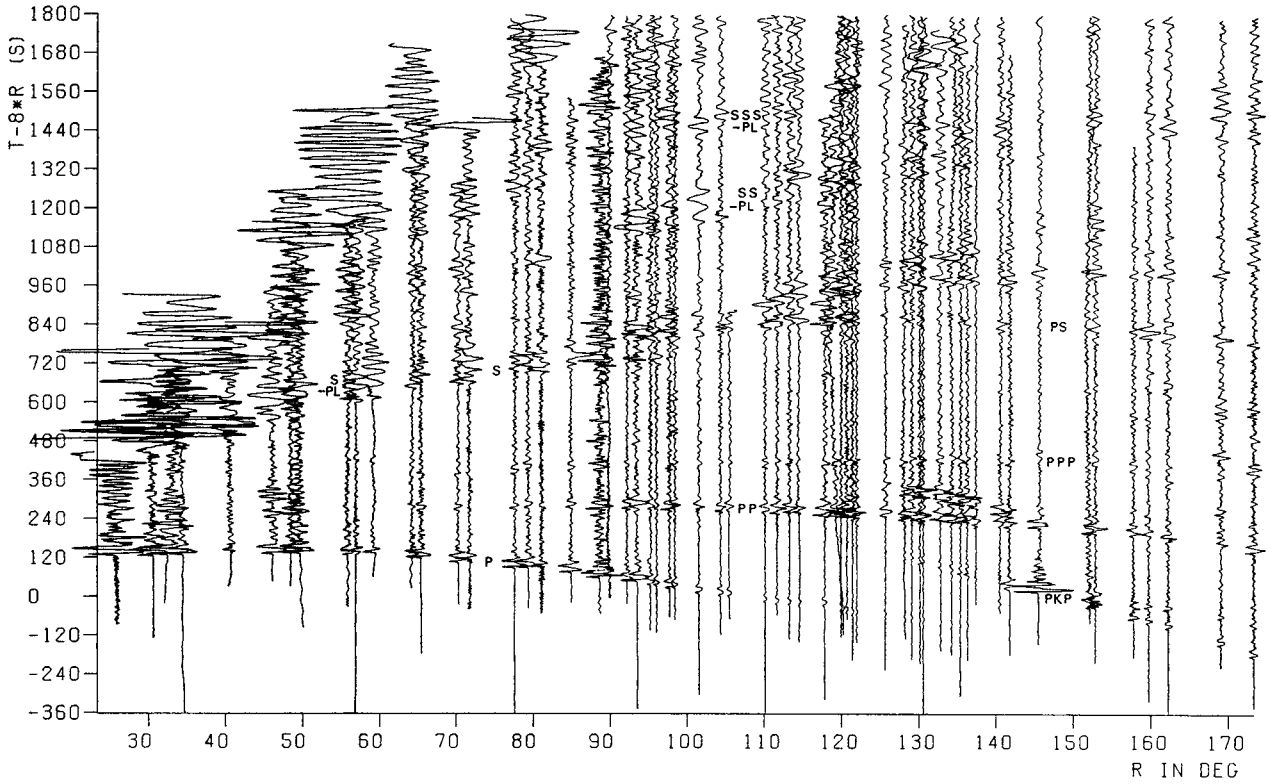

Figure 4: First record section of global seismograms, in which the vertical component is shown (Müller & Kind, 1976).

Gerhard and myself had been working previously in seismic refraction studies of the crust. In this field it had become common at that time to digitize seismograms and to plot sections of the complete recorded waveforms for comparison with synthetic seismograms. We thought it would be interesting to do the same in global seismology. We found a good event, digitized long period WWSSN and CSN film chips and produced a three component global seismic section (Fig. 4; Müller & Kind, 1976). This was the first time that global seismic data could be seen in such a form. Until then practically only picked travel time data had been visualized. This global record section has in the meantime been reproduced in a number of textbooks. Our comparison of the section with complete theoretical seismograms was still somewhat crude, since the reflectivity method had not yet been developed for buried sources. Both of us left Karlsruhe at the end of the seventies but continued to work on the reflectivity method for buried sources. I published in 1978 a buried source version (Kind, 1978) based on an analytical development by Harkrider (1964), and Gerhard published his tutorial in 1985 (Müller, 1985), based on the work of Kennett & Kerry (1979) and Kennett (1983).

References

Fuchs, K., 1968. The reflection of spherical waves from transition zones with arbitrary depth-dependent elastic moduli and density. J. Phys. Earth **16**, 27-41.

Gilbert, F. & A. M. Dziewonski, 1975. An application of normal mode theory to the retrieval of structural parameters and source mechanisms from seismic spectra. Phil. Trans. Royal. Soc. London **178**, 187-269.

Harkrider, D. G., 1964. Surface waves in multilayered elastic media. I. Rayleigh and Love waves from buried sources in a multilayered elastic half-space. Bull. Seism. Soc. Amer. **54**, 627-679.

Kind, R., 1978. The reflectivity method for a buried source. J. Geophys. **44**, 603-612.

Kennett, B. L. N. & N. J. Kerry, 1979. Seismic waves in a stratified halfspace. Geoph. J. R. astr. Soc. **57**, 557-583.

Kennett, B. L. N., 1983. Seismic wave propagation in stratified media. Cambridge University Press, ISBN 0-521-23933-8, vii+342 pp.

Seismic Waves and Complex Media

Michael Korn, Leipzig

Introduction

Gerhard's interest in modeling of seismic waves did not decrease after the reflectivity method had gained worldwide recognition and had developed into a standard tool for seismological interpretations. He continued to work on a variety of approaches for a more complete understanding of the interaction of wave fields with more complex structures.
Among the methods, which emerged during the 1970s and 1980s were the Gaussian beam method, various kinds of finite difference methods, Kirchhoff methods and hybrid methods combing several approaches. Together with a number of students Gerhard has contributed new features and techniques to most of these methods (see, *e.g.*, Korn & Müller, 1983; Müller, 1984; Korn, 1987; Weber, 1988; Kampfmann & Müller, 1989; Emmerich, 1992; Roth *et al.*, 1993).
In this contribution, however, I will concentrate more on a slightly different aspect of his work on the theory of seismic wave fields: the analysis of wave phenomena in complex heterogeneous media that are described by random fluctuations of their elastic properties. In this case only some statistical measures are known and not the exact deterministic distribution of these parameters in space. This facet of Gerhard's work aimed at a more complete understanding of wave field interactions with realistic structures in the Earth, especially at scale lengths, which are short compared to one wavelength. This also sheds some light on limitations and shortcomings of conventional imaging methods, which completely neglect the small-scale part of the heterogeneity spectrum of the Earth. To my opinion, this part of Gerhard's work has not really gained the amount of attention it deserves.
The first time that Gerhard suggested the use of a random medium was in the context of wave field modeling in the Earth's mantle to show the capabilities of a newly developed numerical method. To this end the velocity-depth function down to the core-mantle boundary was superimposed by random fluctuations of a few per cents to form a small-scale heterogeneous medium. The resulting seismograms (Fig. 1) show some of the effects of small-scale velocity perturbations: changes in pulse shapes and amplitudes as well as energy appearing at times between the ordinary seismic phases. At that time this was a purely numerical exercise and no attempt has been made to draw quantitative conclusions from the computations. But soon Gerhard started to look at effects of random structures on wave fields more thoroughly and developed a couple of different approaches to study scattering attenuation, travel time changes and imaging of random structures. In the following some of this work will be summarized.

Scattering Attenuation

When a wave propagates through a medium with fluctuating velocities, it looses energy. This effect is called scattering attenuation. In contrast to anelastic attenuation, where elastic energy is dissipated into heat, scattering attenuation merely is a redistribution of elastic energy in space caused by scattering of parts of the incoming wave energy into directions different from the initial ray path.
In Görich & Müller (1987) a simple theory to compute scattering attenuation of a plane wave propagating through a stack of plane layers with velocities randomly fluctuating around a mean value has been derived under the single backscattering approximation. One only needs to know the autocorrelation function of the velocity fluctuations. With this simple theory 'stratigraphic Q' is described remarkably well, even for rather high rms fluctuations.

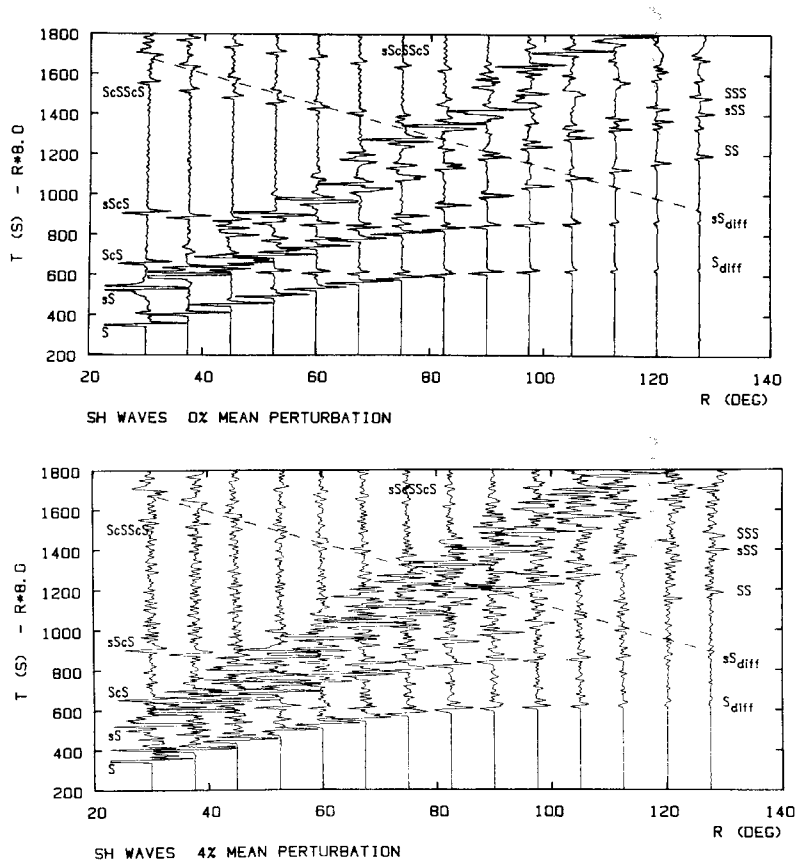

Figure 1: Synthetic seismograms in an Earth model with standard IASPEI91 velocity-depth distribution (top) and superimposed random velocity fluctuations (bottom).

It is well known from anelasticity that attenuation is connected with dispersion, *i.e.*, the phase velocities of waves become dependent on frequency f to assure causal signals. If $Q(f)$ is known and a minimum-phase condition is assumed, phase velocity $c(f)$ can be uniquely determined as derived earlier in the context of anelasticity (Müller, 1983). A complete description of the average pulse shapes in a one-dimensional random medium is therefore obtained by applying a stratigraphic filter $D(f)$ or the corresponding time-domain attenuation operator $D(t)$. A remarkably simple expression for $D(f)$ is obtained by Fang & Müller (1991) as

$$D(f) = \exp\left[-\pi f T\left\{Q^{-1}(f) + i\,\Re\left(Q^{-1}(f)\right)\right\}\right],$$

where $\Re$ denotes the Hilbert transformation and T is travel time.

Fig. 2 shows a comparison of pulse shapes obtained after an input wavelet (bottom trace) has traversed N layers with an rms velocity fluctuation of 12 per cent. The thin lines are the shapes obtained by convolving the input trace with the dissipation operator $D(t)$. Not only the amplitudes but also details of the pulse shapes are successfully predicted, including times later than the duration of the input wavelet.

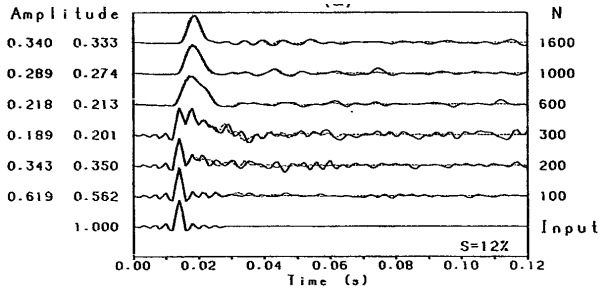

Figure 2: Stratigraphic filtering in a 1D layered medium: input trace (bottom) and resulting traces after passage through N layers. Thick lines: numerical result. Thin lines: application of dissipation operators.

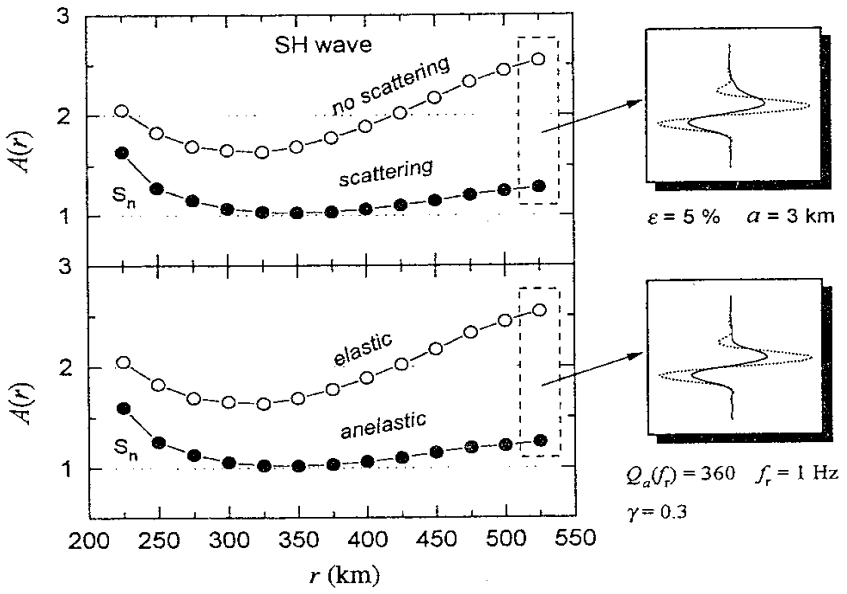

Figure 3: Anelastic (top) versus scattering attenuation (bottom) for Sn wave propagation.

Fang & Müller (1996) extended this work to three-dimensional random media. Although the validity of the minimum-phase assumption has not been strictly proven, numerical results show that in general the dissipation operator approach works well. Scattering attenuation has thus been put into exactly the same theoretical framework as anelasticity, and therefore can be easily implemented, *e.g.*, into reflectivity codes. Fig. 3 (from Fang & Müller, 1996) shows an example of Sn wave propagation in a crustal model with either random heterogeneity or anelasticity. The amplitude versus distance curves as well as the pulse shapes are almost identical in both cases. In essence that means that an anelastic Q of 360 at 1 Hz or a random heterogeneity of 5 per cent rms fluctuation and 3 km correlation length have the same effect on the attenuation of direct Sn waves and therefore heterogeneity and anelasticity cannot be distinguished by looking at the transmitted wavelets only.

Travel Times and Velocity Shift

Travel times are the prime observational quantity derived from seismic wave fields. Many methods like travel time tomography solely rely on the inversion of accurately observed travel time residuals. Gerhard and his coworkers used both ray-theoretical and wave-theoretical methods to study travel times in random media.

Fig. 4 shows a synthetic record section of an initially plane wave after propagating a distance L through a medium with correlation length a and rms perturbation ε (top). The first arrivals fluctuate around a mean value that is slightly different from the value expected from the average slowness of the random medium (dashed line, middle panel). A simple theory based on ray-theoretical considerations was developed in Müller *et al.* (1992) to connect the autocorrelation functions of the velocity fluctuations of the medium and travel time fluctuations of the wave field. Thus from the observed travel time correlation (bottom) the random medium parameters $\tilde{\varepsilon}$ and $\tilde{a}$ can be inverted. Furthermore, calibrating the inversion results with synthetic calculations of the complete wave field can extend the ray-theoretical limits.

A first application of this theory to a data set recorded in the Baltic Sea was performed by Roth (1997). He interpreted the travel time fluctuations of the Pg wave on a closely spaced profile between 30 and 80 km offset (Fig. 5). After subtracting the travel times of a simple velocity-depth model from the data, the autocorrelation function of the remaining residuals yielded correlation lengths of 330 – 660 m and rms fluctuations of 2.2 – 5 per cent.

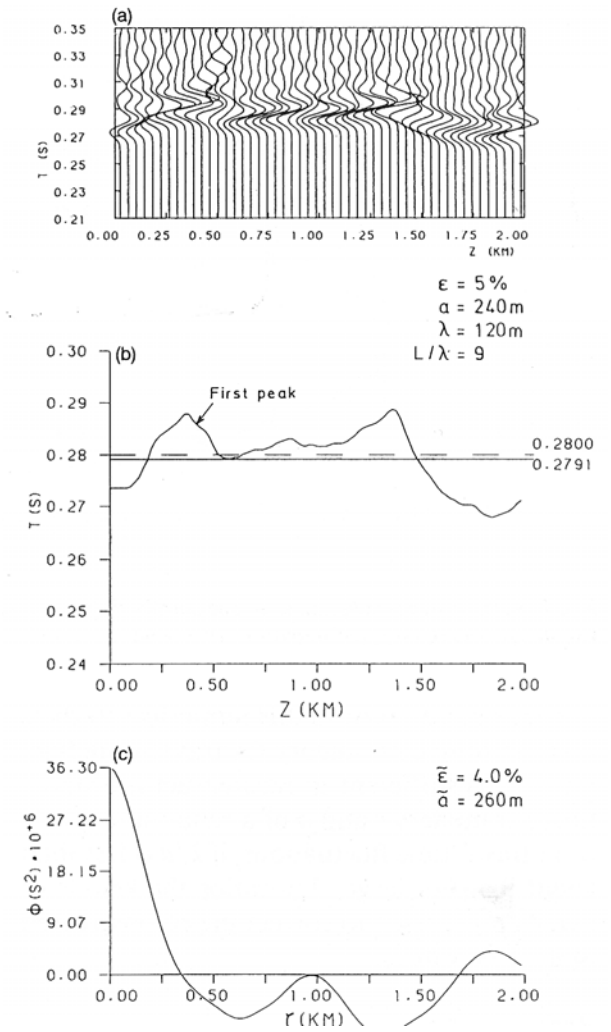

Figure 4: (a) Synthetic seismograms in a random medium, (b) travel time fluctuations, and (c) their autocorrelation function. See text for further explanation.

This rather high upper-crustal heterogeneity corresponds well with the strong reflectivity seen in reflection data from the same region.
The observation from Fig. 4 that waves in a random medium travel faster than in the corresponding medium with the same average slowness has been called 'velocity shift' by Müller *et al.* (1992). It can be qualitatively explained by the fact that multiply scattered waves travel along fast paths. The velocity shift has been studied into great detail by Roth *et al.* (1993). The relative velocity change $\delta v/v$ is in the order of one per cent and increases with travel path L and fluctuation ε, if wavelength λ is much smaller than correlation length a. When λ increases, the velocity shift

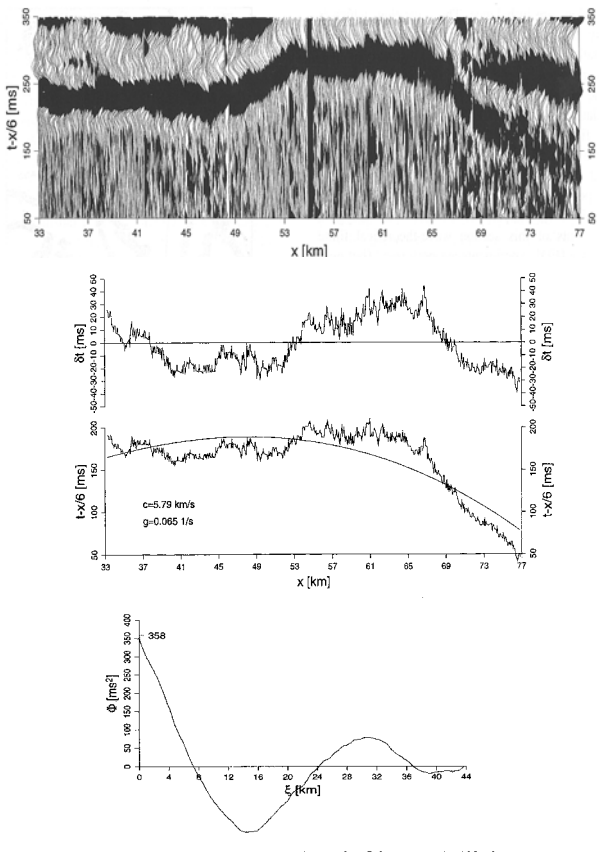

Figure 5: Top: Pg wave section. Middle: travel times. Bottom: autocorrelation function of travel time residuals with respect to a smooth background model (solid line in middle panel).

is reduced, *i.e.*, velocity dispersion is observed (Fig. 6). The velocity shift itself is small enough that it will not have consequences on the interpretation of velocity-depth profiles in terms of chemical composition and phase of minerals and rocks. Its dispersion, however, is of the same order of magnitude as the observed dispersion for mantle S waves between the periods of free oscillations and short period body waves. This is normally interpreted as caused by anelasticity. Given the effect of the velocity shift, one may speculate that statistical heterogeneity explains much of the observed velocity dispersion, and that the influence of anelasticity may have been overestimated in the past. Again, this work supports the claim that scattering and anelasticiy, although physically very different, are phenomenologically very similar: both cause wave attenuation and wave dispersion. Therefore it will be difficult to discriminate between the two.

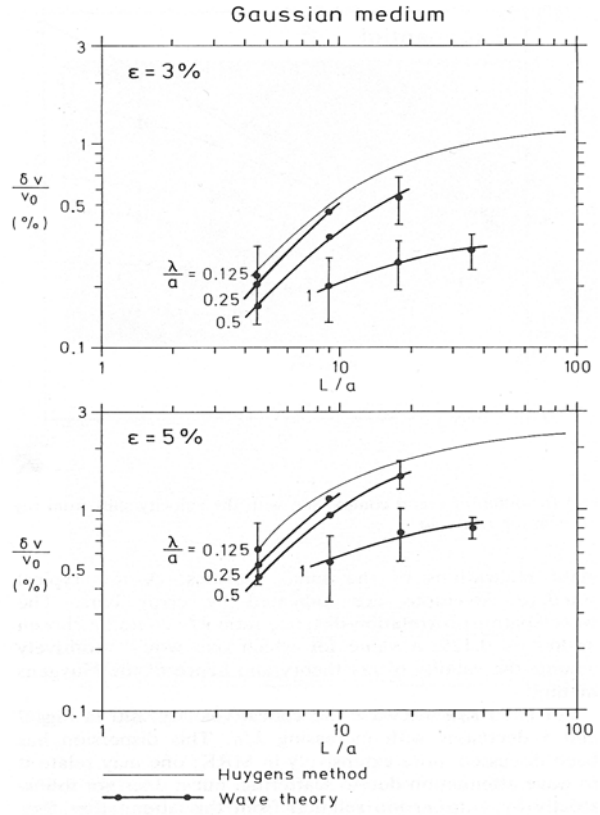

Figure 6: Relative velocity shift $\delta v/v_0$ for various lengths of travel paths L and wavelengths λ. The thin line is obtained by a numerical method for computing first arrival travel times; the thick lines are from full wave field finite difference calculations.

Imaging of Random Structures

Imaging procedures like tomography or migration are normally used to retrieve deterministic heterogeneous structures. If a random small-scale structure is present on top of that, how does it influence the imaging results? Gerhard has tried to give answers to several of these problems.

Ray Tracing in Random Media

Geometric ray theory is the usual way to calculate travel times in heterogeneous media. Kinematic ray tracing, however, does not give the travel times of diffracted waves, which propagate over the fast parts and are diffracted around the slow parts. In a random medium such diffractions will be the first arrivals. Hence it is of practical importance to test the applicability of ray tracing in such cases. Witte *et al.* (1996) compared the travel times of plane waves in a random medium obtained by kinematic ray tracing to those obtained by a finite difference solution of the eikonal equation without any ray computations. In Fig. 7 a homogeneous background medium was superimposed by random heterogeneities with Gaussian autocorrelation function and 3 per cent rms fluctuations. The ray diagram in Fig. 7 clearly shows that even in such a mildly heterogeneous medium systematic focusing and defocusing only occurs for short travel paths. Later on raybundles become so divergent that their rays sense different substructures and propagate independently; regular ray-field structure is lost.

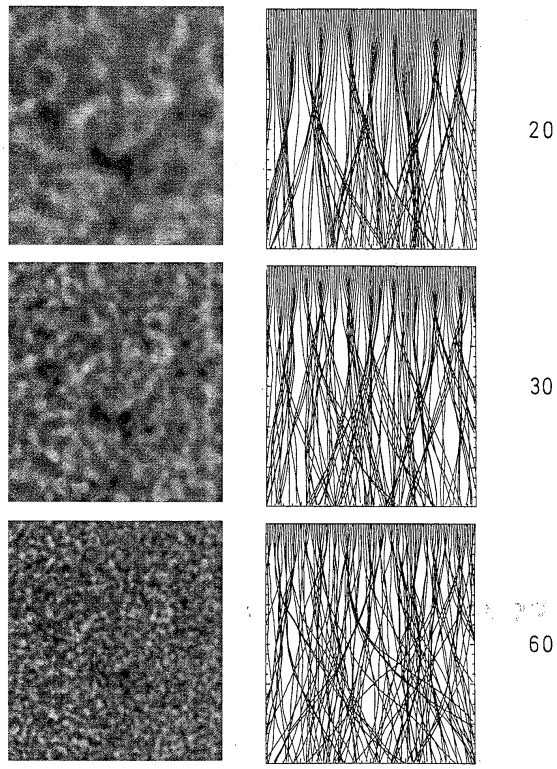

Figure 7: Left: Visualization of a Gaussian random medium. Right: Corresponding ray diagrams. Rays travel from top to bottom. The numbers on the right are the ratios of path length to correlation length.

The corresponding travel times (Fig. 8) also show a very diffuse character when L is increased. Individual travel time branches loose their continuity, their scatter increases, and finally they develop into a cloud of points without structure. In contrast, the first-arrival travel times computed with the eikonal solver including diffractions show a relatively smooth continuous behavior (dotted lines). They are generally early with respect to the

ray-tracing times, as expected from the velocity shift.

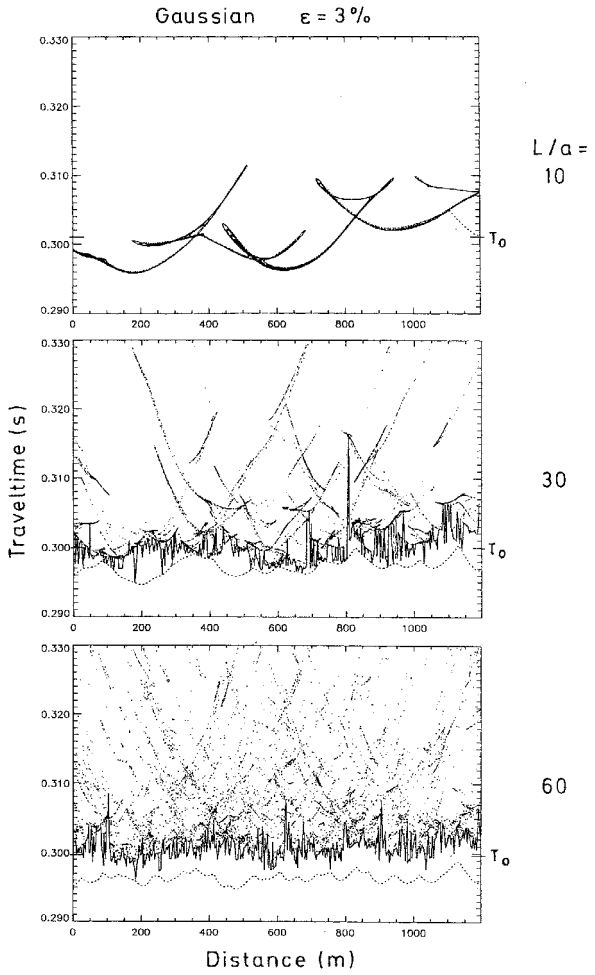

Figure 8: Travel times for the models of Fig. 7. Dashed line is from eikonal solver; points are from kinematic ray tracing.

The problems of ray tracing in random media are evident from Figs. 7 and 8. Only for sufficiently smooth and weak fluctuations and for short travel paths it gives correct arrival times. Otherwise there is a bias towards longer travel times, *i.e.*, smaller velocities and pronounced short-scale variations with distance. For reasonable assumptions on mantle heterogeneity, the bias can be of the order of one per cent for typical teleseismic ray paths. This is already significant for global tomographies employing body-wave travel times.

Ray Parameters of the Core Diffraction P_{diff} and Mantle Heterogeneity

The regional structure of the lowermost mantle and the core-mantle boundary itself has been of utmost interest to seismologists for a long time. The problem of determining deep-seated lateral heterogeneity in the Earth, located below shallow-seated heterogeneity, however, is like looking through a very irregular glass window. Several authors have attempted to measure regional variations of the ray parameter of the core diffraction P_{diff} to infer the structure of the D" zone. In this case one needs to correct for the travel time effects of the mantle heterogeneities above D". Usually, the corrections are taken from tomographic mantle models. Hock *et al.* (1997) tried to quantify the effects of upper mantle heterogeneity on scale lengths of a few hundred kilometers and velocity variations of up to 3 per cent on the P_{diff} ray parameters by modeling the upper mantle as a random medium and calculating corresponding travel time fluctuations (Fig. 9). They found that the corrections to the measured P_{diff} ray parameters can reach several per cent, which is in the same order of magnitude as the observed regional differences. As a consequence, they come to the pessimistic conclusion that regionalization of D" with P_{diff} requires a detailed knowledge of mantle heterogeneity, in particular of the upper mantle, which is currently not available.

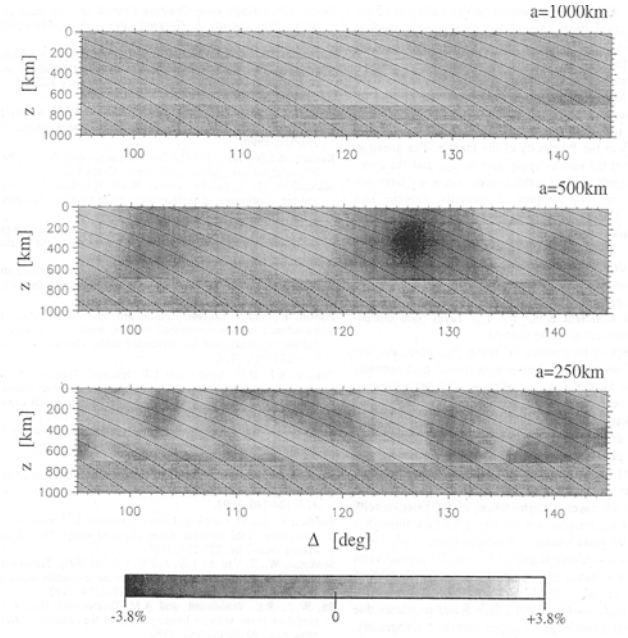

Figure 9: Slowness fluctuations in upper mantle models with different correlation lengths *a*. The lines are isochrones for P_{diff} waves at 15 sec intervals.

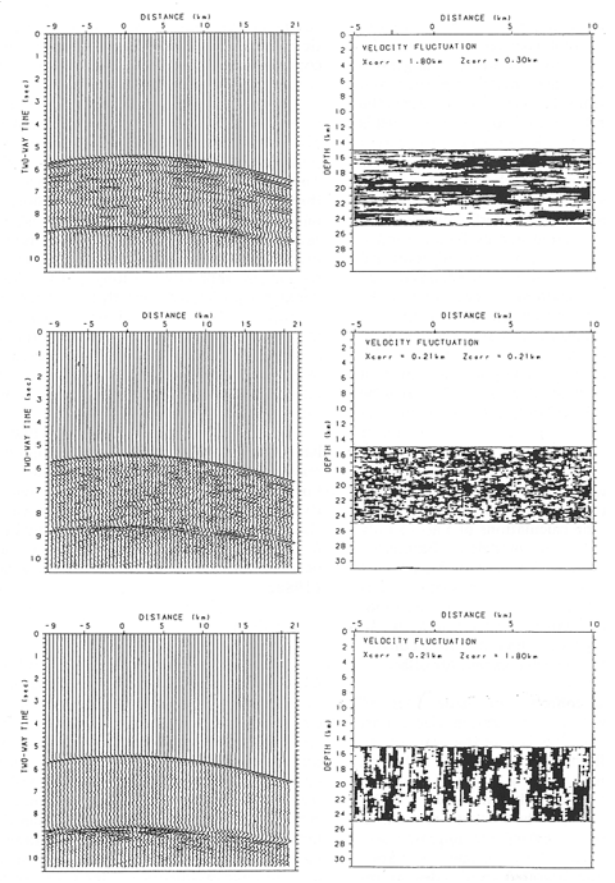

Figure 10: Right: Crustal models with random lower crust. Left: Corresponding single shot sections.

Migration of Random Crustal Structures

Emmerich *et al.* (1993) investigated crustal models with a lower crust containing random small-scale heterogeneous structures overlain by a horizontally stratified upper crust. This way they tried to simulate the results of deep seismic soundings, which often show strong reflected energy from the lower crust, whereas the upper crust seems to be more or less transparent. The numerical studies were done with a hybrid method for the computation of synthetic seismograms (Emmerich, 1992). Three types of models with horizontally elongated, isotropic, and vertically elongated random structures are shown in Fig. 10. For horizontally elongated scatterers there are strong reflections coherent over a horizontal distance, which is longer than the correlation length. Reflections from the Moho show considerable amplitude and phase fluctuations. For isotropic scatterers the coherency is much weaker, a result which is rather different from what would be expected from an ensemble of point scatterers. The Moho reflection can hardly be outlined and is followed by a coda consisting of energy, which is multiply scattered within the lower crust. Vertically elongated scatterers give only weak reflections, but strongly influence the reflection from the Moho forming a complex pattern of reflected and scattered energy. This may be easily misinterpreted in terms of a complex reflector structure instead of a complex overburden.

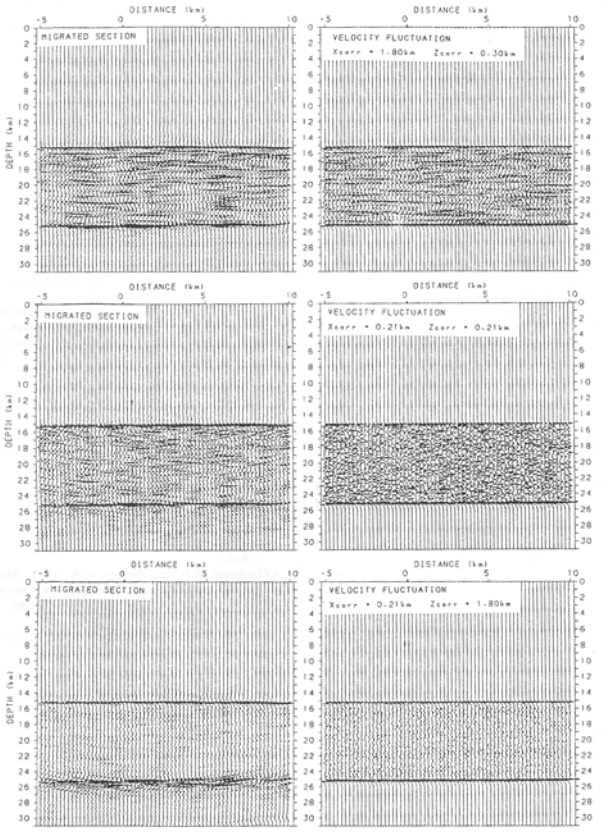

Figure 11: Left: Migrated sections for the models of Fig. 10. Right: Vertical derivative of velocities.

The record sections were then migrated with a fast frequency-wavenumber migration (Müller & Temme, 1987). The result is shown in Fig. 11. For the horizontally elongated scatterers the migration is partly successful, but there is also some disagreement. The coherent elements are generally too long and the Moho depth is not migrated correctly everywhere. For the other two cases there is almost no similarity between the true and the migrated structure. The migrated sections contain artificial coherent reflecting elements, which would be wrongly interpreted as structural elements.

Final Remarks

For more than ten years Gerhard together with a number of coworkers and students has studied wave propagation in complex heterogeneous media described by random velocity distributions. About a dozen publications and several PhD and diploma theses resulted from that work. At a first glance many of the posed questions seem to be of mainly academic interest. A closer look, however, reveals that most of the obtained results bear immediate consequences for the interpretation of the heterogeneous structure of the Earth, on scales ranging from global lateral mantle structure to crustal reflectors. It is my hope that this important part of Gerhard's work will continue to get the attention it deserves from other seismologists, and that it will stimulate future research in this exciting field.

References

Emmerich, H., 1992. PSV-wave propagation in a medium with local heterogeneities: a hybrid formulation and its applications. Geophys. J. Int. **109**, 54-64.

Korn, M., 1987. Computation of wavefields in vertically inhomogeneous media by a frequency domain finite-difference method and application to wave propagation in earth models with random velocity and density perturbations. Geophys. J. R. astr. Soc. **88**, 345-377.

Roth, M., 1997. Statistical interpretation of traveltime fluctuations. Phys. Earth Plant. Inter. **104**, 213-228.

Weber, M., 1988. Computation of body-wave seismograms in absorbing 2-D media using the Gaussian beam method: comparison with exact methods. Geophys. J. **92**, 9-24.

Migration: Reconstruction of Structures from Wavefields

Stefan Buske, FU Berlin

Introduction

Seismic migration was a part of Gerhard Müller's research interests since about 1980. From then on he and his working group have investigated various aspects of this theoretically challenging and industrially important branch of seismic wave propagation. The title of this paper is chosen as a reminder of his lecture course with the same name. He first gave this course in the winter term 1985/86 and the notes were continuously updated based on the outcomes of his work (Müller, 1986 – 1997). Here, the related developments and results are summarized in a more or less chronological order from the viewpoint of a working group member. It is neither meant as a tutorial, nor does it contain any reference to other national or international work on this subject. However, the attentive reader will notice the typically comprehensive and high level of Gerhard's work compared with simultaneously developed migration techniques.

This compilation starts with a short introduction to the basics and principles of migration. This leads to the simplest geometrically based migration techniques, the *ray-geometrical migration* as well as the *diffraction stack*. Then the methods based on the wave equation are described, namely *finite-difference-* (FD), *frequency-wavenumber-* and *Kirchhoff migration*. To keep the paper short and concise the focus is on examples rather than on extensive mathematical derivations. Furthermore, some specific research results are mentioned, which have strong links to Gerhard's other working directions (*e.g.*, investigations on intrinsic attenuation or on wave propagation in random media).

The principal aim of seismic migration is the reconstruction of reflectors at their true position in the subsurface. The recorded wavefield is used to restore a certain "element of the reflector" from the corresponding "element of the reflection". In this sense, the "reflection element" *migrates* into its origin: the "reflector element" (see Fig. 1). The core of any migration method is the extrapolation of the recorded wavefield back in time and down into the subsurface. Therefore, migration can be regarded as an inverse procedure to seismic modeling in which the reflection element is constructed from the corresponding reflector element. Migration can be formulated by means of simple geometrical considerations or by advanced wave-equation based techniques. It can be performed for pre- or post-stack data as well as for other arrangements of these data (CMP-, zero-offset- or plane-wave-sections, shot gathers, etc.) either in the time or depth domain. The final migration result should include the shape and geometry of the reflector as well as its properties (reflection coefficients, etc.).

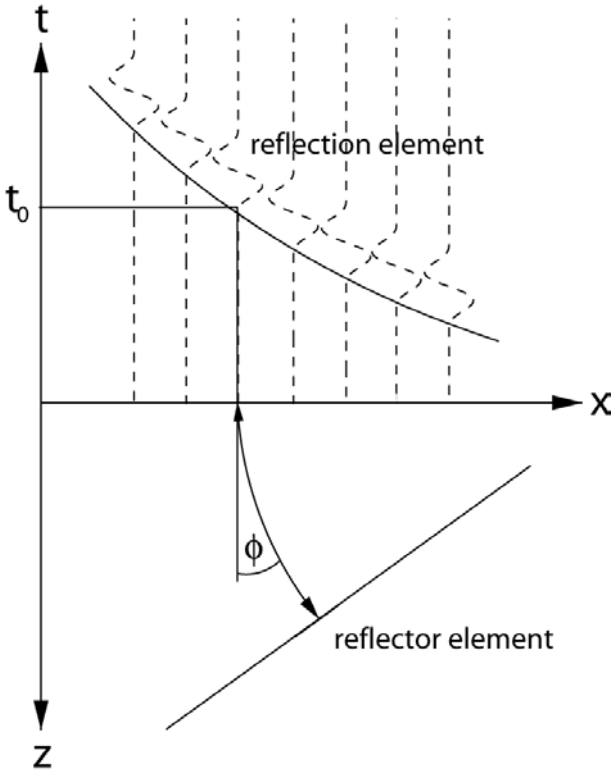

Figure 1: Ray-geometrical migration.

Migration Techniques Based on Geometrical Considerations

Ray-Geometrical Migration

Gerhard started his work on migration with a purely geometrical approach commonly referred to as *ray-geometrical migration*. For a zero-offset travel time curve, the reflection element is connected to the corresponding reflector element by a simple relation: the slope of the reflection element in the time domain is determined by the take-off angle of the corresponding zero-offset ray and the velocity at its surface position (eq. (1) and Fig. 1).

$$\frac{dx}{dt} = \frac{-\frac{1}{2}v(x, z=0)}{\sin(\phi)} \qquad (1)$$

With the help of this formula the reconstruction of the reflector can easily be performed piecewise. First, the travel time curve is picked. Then, for each reflection element, the slope is calculated and a ray is traced starting at an angle ϕ computed from equation (1) at the corresponding surface position. The ray is stopped after a time $t_0 / 2$ and the reflector element is drawn perpendicular to this ray at its end point. This procedure can be implemented interactively, it is fast and it can be formulated for arbitrary velocity models. However, it requires picking, which is a crucial procedure in the case of bad data quality and for large data sets. Furthermore, it is a purely geometrical approach, which does not take into account any amplitude information. This method was the subject of Uwe Block's diploma thesis (1987) and moreover it was the starting point for all migration activities in Gerhard's group.

Diffraction Stack

Another migration technique, which is also based only on geometrical considerations, assumes that every point in the subsurface can be regarded as a possible point diffractor (P) (see Fig. 2). The sum of the traveltime from the source to this diffractor (t_i) and from the diffractor to every receiver at the surface (t_d) yields the corresponding diffraction curve. Summing the amplitudes along the diffraction curve through the observed wave field *U(x,t)* yields a "high" value only if a diffractor exists at this position. Otherwise the sum is negligibly small. An image of the whole subsurface – the migrated section *M(x,z)* – is obtained by performing this stack along the diffraction curves for all subsurface points on a grid (eq. (2)).

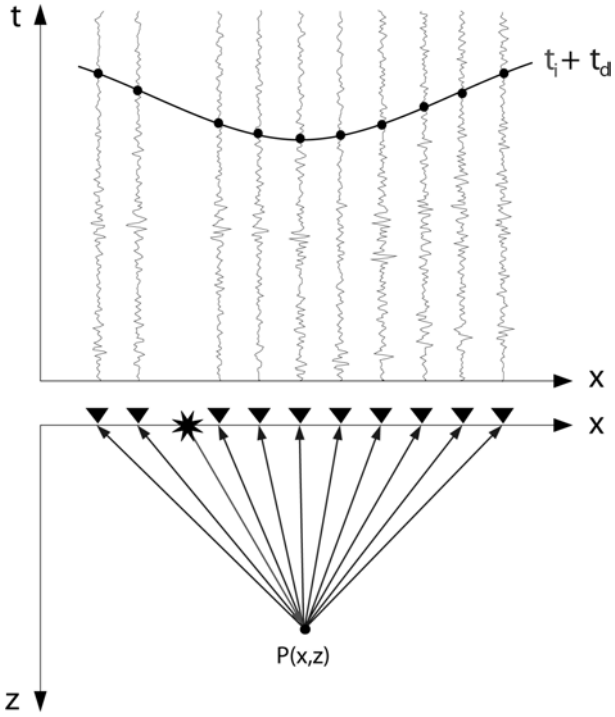

Figure 2: Diffraction stack.

$$M(x,z) = \sum_{j=1,nrcv} U\left(x_j, t_i(x,z) + t_d(x_j,x,z)\right) \qquad (2)$$

According to Huygens's principle, a reflector appears in the migrated section as the result of constructive interference of many diffractors. For a medium with constant velocity, the diffraction curves are hyperbolas, which can be analytically calculated. In the case of arbitrary velocity functions the diffraction curves have to be computed numerically. Furthermore, the whole procedure can be extended easily to 3D by summing along diffraction surfaces. The diffraction stack technique is a kind of "father" to Kirchhoff migration, which itself is one of the wave equation based methods described, among other things, in the next section.

Migration Techniques Based on the Wave Equation

Another way of migrating the reflection element into the reflector element is by using the wave equation. In this case, a seismic experiment is considered as a "downgoing" wave part of which is reflected and converted into an "upgoing" wave. In this context, migration is nothing more than the determination of the spatial origin of the upgoing wave, *i.e.*, the position of the reflector. In order to reconstruct the reflector, two steps have to be performed:

1. *Wave field extrapolation*: the wave field $U(x, z = 0, t)$ recorded at the surface is propagated back in time down into the subsurface using the wave equation:

   $$U(x, z = 0, t) \Rightarrow U(x, z, t)$$

2. *Imaging*: at every subsurface point the backpropagated wave field is sampled at the time when the downgoing wave arrives (t_i = imaging time), *i.e.*, when it is reflected:

   $$M(x, z) = U(x, z, t_i(x, z))$$

The migrated section *M(x,z)* is an image of the subsurface; it represents a measure of the amount of energy which is reflected at a certain subsurface point. The second step mentioned above is common to all migration methods based on the wave equation. However, the first step can be different since the backpropagation is realized by solving the wave equation. A variety of methods exist to solve the wave equation numerically. Here, we consider only the three major techniques, namely *finite-difference*- (*FD*), *frequency-wavenumber*- (ω-*k*) and *Kirchhoff* methods. In the following they are presented in the chronological order that they were investigated within Gerhard's group. No detailed derivations are given here, but these are presented in precise and didactically perfect way (as always) in Gerhard's lecture notes (Müller, 1986 – 1997).

Finite Difference Migration

Fourier transforming the wave field with respect to the spatial coordinates and time and inserting the result into the wave equation yields the well-known *dispersion relation*. An approximation of this relation and a back transformation results in a so-called one-way wave equation, which is then solved using the method of finite differences. In his PhD thesis, Paul Temme elaborated on this technique with the help of synthetic seismograms (Temme, 1983). From the migration of single shot gathers he managed to reconstruct laterally varying reflection coefficients for an inclined reflector. Additionally, he studied the migration of CMP gathers and plane-wave sections and compared the results (Temme, 1984).

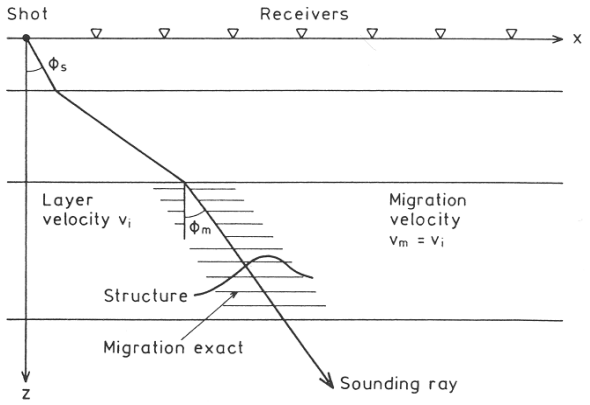

Figure 3: Principle of the "fast" ω-*k* migration (from Emmerich *et al.*, 1993).

Frequency-Wavenumber Migration

A Fourier transformation with respect to only the horizontal coordinates and time results in an equation, which can be solved in the frequency domain. The Fourier transform of the recorded wave field at the surface can be propagated back into the subsurface by a simple phase-shift operation. With the help of Fast-Fourier-Transform techniques, this method became very popular. It was Getahun Terefe (1985) who firstly started to work on this subject in Gerhard's group. Again, it was Paul Temme who became interested in this topic and who developed together with Gerhard the "fast" ω-*k* migration technique (Temme & Müller, 1986; Müller & Temme, 1987). This extension of the usual "recursive"

implementation of ω-k migration proved to be very efficient because it replaced the complete downward back propagation of the wavefield by a number of "directional" migrations along pre-specified "sounding rays" (see Fig. 3). The superposition of a small number of these sounding ray migrations is usually sufficient to deliver a good image of the subsurface, thereby saving a lot of computing time (see Fig. 4). Jürgen Zwielich (1989) extended this work and Helga Emmerich (1992) finally applied it to a data set acquired over a salt pillow structure in Northern Germany (Fig. 5 top).

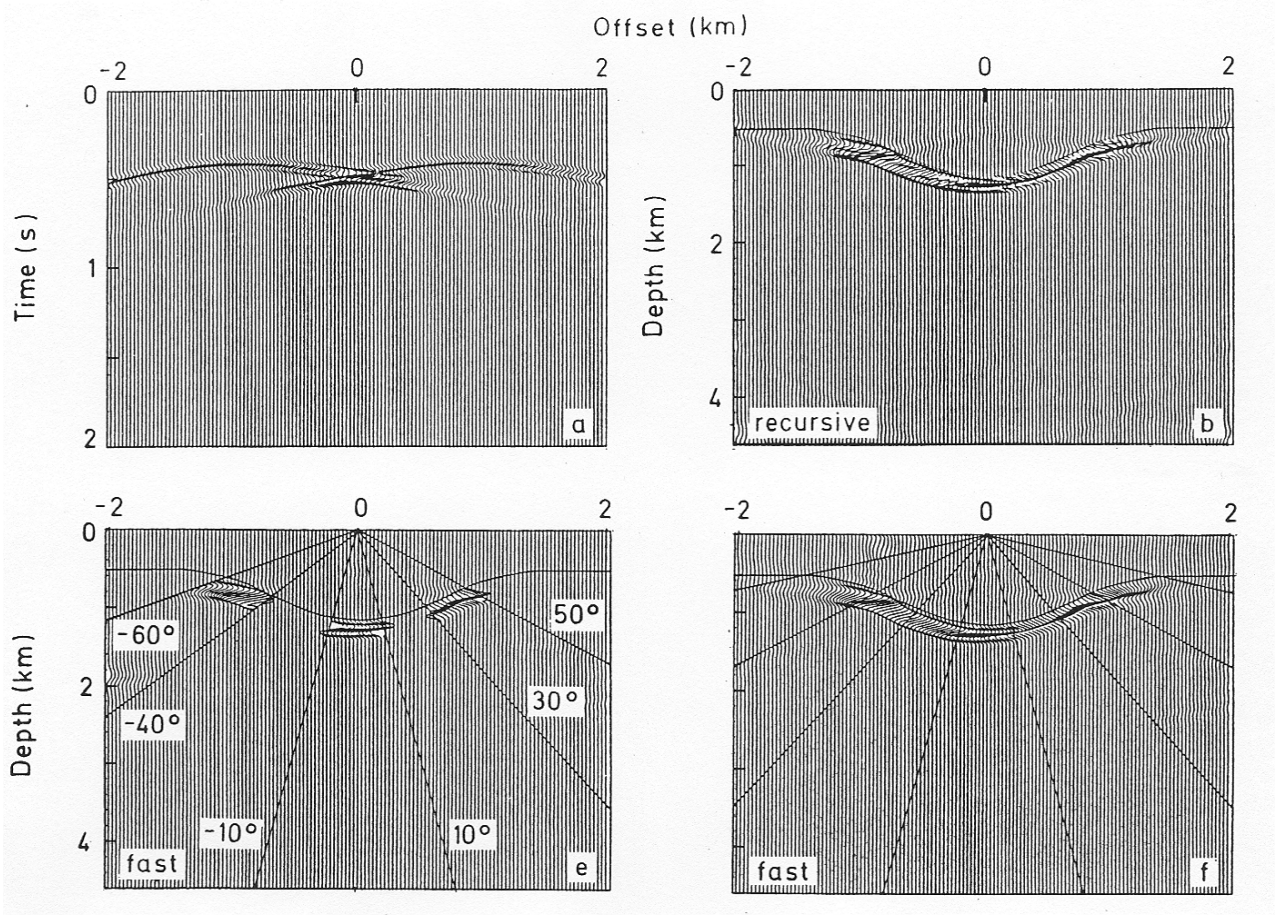

Figure 4: Comparison of "recursive" and "fast" ω-k migration for a syncline (modified after Emmerich *et al.*, 1993).

Kirchhoff Migration

A one-dimensional Fourier transformation of the wave equation with respect to time yields the Helmholtz equation, which can be solved in the frequency domain. A back transformation leads to the well-known Kirchhoff formula, which can be written in such a form that the migrated section is a weighted diffraction stack integral over the filtered wave field recorded at the surface. This migration technique is extremely flexible since it can be implemented easily for arbitrary source and receiver locations. Combination with an efficient eikonal solver for the computation of the travel times from the source and the receivers to the subsurface points allows the use of almost arbitrary velocity models. This method has been tested thoroughly on various models (Buske, 1994), including synthetic test models as well as the salt pillow structure mentioned above (see Fig. 5 bottom). Later, the Kirchhoff migration code was extended to three dimensions and applied to the ISO89-3D data set from the KTB area (Buske, 1999a; 1999b). The resulting images revealed the three dimensional shape of the prominent Erbendorf body and the SE1 reflector (Fig. 6). The latter is split off into two separate parts below 6 km depth and the KTB drill hole penetrates the SE1 reflector in an

area where its image is strongly blurred. Later, Volker Oye (2000) applied Kirchhoff migration to the KTB8502 profile from the same area with special emphasis on sophisticated trace correction factors and amplitude treatment within the migration.

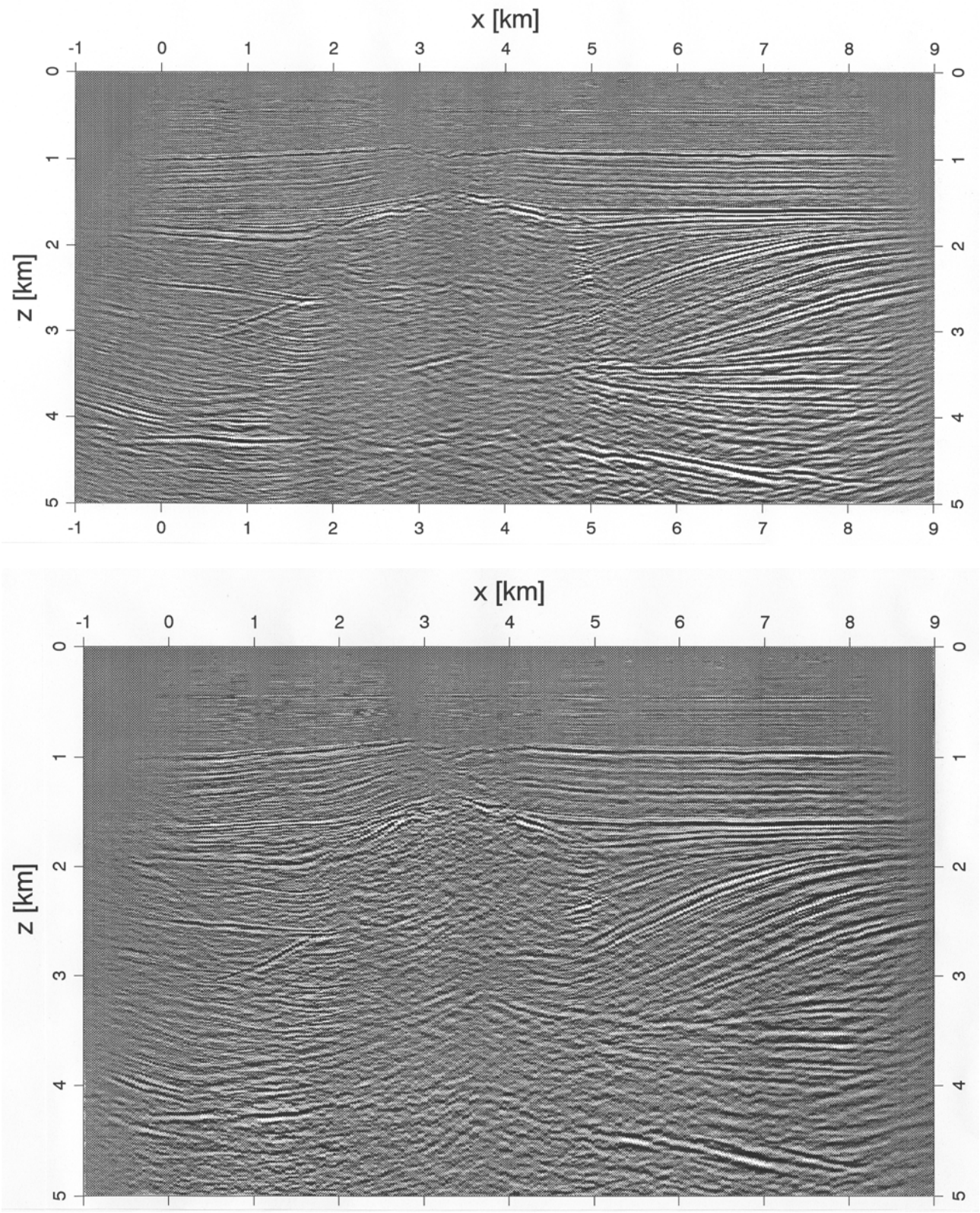

Figure 5: "Fast" ω-k migration (top, from Emmerich, 1992) and Kirchhoff migration (bottom, from Buske, 1994) applied to a salt pillow structure from Northern Germany.

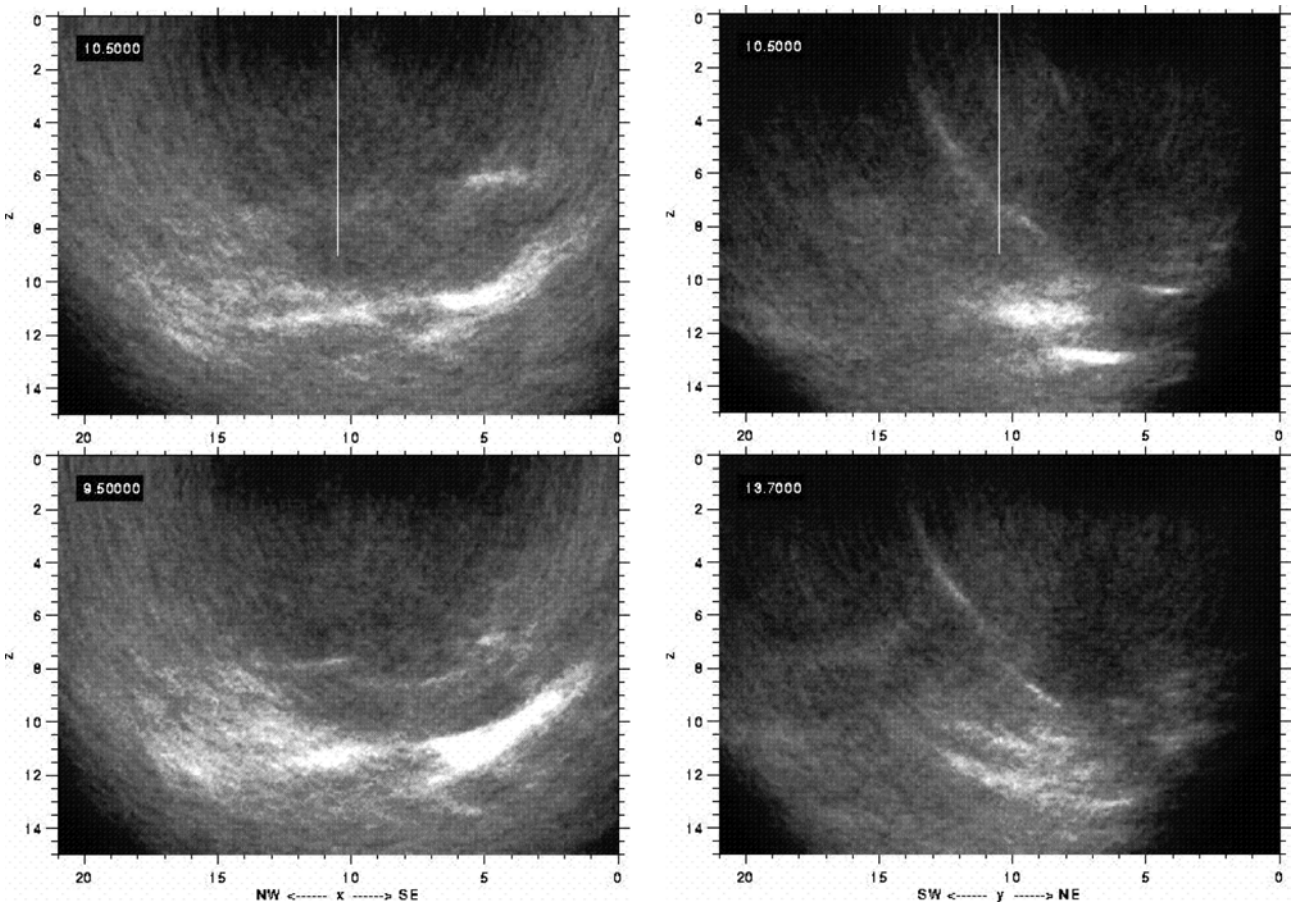

Figure 6: Slices through the volume obtained by 3D Kirchhoff migration applied to the ISO89-3D data set (from Buske, 1999a). The borehole is marked in the upper images; it penetrates the SE1 reflector in an area where its image is blurred. The lower images show that the SE1 reflector is split off below a depth of 6 km.

Further Studies

Finally, it should be mentioned that some special studies have been performed within these main branches of migration. Helga Emmerich *et al.* (1993) started an interesting investigation into the influence of a statistically heterogeneous overburden on the migrated image. They found that according to the subhorizontal recording geometry along the surface subhorizontal features also dominate the image although the orientation of the heterogeneity within the medium can actually be subvertical. This fact is often underestimated and might lead to hasty and false geological interpretations. Charles Toutou (1997) incorporated the influence of intrinsic absorption into migration and he implemented the corresponding correction terms into frequency wavenumber migration as well as into Kirchhoff migration. His work included applying the method to synthetic models and DEKORP data. Finally, an interesting study related to migration has been undertaken by Matthias Zillmer *et al.* (2002). They analysed in detail the reflections from the above-mentioned SE1 reflector as well as from the Erbendorf body with respect to their reflection coefficients. Their results are described in this volume within a separate paper.

Final Remarks

Due to the limited length of this summary, only a brief outline of the migration techniques treated in Gerhard's group is possible. The examples presented here give only a short insight into the cornerstones of the work performed, but the aim is to generate interest and to provide a starting point for further reading. However, for those considering further work on the subject of migration, the best starting point is, without

doubt, all of Gerhard's lecture notes, not only those dealing with the *reconstruction of structures from wavefields*.

References

Block, U., 1987. Strahlenseismische Migration – Methode und Anwendung auf synthetische und gemessene Daten. Dipl. Arbeit, Institut für Meteorologie und Geophysik, Universität Frankfurt, 85 pp.

Buske, S., 1994. Kirchhoff-Migration von Einzelschuss-Daten. Dipl. Arbeit, Institut für Meteorologie und Geophysik, Universität Frankfurt, 117 pp.

Buske, S., 1999a. Three-dimensional Kirchhoff migration of deep seismic reflection data. Geophys. J. Int. **137**, 243-260.

Buske, S., 1999b. 3D prestack Kirchhoff migration of the ISO89-3D data set. Pure Appl. Geophys. **156**, 157-171.

Emmerich, H., 1992. Erprobung der schnellen Frequenz-Wellenzahl-Migration an reflexionsseismischen Daten. Internal report, Deilmann-Erdöl-Erdgas.

Oye, V., 2000. Wahre Amplituden reflexionsseismischer Daten und Migration. Dipl. Arbeit, Institut für Meteorologie und Geophysik, Universität Frankfurt, 94 pp.

Temme, P., 1983. Rekonstruktion von seismischen Reflektoren – Grundlagenuntersuchungen an synthetischen Seismogrammen. Dissertation, Universität Frankfurt, 100 pp.

Temme, P., 1984. A comparison of common-midpoint, single-shot and plane-wave depth migration. Geophysics **49**, 1896-1907.

Terefe, G., 1985. Tiefenmigration im Frequenz-Wellenzahl-Bereich. Dipl. Arbeit, Institut für Meteorologie und Geophysik, Universität Frankfurt, 87 pp.

Toutou, C., 1997. Berücksichtigung von Absorption bei der Migration seismischer Daten. Dissertation, Universität Frankfurt, 209 pp.

Zwielich, J., 1989. Rekursive und schnelle Frequenz-Wellenzahl-Migration von Einzelschuss-Daten bei tiefenabhängiger Geschwindigkeit. Dipl. Arbeit, Institut für Meteorologie und Geophysik, Universität Frankfurt.

Gerhard Müller – Investigations of the Earth's Mantle

Johannes Schweitzer, NORSAR

Introduction

Gerhard Müller's contributions to the investigation of the structure of the Earth's mantle was inextricably linked to his decades long interest in calculating theoretical travel times of seismic waves and theoretical seismograms in progressing by more complex media by using different theoretical approaches and numerical realizations. Gerhard started with simple horizontally layered models before developing, together with his scholars and co-workers, very complex and laterally heterogeneous models. During the 1970s, he developed his method to transform spherical models of the Earth structure into theoretically equivalent, horizontally layered models (Müller, 1971a; 1973c; 1977b). This theoretical approach was very important for all his studies on the deeper structure of the Earth. With the Earth Flattening Approximation, travel times and theoretical seismograms for realistic Earth models can be calculated which can subsequently be compared with observed seismograms.

Using these tools, Gerhard investigated seismic velocities, densities, attenuation of seismic waves and the principal structure of the Earth's interior. For example, Gerhard published together with Rainer Kind globally observed long period seismogram sections of vertical, radial and transverse components for an event near Sumatra and compared these sections with theoretical seismograms calculated for P and SV energy (Müller & Kind, 1976). Some years later, he completed this work together with Wolfgang Schott by calculating theoretical seismograms for SH waves and comparing them with observed data (Müller & Schott, 1981).

In this overview on Gerhard's studies related to the Earth's mantle, I will concentrate on investigations of body waves since most of his work on surface waves was related to the Earth's crust.

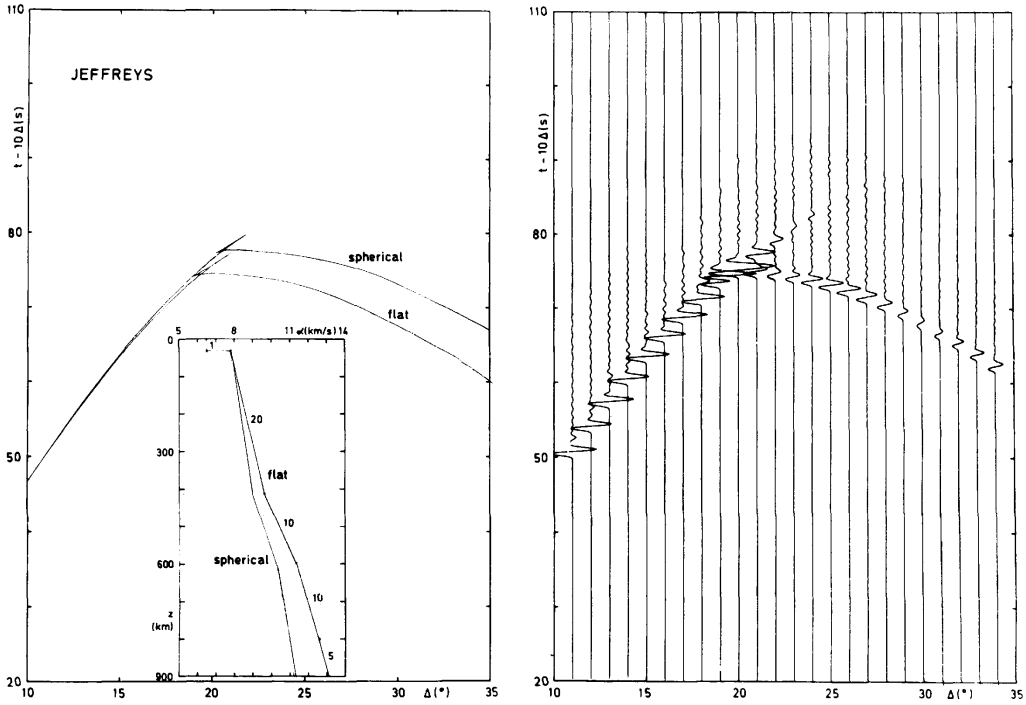

Figure 1: One of Gerhard Müller's first applications of the Earth-Flattening Approximation when calculating theoretical seismograms for an upper mantle model (Fig. 1 from Müller & Mayer-Rosa, 1971).

Upper Mantle Structure

Gerhard's first publication on upper mantle structure was published in the Proceedings of the ESC meeting in Luxembourg, 1971 with Dieter Mayer-Rosa as co-author. Already in this paper all methods came together, which Gerhard used to study the Earth; he applied a first version of his Earth Flattening Approximation, compared theoretical travel times and seismograms for different models of the uppermost mantle and measured amplitude distance curves (Müller & Mayer-Rosa, 1971). In this text the authors also already mentioned the need for correcting observed amplitude data for source radiation. Only then observed amplitudes of different events can be compared with amplitudes of theoretical seismograms (Fig. 1).

SKS Precursors

In the late 1970s and early 1980s, Gerhard, together with Sonja Faber, investigated precursors to SKS phases, which can often be observed in long-period seismograms (Faber & Müller, 1980). Precursor observations of the March 4, 1977 intermediate focus event in Romania at North American stations were the starting point for these studies. At this epicentral distance, theoretical seismogram calculations supported only one interpretation: the observed precursors were SV-to-P conversions from the mantle transition zone at about 11 to 13º distance from the observing stations. The set of precursor observations was extended by data from Tonga-Fiji events, for which SV-to-P conversions can also be observed at North American stations (Fig. 2). Both data sets were then used to discuss models of the discontinuities in the upper mantle transition zone.

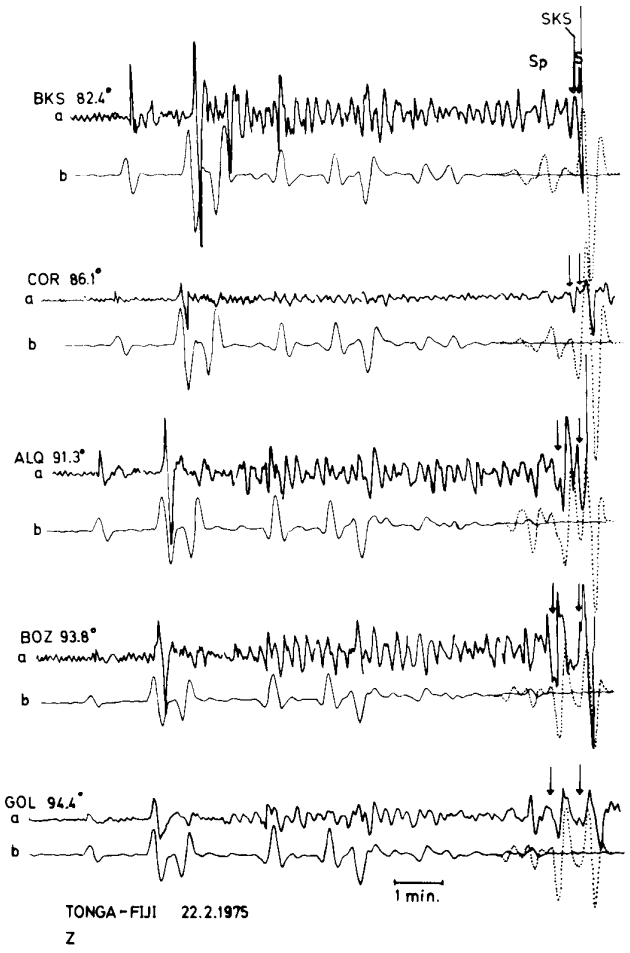

Figure 2: Observed and modeled long period seismograms showing SKS precursors (Sp) observed at stations in North America (Fig. 16 from Faber & Müller, 1980).

This study was continued with a systematic search for such converted phases at European stations, most of them observed with the, at that time newly established, Gräfenberg Array (Faber & Müller, 1984; Müller *et al.*, 1986). Again, the theoretical seismograms helped to interpret the data and to distinguish between different models.

The Phase pMP

The next study concerning precursors of regular seismic phases was initiated by observations at the Gräfenberg array where for deep focus events precursors, arriving shortly before the surface reflection pP, could sometimes be observed. Soon it became clear that these precursors are pP energy reflected from the underside of the Mohorovičić discontinuity, called pMP (Fig. 3). In his Diploma Thesis, Thomas Schenk investigated this phenomenon in detail for Japanese events observed at stations in Europe and North America and, in this way, measured the crustal thickness of remote areas (Schenk *et al.*, 1989).

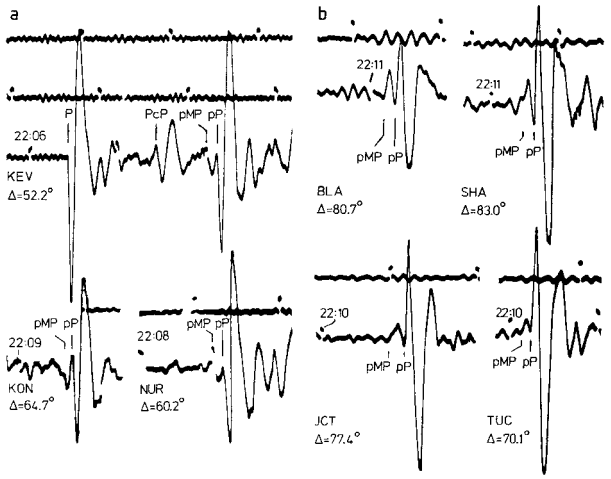

Figure 3: Example of pMP observations at European (a) and North American (a) stations (Fig. 6 from Schenk *et al.*, 1989).

During the late 1970s and 1980s, Lev Vinnik, Rainer Kind and other authors developed the ideas on P-to-SV conversions in upper mantle and crust arriving in the P coda on the radial component, a method today known as receiver function analysis. Gerhard was of course interested in knowing the potentials and limitations of this method and initiated the theoretically oriented Diploma Thesis of Benno Kolbe on this topic (Kolbe, 1990). More oriented towards data interpretation was the last Diploma Thesis concerning the upper-mantle structure which Gerhard supervised: the first systematic investigation of SKS and SKKS splitting at the broadband stations of the German Regional Seismic Network (GRSN) by Martin Knappmeyer (Knappmeyer, 1994).

Lower Mantle and D"

As far as I am aware, the first work of Gerhard on seismic phases especially sensitive to the structure of the lower mantle was when he worked together with Rainer Kind on extensions of the reflectivity method (Kind & Müller, 1975). They calculated long period seismogram sections for SV- and P-phase energy and discovered unknown pulse distortions of the SKS onsets at epicentral distances larger than about 110º. Very soon it became clear that this pulse distortion was due to an SV-to-P-to-SV converted phase, which travels for some part of its path along the core-mantle boundary (CMB) as a P-diffracted wave. The existence of this theoretically found phase, called SPdiffKS or SKPdiffS, was then confirmed by observing similar pulse distortions on records of long period WWSSN seismograms (Fig. 4 and see also Fig. 3 of R. Kind's contribution).

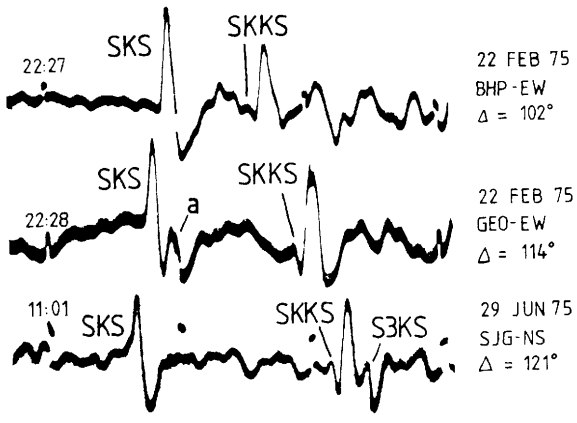

Figure 4: Example for the pulse distortion (a) of the SKS onset in 114º due to the CMB diffractions SKPdiffKS and SPdiffKS (Fig. 2 from Schweitzer & Müller, 1986).

In recent years, this phase again came into the focus of seismologists when other authors used it to demonstrate the existence of Ultra Low

Velocity Zones at the CMB (*e.g.*, Garnero *et al.*, 1998) without considering that this phase cannot be interpreted with a ray theoretical approach.
During the following two decades, Gerhard worked together with Diploma- and PhD-students and colleagues again and again on problems linked to the structure of the CMB, the lower mantle and in particular of D".

PcP Amplitudes
Still in Karlsruhe, Gerhard together with Abdel Hafiz Mula and Søren Gregersen investigated long-period PcP amplitudes (Müller *et al.*, 1977), which are sensitive to the reflection coefficient and thereby to the velocities and densities on both sides of the CMB. The amplitudes were normalized by correcting them for the radiation pattern of the sources and then dividing by the (also radiation pattern corrected) amplitudes of the direct P phase. This procedure corrects for different event magnitudes and reduces the influence on the PcP amplitudes of lateral heterogeneities along the paths in the mantle, in particular near the sources.
After moving to Frankfurt, Gerhard continued and extended his investigation of the lower mantle structure and the D" region together with Jörg Schlittenhardt (Schlittenhardt, 1984; 1986; Müller *et al.*, 1986), Thomas Spies (1985), and in theoretical studies together with Wolfgang Kampfmann (Kampfmann & Müller, 1989) and Helga Emmerich (1991; 1993). Thomas Spies investigated in his Diploma Thesis 11 more events than Hafiz Mula and confirmed the large scatter in the amplitude ratios found earlier. However, this study clearly demonstrated a geographical dependency of the observed amplitude ratios and that most data are compatible with simple velocity models for the lower mantle like PREM. This finding was confirmed by the parallel investigation of PcP-P travel-time differences, which could also be best explained by a PREM-like velocity structure in D" with some additional regional velocity anomalies.
Jörg Schlittenhardt investigated PcP/P short period amplitude ratios at larger distances. He investigated P and PcP observations from the Gräfenberg Array and from NORSAR. The direct P phase and the core reflection PcP can be separated at large distances by applying array techniques. Jörg Schlittenhardt found very low PcP/P amplitude ratios with respect to all discussed models of D" and the CMB. He found that the amplitudes of PcP are strongly influenced by the attenuation of P energy in D" and, in order to explain the observed data, he proposed laterally strongly varying attenuation in D" (Fig. 5).

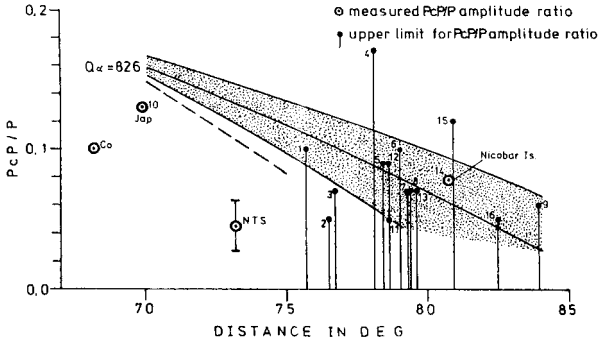

Figure 5: Observed low PcP / P amplitude ratios and different Q models for D" (Fig. 10 from Schlittenhardt, 1986).

Some years later, Gerhard together with Wolfgang Kampfmann published an alternative model for low PcP amplitudes. Theoretical seismograms calculated with the Kirchhoff theory for a rough CMB surface can also easily produce the observed large scatter in reflected PcP amplitudes (see Fig. 3 of A. Souriau's contribution). Gerhard's PhD student Helga Emmerich extended this study for ScS waves (Emmerich, 1991; 1993) and confirmed the PcP results of Kampfmann & Müller (1989).

The Core Diffractions Pdiff and Sdiff
During his time in Karslruhe, Gerhard began to investigate the velocity gradient in D" together with his PhD student Hafiz Mula. For this study they measured on long period seismogram sections the ray parameter of Pdiff and Sdiff (Mula & Müller, 1980). They found that long period Pdiff and Sdiff waves propagate with a non-ray-theoretically defined velocity in D" but with a signal period dependent on the average velocity in D" (Fig. 6). Extreme velocity gradients as discussed in the literature at that time could be ruled out as

global features. These results were then further supported by an independently published study of Hafiz Mula, in which he measured and modeled the amplitude decay of Pdiff and Sdiff (Mula, 1980; 1981).

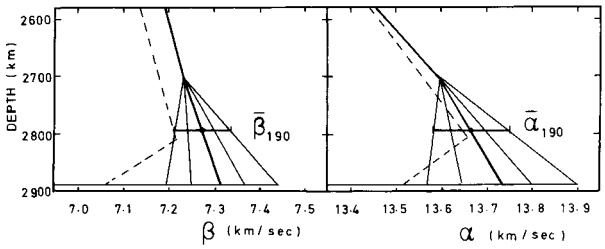

Figure 6: Shows the investigated range in the lower most 190 km of the Earth's mantle for the effective velocity for long period Pdiff and Sdiff (Fig. 11 from Mula & Müller, 1980).

The last time Gerhard worked on core diffractions was when he, together with Silke Hock, Michael Roth, and Helga Emmerich mapped the geographical dependence of ray-parameter measurements of Pdiff (Hock, 1992; Hock *et al.*, 1997). In this study, they found not only drastic differences in the ray parameter for Pdiff but also a strong dependency of these differences from applied corrections for lateral heterogeneities in the mantle as a whole.

No First Order Discontinuity on Top of D"

Finally, I will conclude with results from studies of Gerhard on the lower mantle velocity structure in which I personally was involved. During the early 1980s, Thorne Lay and co-workers published several studies (*e.g.*, Lay & Helmberger 1983), in which they proposed the discovery of a new global discontinuity on top of D". These publications were not without any contrary reactions and one of the studies was made in Frankfurt (Schlittenhardt *et al.*, 1985). Following Lay's idea, such a discontinuity will produce very pronounced and observable effects on long period seismograms outside the distance range investigated by Lay. In our study, we could show with several seismogram sections that such pronounced effects cannot be observed and that therefore the idea of a global discontinuity on top of D" is not in agreement with observed data and is therefore wrong (Fig. 6).

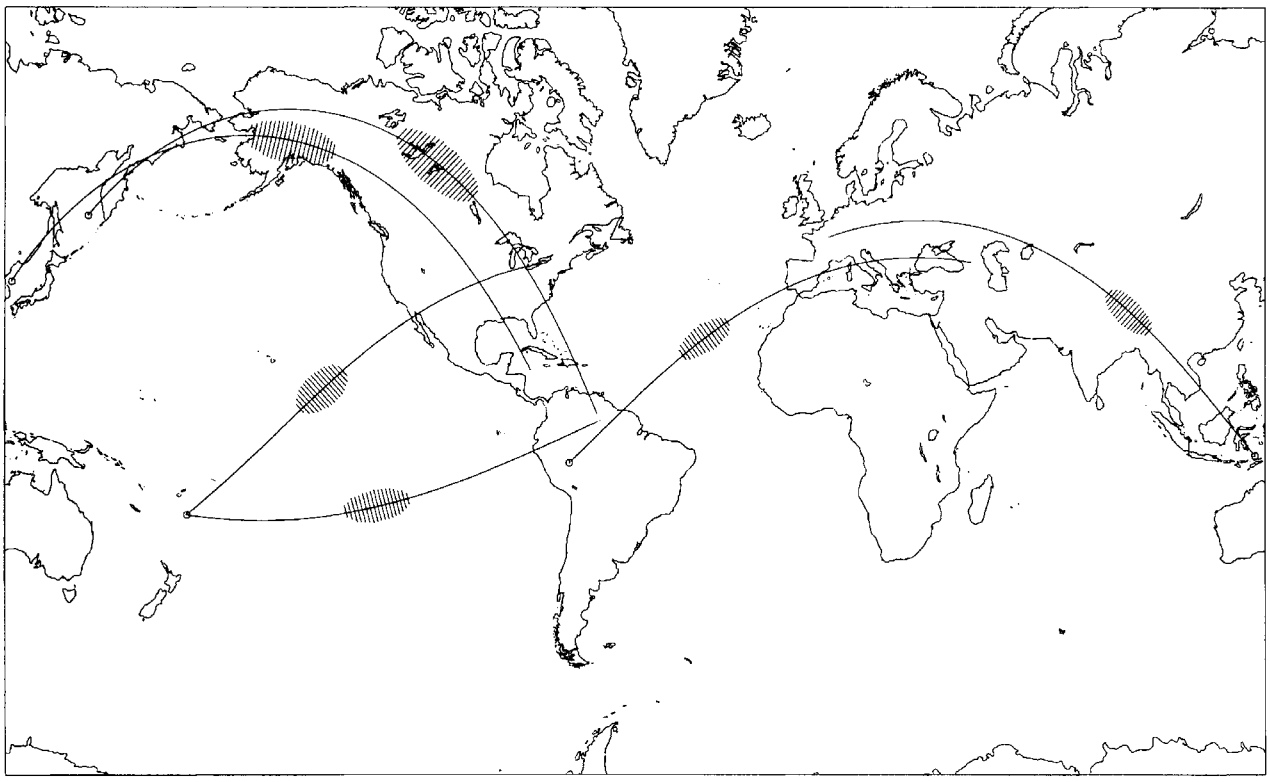

Figure 7: The hatched areas mark the regions for which no evidence was found for a seismic discontinuity on top of D" (Fig. 6 from Schlittenhardt *et al.*, 1986).

During the work on my Diploma Thesis, it became evident that observed anomalous SKKS-SKS travel-time differences and amplitude ratios SKS/SKKS, earlier interpreted as effect of the velocity structure in the outer core (Kind & Müller, 1977), are best explained by lateral heterogeneities in the lower mantle (Schweitzer, 1985; Schweitzer & Müller, 1986). Consequently, I modeled in my PhD thesis these observed effects and could present the first S-velocity model of the now well-known velocity anomaly in the lowermost mantle below the Pacific (Schweitzer, 1990).

Resume

Teaching us students Gerhard initiated numerous Diploma- and PhD-theses. He substantially contributed to the results and the quality of all these academic publications, which later often became the nucleus of one of the many publications with Gerhard as co-author. Therefore, I cannot separate these academic publications from Gerhard's own publications but see them all as one contribution to our knowledge about the Earth's interior.
This January, it was 18 years ago that I finished my Diploma and 13 years ago that I delivered my PhD thesis, both supervised by Gerhard. I will never forget and always be thankful for this scientific education and for his critical but always-fair stimulation of my studies and that, whenever I needed it, he was present in his open office ready for help and exchange of ideas.
In his unique kind of deeply looking into geophysical problems and critically but constructively reviewing research results, Gerhard will be remembered as an extraordinary scientist and as high quality academic teacher.

References

Emmerich, H., 1991. Kombination von Finite-Differenzen-Verfahren und Frequenz-Wellenzahl-Filtern zur Modellierung der Wellenausbreitung in lokal komplexen Medien. Dissertation, Universität Frankfurt, 142 pp.

Emmerich, H., 1993. Theoretical study on the influence of CMB topography on the core reflection ScS. Phys. Earth Planet. Int. **80**, 125-134.

Garnero, E. J., J. Revenaugh, Q., Williams, T. Lay & L. H. Kellog, 1998. Ultra-low velocity zone at the core-mantle boundary. In: Gurnis *et al.* (editors). The core-mantle boundary region, Am. Geophys. Un., ISBN 0-87590-530-7, 319-334.

Hock, S., 1992. Bestimmung des Strahl-parameters der am Erdkern diffraktierten P-Welle zur Untersuchung der Basis des Erdmantels. Dipl. Arbeit, Institut für Meteorologie und Geophysik, Universität Frankfurt, 8+124 pp.

Knappmeyer, M., 1994. Doppelbrechungs-analyse von SKS- und SKKS-Phasen an den Stationen des German Regional Seismic Network. Dipl. Arbeit, Institut für Meteorologie und Geophysik, Universität Frankfurt, 125 pp.

Kolbe, B., 1990. Theoretische Seismogramme der Mantel-P-Welle mit Konversions-phasen – Analyse mit der Methode von Vinnik. Dipl. Arbeit, Institut für Meteorologie und Geophysik, Universität Frankfurt, 144 pp.

Lay, T. & D. V. Helmberger, 1983. A lower mantle S-velocity triplication and the shear velocity structure of D". Geophys. J. R. astr. Soc. **75**, 799-837.

Mula, A. H. G., 1980. Ray parameter and amplitudes of long period diffracted waves and the velocities and the Q structure at the base of the mantle. Dissertation, Universität Karlsruhe, 107 pp.

Mula, A. H. G., 1981. Amplitudes of diffracted long-period P and S waves and the velocities and Q structure at the base of the mantle. J. Geophys. Res. **86**, 4999-5011.

Schenk, T., 1988. Die an der Moho reflektierte pP-Vorläuferphase pMP – Beobachtungen und Krustenuntersuchungen. Dipl. Arbeit, Institut für Meteorologie und Geophysik, Universität Frankfurt, 135 pp.

Schlittenhardt, J., 1984. Array-Untersuchungen von reflektierten und diffraktierten Kernphasen. Dissertation, Universität Frankfurt, 159 pp.

Schlittenhardt, J., 1986. Investigation of the velocity- and Q-structure of the lowermost mantle using PcP/P amplitude ratios from arrays at distances of 70° – 84º. J. Geophys. **60**, 1-18.

Schweitzer, J., 1984. Laufzeiten und Amplituden der Phasen SKS und SKKS und die Struktur des äußeren Erdkerns. Dipl. Arbeit, Institut für Meteorologie und Geophysik, Universität Frankfurt, 117 pp.

Schweitzer, J., 1990. Untersuchungen zur Geschwindigkeitsstruktur im unteren Erdmantel im Bereich der Kern-Mantel-Grenze unterhalb des Pazifiks mit Scherwellen. Dissertation, Universität Frankfurt, 134 pp.

Spies, T., 1985. Untersuchung der seismischen Geschwindigkeiten an der Basis des Mantels mit Amplituden und Laufzeiten der Kernreflexion PcP. Dipl. Arbeit, Institut für Meteorologie und Geophysik, Universität Frankfurt, 137 pp.

Anelasticity of Earth Materials

Hans Berckhemer, Frankfurt

Introduction

This is a somewhat shortened version of my talk in Neustadt, in particular with respect to figures and experimental parts.
For the Frankfurt institute the year 1978 was a very successful one in a twofold sense. A full (C4) professorship for mathematical geophysics had been newly created. It was the first one of this kind in Germany. But in particular we succeeded in occupying this chair with our favoured candidate Gerhard Müller.
In the sixties mathematical geophysics was treated in Frankfurt only in seminars in cooperation with the theoretical physicist Bernhard Mrowka and later, up to his appointment in Clausthal, by Horst Neugebauer. At this place I should like to gratefully remind to Bernhard Mrowka, who had, although tied to the wheelchair, always with subtle humour and critical sense guided the students.
Gerhard Müller was known as a critical, but extraordinary profound and creative scientist, and a dedicated academic teacher. In a short time he had gathered together a group of able students from whom more than a dozen valuable dissertations came out. Although Gerhard and I were quite different in scientific mind and interests our very good collegial cooperation was based on mutual respect and appreciation. If in recent years our personal relationship had been deepened, this may not at least be due to a common scientific interest in rock fracture processes and in experimental problems.
In the seventies my interest shifted from purely seismological subjects to petrophysical experiments related to earthquakes and geodynamics. So our fields of activities have supplemented each other quite well and this I should like to show in this paper. I shall deal with non-elastic properties of Earth materials.
Even seismologists are frequently not aware, that the possibility for a deterministic investigation of the Earth's interior by seismic body waves depends on the fact that the Earth is <u>not</u> an ideal elastic medium but that the seismic motion decays after some time by anelastic absorption of wave energy. Otherwise the Earth would be populated with a very complex pattern of chaotic noise. As much as 10^{17} Ws seismic energy have to be consumed annually in the Earth. The question of damping of seismic signals arises in particular if the energy radiated from the seismic source has to be considered. The signal has to be corrected properly, preferably in the frequency domain (see *e.g.*, Lindenfeld & Berckhemer, 1995).

Definitionen für Q

$Q = \frac{2\pi E}{\Delta E} \approx \frac{\pi \omega}{2\alpha}$ Schwinger-Güte
α = Abklinggrösse pro s

$Q = \frac{\omega}{2c\beta}$ Fortschreitende Welle
c = Ausbreitungsgeschwindigkeit
β = Schwächungskoeffizient pro m

$Q = \frac{k'}{2k''(\omega)}$ Komplexe Wellenzahl

$Q = \frac{M'}{M''}$ $M = M' + iM'' = A\,e^{i\varphi}$ komplexer Modul

$Q^{-1} = \tan\varphi$

Frequenzabhängigkeit von Q

$Q \approx \omega^{\gamma}$

$0 < \gamma < 1$ $\gamma = ?$

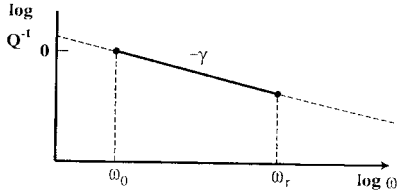

Normierungen

$$Q(\omega) = Q(\omega_r) \cdot \left(\frac{\omega}{\omega_r}\right)^{\gamma}$$

ω_r = Referenzfrequenz z.B. Eckfrequenz des seismischen Absorptionsbandes
oder

$$Q(\omega) = 1 \cdot \left(\frac{\omega}{\omega_0}\right)^{\gamma}$$

wobei bei $\omega = \omega_0$, $Q(\omega_0) = 1$

Figure 1: Definitions of Q and frequency dependence.

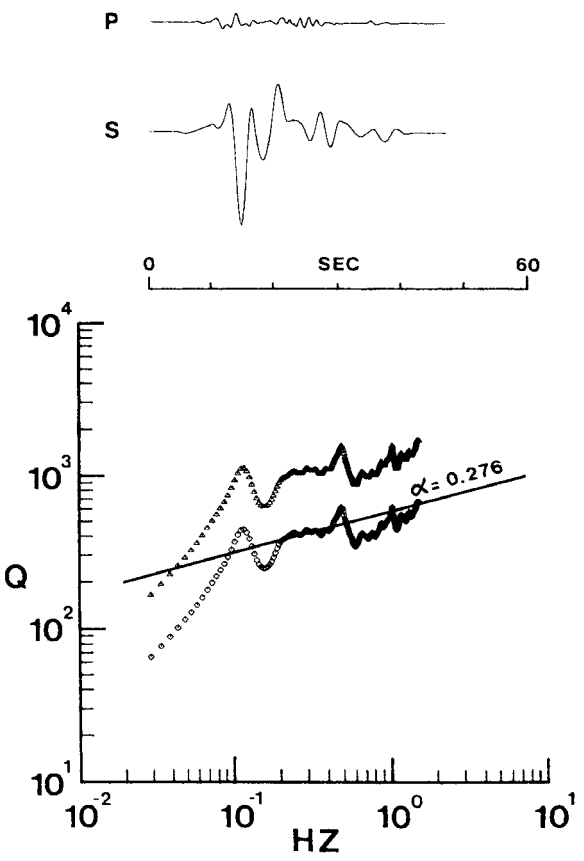

$$Q(f) = \frac{\pi \cdot f \cdot t'}{\ln(S(f)/P(f)) - \ln m} \sim f^{a}$$

Figure 2: Determination of frequency dependence of Q from S / P spectral ratio of teleseismic event, Honshu 7. March 1978 (Ulug & Berckhemer, 1984). In this figure α is used as name for the exponent of *f* and not γ.

M. Lindenfeld has recently estimated the dramatic losses of body wave energy along the seismic wave path for numerous teleseismic events of different energy and epicentral distance. Only 2 – 10 % of the radiated energy reaches the teleseismic stations.

Let us start with some basic definitions of anelastic absorption (Fig. 1). The quality factor Q was originally introduced in communication engineering as the measure for the damping of an oscillating electronic circuit. 1 / Q is the relative loss of energy per oscillation. For propagating waves Q can be expressed by the attenuation coefficient per unit length of the ray path or by the complex wave number. In Müller's approaches as well as in relevant experiments the definition of Q by the ratio of the real to imaginary part of the complex elastic modulus was used. This definition is applicable, if the system is linear and causal. In this case the real and imaginary part are uniquely connected by the so-called Kramers-Kronig relation, of which Müller makes consequent use.

The seismological experience but also the laboratory experiments have shown, that Q increases rather weakly, but never the less significantly with frequency. How large is this frequency dependence? This was an open question two decades ago. Müller has applied the usual power-law approach, leaving at first the exponent γ open. Q may be standardized by an arbitrary reference-frequency ω_r or by ω_0 where ω_0 is the frequency for Q = 1.

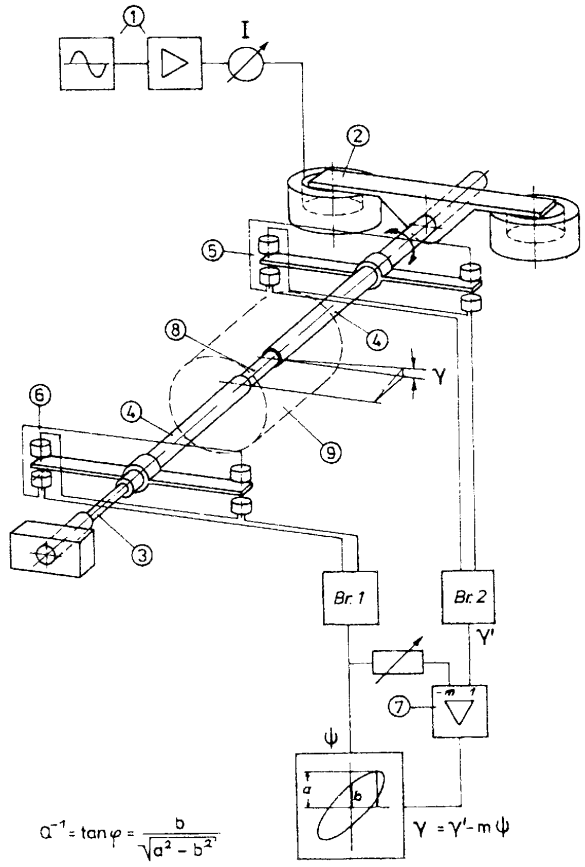

Figure 3: Apparatus for forced harmonic torsion experiments at high temperature (8: rock sample, 5, 6: measuring devices for torsion strain and stress, 9: oven) (Berckhemer *et al.*, 1982).

We have tried in two completely independent ways to find the exponent γ, on the one hand by a special analysis of P- and S- waves of teleseismic signals and on the other hand by investigation of crust- and mantle rocks at high

temperature in the laboratory. In his PhD thesis A. Ulug derived under certain assumptions from the spectral ratio of P and S the frequency dependence of Q and received values of γ between 0.25 and 0.5. A sample is shown in Fig. 2. To measure the complex modulus in the laboratory, cylindrical rock samples of crust- and mantle rocks were exposed to harmonic torsion and the deformation measured at frequencies of 0.03 – 10 Hz at temperatures up to 1400 C° in a newly developed device. (Fig. 3) In these experiments and their evaluation E. Aulbach, W. Kampfmann and H. Schmeling took an important part. Results for a sample of Balmuccia peridotite are shown in Fig. 4. The power-law dependence of Q on frequency is restricted to a certain frequency band. At higher frequencies and lower temperature an upper corner is seen in the Q spectrum as already postulated by D. Anderson and J. B. Minster (1980).

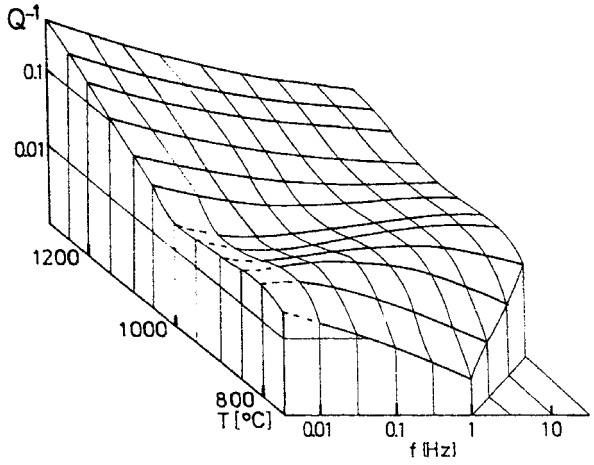

Figure 4: Q^{-1} of Balmuccia- Peridotite as a function of frequency and temperature. Upper absorption band corner visible at high frequency and low temperature.

Now to the theoretical approach of Gerhard Müller for linear, viscoelastic solids (Müller, 1983). The stress- strain relation can be written in the well known form of Hook's law where, however, $M(\omega)$ is a complex, frequency dependent modulus. Müller obtains by means of the Kramers-Kronig equation a relation between M' and M". For $Q(\omega) = (\omega / \omega_0)^{\gamma}$. Müller was able to compute for all rational fractions of γ exact and approximate solutions, where, of course, the Q-spectrum did not contain absorption corners. Here the function $I(\omega,\gamma)$ is given only in an approximate form. Of interest are in particular the limiting values for high and low frequencies, which result from the relaxation function R(t) (system response to a step in displacement) and from the creep function K(t) (system response to a step in stress). This is on the one hand $R(t\rightarrow 0) = M(\omega\rightarrow\infty)$ the unrelaxed modulus of an ideal elastic Hook body. Of basic importance in Müller's approach is, however, that also a limiting value for very low frequencies or long times $K(t\rightarrow\infty)$ can be given. For constant ω_0 this corresponds exactly to the property of the classical Maxwell body, where the viscosity is defined as $\eta = M(\infty) / \omega_0$. For $0 < \gamma < 1$ it follows (Fig. 5)

$$\eta = M(\omega_r)\, Q(\omega_r)^{\gamma} / \omega_r$$

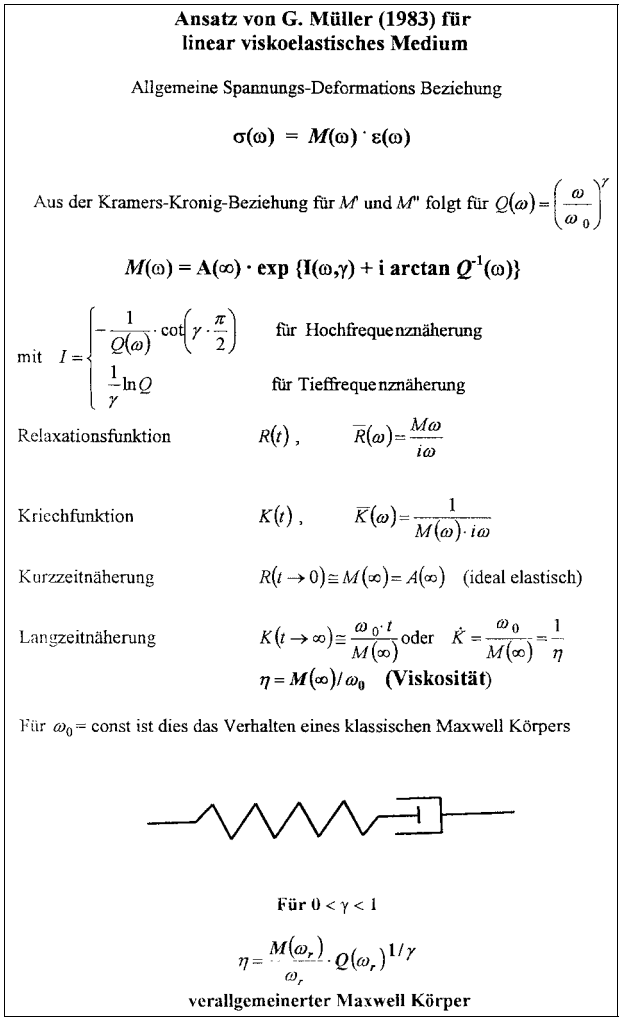

Figure 5: Approach by G. Müller (1983) for absorption in viscoelastic media.

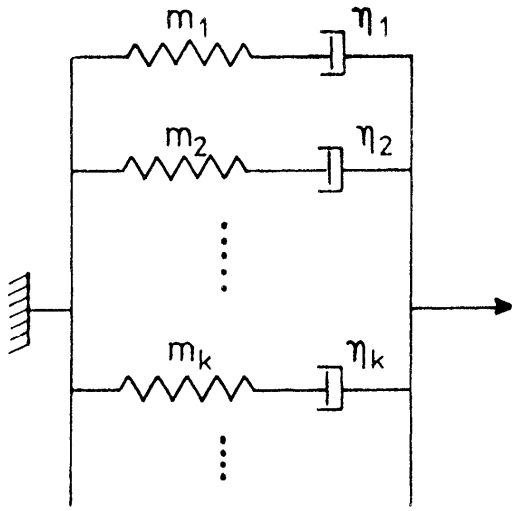

Figure 6: Rheological model of the generalized Maxwell body.

This, however, is the important link between anelastic damping and creep processes, including stationary creep. Müller showed that this could not longer be described by a single Maxwell body but by a spectral distribution of Maxwell bodies, a so-called generalized Maxwell body, for which the viscosity depends strongly on frequency. It may be visualized by a set of parallel Maxwell elements with different parameters (Fig. 6).

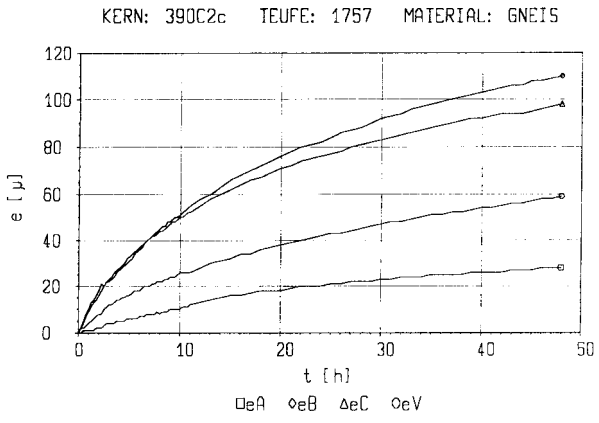

Figure 7: Strain retardation measurements (in different directions) at Gneiss – KTB deep drill core as an example for Primary Creep.

The relation of Q and the viscosity is of primary importance, because Q in the Earth is a measurable quantity while, except for postglacial rebound, experimental observation of the flow viscosity in the Earth mantle is hardly be possible. The attempt to link Q and η has, on a purely empirical basis, already been made by D. Anderson in 1966 who got $\eta / Q = 4 \times 10^{18}$ Pas. Müller has given a theoretically founded relation, although under the condition that both processes are physically similar, which has to be proved.

So far we have only considered damping of seismic waves and stationary flow. But what is in between them? First let us look at an experimental case. At room temperature we have measured the strain retardation at freshly recovered KTB drill cores (Fig. 7). The elastic stress has already been released in the drill hole during overcoring. The time dependent strain retardation we see on Fig. 7 is called Primary Creep or Transient Creep. How does this look like in Müller's theory of generalized Maxwell bodies? He had the stress relaxation and the postglacial uplift of Canada and Fennoscandia in mind (Müller, 1986a). In principal the relaxation process can be expressed by the relaxation spectrum r(ώ) of the generalized Maxwell body (Fig. 8).

Verallgemeinerte Maxwell Rheologie und die postglaziale Anhebung von Kanada und Fennoskandien, G.Müller 1986

Relaxationsfunktion

$$\mathbf{R(t) = H(t)\cdot\int_{\sigma}^{\infty} r(\acute{\omega})\cdot \exp(-\acute{\omega}t)\cdot d\acute{\omega}}$$

r(ώ)= Relaxationsspektrum für **Verallgemeinerten Maxwellkörper CMB** mit Verteilung von Federkonstanten, Viskositäten, Modellparameter, Relaxationsfrequenzen ώ oder Relaxationszeiten $\tau = 1/\acute{\omega}$

3 Modelltypen:

I CMB-Spektrum mit variablem Modellparameter

II CMB-Spektrum definiert durch Q-Spektum

III CMB-Spektrum definiert mit allgemeiner Spannungs-Deformations Beziehung

Figure 8: Generalized Maxwell rheology (Müller, 1986a).

All these models are uniquely determined by only 3 parameters. Müller has studied 3 classes of models for r(ώ). All of these models are uniquely determined by 3 parameters. Here we will consider only his type II, which is closest to our definition of the frequency dependence of Q. The relaxation function corresponds (Fig. 9) to Primary Creep and has also large similarity with the experiment. If one

considers the postglacial land uplift as process of Primary Creep even details (dots) in the melting history of the ice can well be described by the theory, if for the viscosity $\eta = 10^{23}$ Pas is taken. The agreement is best for m = 4, equivalent to $\gamma = 0.25$. The viscosity values used in the models, however, are 1 to 2 orders of magnitude higher than those obtained by interpretation of stationary, linear creep. Müller considers this as one of the major results of his approach. If we extrapolate with Müller from some thousands of years to 100 to 300 million of years, which means to convection in the Earth's mantle and to plate tectonics, this would change the viscosity only little.

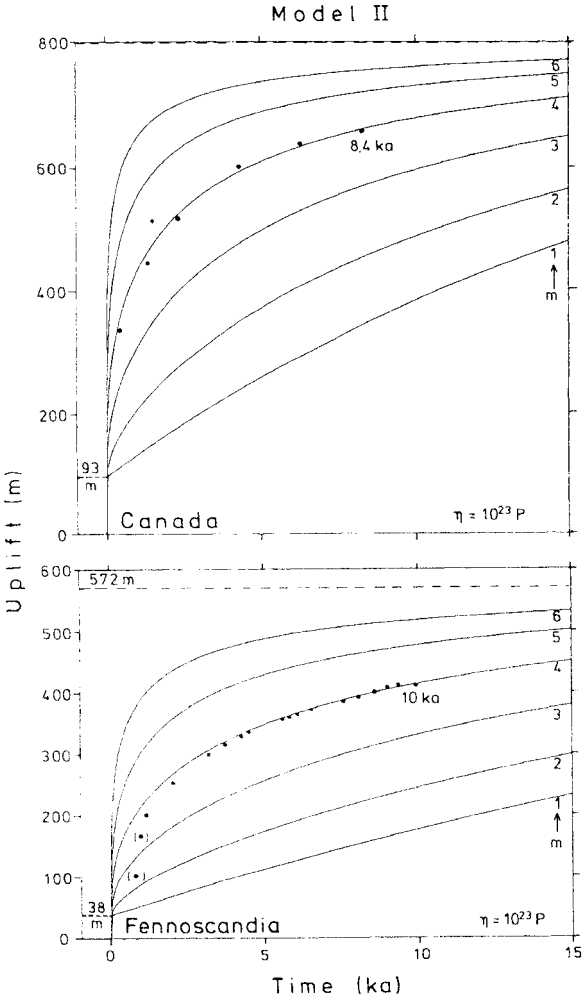

Figure 9: Theoretical curves for Primary Creep and observed isostatic uplift (dots) at Canada and Fennoscandia for $\eta = 10^{23}$ P and different exponents m = $1/\gamma$ for the frequency dependence of Q.

The question is whether the assumption of linear viscoelasticity is realistic. In Dorn's general creep equation this would need a stress exponent of n = 1 (diffusion creep). Whether diffusion creep or power-law creep with n = 3 – 4 prevails depends on temperature, deviatoric stress σ and grain size. This shows the Ashby- diagram (Fig. 10) for polycrystalline olivine of 0.1 mm grain size. The temperature may be between 0.5 and 0.8 of the melting temperature. Except for active zones like Hot Spots the shear stress may be very small, perhaps 0.1 – 5 MPa. So we are just in the boundary zone between linear diffusion creep and power law dislocation creep. In a recent review paper Karato & Wu (1993) stated that the flow laws in the mantle are still not yet assured and that the mantle is in transition between linear and power law creep. We may draw the conclusion that the assumption of linear creep may not be unrealistic. But we have to keep in mind that at the large variety of possible rheological microprocesses the description by a single law would be a courageous attempt.

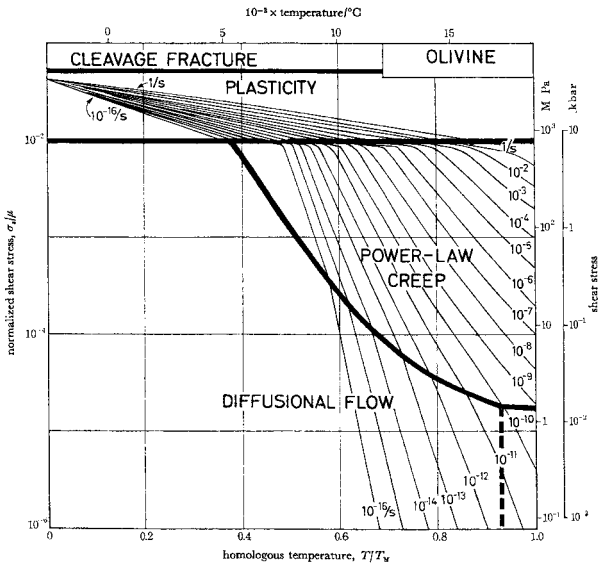

Stationäres, sekundäres Kriechen

$$\dot{\varepsilon} = C_0 \cdot \tau^n \cdot \exp(-E_C / RT)$$

Dorn Gleichung

C_0 = Vorfaktor=f (Material, Korngröße usw.)
E_C = Aktivierungsenergie für Fehlstellendiffusion
n = 1 Diffusionskriechen (Newton'sches Fließen)
1< n < 4 Versetzungskriechen, Potenz-Gesetz-Kriechen

Figure 10: Ashby-diagram for high temperature stationary creep of polycrystalline olivine of 0.1 mm grain size.

Certainly Gerhard Müller, as a critical scientist, has not expected that the total rheology of the Earth mantle can be described by a single process, but probably felt satisfaction that in nature so many things can be formulated mathematically according to a few rules.

References

Berckhemer, H., W. Kampfmann, E. Aulbach & H. Schmeling, 1982. Shear modulus and Q of forsterite and dunite near partial melting from forced-oscillation experiments. Phys. Earth Planet. Inter. **29**, 30-41.

Karato, S. & P. Wu, 1993. Rheology of the Upper Mantle: A Synthesis. Science **260**, 771-778.

Lindenfeld, M. & H. Berckhemer, 1995. Seismic energies of earthquakes and relationships to other source parameters. Tectonophyiscs **248**, 171-184.

Ulug, A. & H. Berckhemer, 1984. Frequency dependence of Q for seismic body waves in the Earth's mantle. J. Geophys. **56**, 9-19.

Core Studies: A Brief Retrospective of Gerhard Müller's Work

Annie Souriau, Observatoire Midi-Pyrénées, Toulouse

A brief retrospective of Gerhard Müller's work about the structure and physics of the core is presented. This work concerns mostly seismology, in particular studies based on the comparison of long period body wave records with theoretical seismograms obtained using the reflectivity method. Theoretical studies on the propagation of core phases have also been performed, as well as studies concerning the energy budget related to inner core crystallization.

Introduction

At the beginning of the seventies, the structure of the liquid core and solid inner core had been investigated mostly from the travel times and amplitudes of short period core phases. Several P-velocity models had been proposed, which correctly fit the travel times of the PKP phases (P-waves refracted inside the core), as well as the general trend of the amplitude variations observed along the different branches (Bolt, 1964; Engdahl, 1968; Hales & Roberts, 1971; Buchbinder, 1971; Qamar, 1973). The liquid core and inner core radii had been determined with a rather good accuracy from the travel times of the waves reflected at these interfaces, PcP and PKiKP. An estimate of the density jump at the inner core boundary had been obtained from the amplitude ratio of PKiKP/PcP at vertical incidence (Bolt, 1972). On the other hand, the eigenmodes had given a global picture of the core, and provided the strongest argument in favour of the rigidity of the inner core (*e.g.*, Gilbert & Dziewonski, 1975).

However, many problems remained unanswered, for example: Is the liquid core a perfect liquid (*i.e.*, with null rigidity)? Is it, or not, stratified? Is it possible to observe topography at the core-mantle boundary? What is the velocity profile inside the inner core? All these questions are strongly linked to the physics of the core and to the differentiation process of the Earth, which were (and are still) poorly known. In particular, the structure near the inner core boundary could provide information on the crystallization process, and on the presence of partial melting at the top of the inner core. Also, the energy budget in relation to inner core formation and magnetic field generation was an open question.

The advances made by Gerhard Müller and his team concerning the structure of the core are based in a large part on the use of synthetic seismograms, generated with the reflectivity method (Fuchs & Müller, 1971; Müller, 1985), combined to the use of the flat Earth approximation (Müller, 1973c; 1977b). This approach makes it possible to model core phases with a good accuracy up to epicentral distances of about 160°, other methods having to be used close to the antipodes (Choy *et al.*, 1980a; 1980b). On the other hand, long period records with worldwide-distributed stations were available thanks to the "World Wide Standard Seismograph Network" (WWSSN), even so digitizing these analog records for computer use required a great effort. G. Müller based several of his studies on the modelling with synthetics of the waveforms of WWSSN records, keeping always in mind the concern of the physical significance of his results. He also made interesting contributions concerning theoretical problems related to the energy budget of the core. The following sections will attempt to give, through selected examples, an appraisal of his most important contributions to the knowledge of the Earth's core.

No First Order Discontinuity at the Base of the Liquid Core

Precursors to PKiKP, the phase reflected at the inner core boundary, are sometimes observed on short period records at epicentral distances around 120 to 136º. Bolt (1964) interpreted them as evidence of a first order discontinuity

inside the liquid core at about 450 km above the inner core boundary (ICB): waves reflected at this discontinuity would indeed arrive earlier than PKiKP. Such a discontinuity implies that the liquid core is made of at least two layers of immiscible fluids, a result which has strong implications on the chemical composition of the Earth, as well as on Earth rotation. Müller (1973b) showed that, if this discontinuity exists, it gives an additional branch to the usual PKP branches (Fig. 1), which must be detectable on long period records. The comparison of synthetics with WWSSN data shows that it is not the case (Müller, 1973b; 1975a). Thus this discontinuity is not the convenient explanation of the PKiKP precursors. Following Cleary & Haddon (1972) and Doornbos & Vlaar (1973), Müller (1973b) proposed that scatters at the base of the mantle could be responsible for the precursors.

The P- and S-Velocity Profiles and the Attenuation Beneath the Inner Core Boundary

The knowledge of the inner core structure immediately beneath the inner core boundary is essential to understand core formation, and to know its chemical and physical state. The S-velocity profile is particularly important, as it may help detecting possible partial melting at the top of the inner core. Müller (1973b) investigated this region by analysing the PKP wave at the vicinity of the D-cusp, *i.e.*, at the epicentral distance where the diffracted wave PKIKP and the reflected wave PKiKP interfere, close to 120 – 130º. This distance range is the best one to constrain the S-structure immediately below ICB. In order to check the various core models, the analysis has been extended to larger distances, up to 160 degrees.

One of the main difficulties is the trade-off between S-velocity and density at ICB, which influence in the same way the reflection coefficient of PKiKP. A density jump at ICB close to 1 g/cm^3 has been adopted, in agreement with the value obtained from the PKiKP reflection coefficient at nearly vertical incidence (Bolt, 1972).

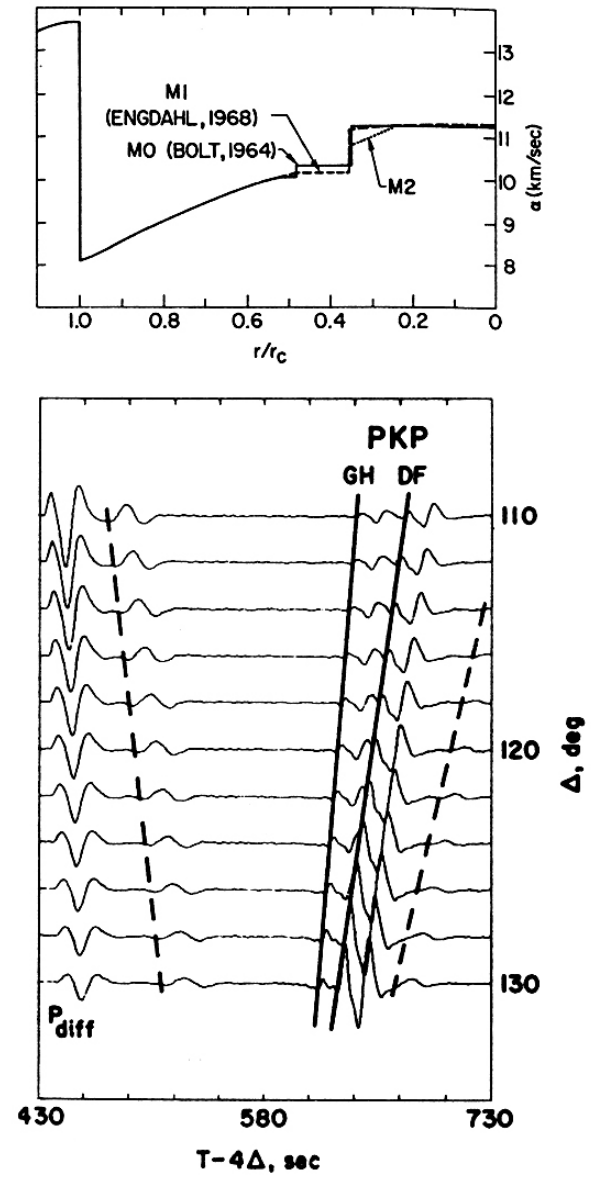

Figure 1: Test of three core models. Top: Model M0 (Bolt, 1964) exhibits a discontinuity inside the liquid core, M1 (Engdahl, 1968) is a smooth model, M2 (Müller, 1973b) is similar to M1 but with a smaller velocity gradient at the top of the inner core. Bottom: Long period synthetic seismograms for model M0: a precursor to PKP-DF is predicted, but it is not observed in the data, leading to reject the hypothesis of a discontinuity at the base of the liquid core. Dashed lines correspond to numerical artefacts (after Müller, 1973b).

Long period WWSSN records for five selected events in Indonesia, Philippine and New-Hebrides Islands have been compared to synthetic seismograms computed for various values of the inner core velocities: S-velocity below ICB ranges from 0 km/s to 5 km/s, and the P-velocity jump at ICB is either 0.6 km/s or 1 km/s. The selection of the best models is

made by comparing the amplitude-distance curves for observed and computed PKP phases (Fig. 2). Another method, based on the comparison of the PKP/P_{diff} amplitudes (where P_{diff} is the P-wave diffracted at core-mantle boundary), avoids the correction for instrumental response, but is more sensitive to the presence of heterogeneities in the D" layer at the base of the mantle.

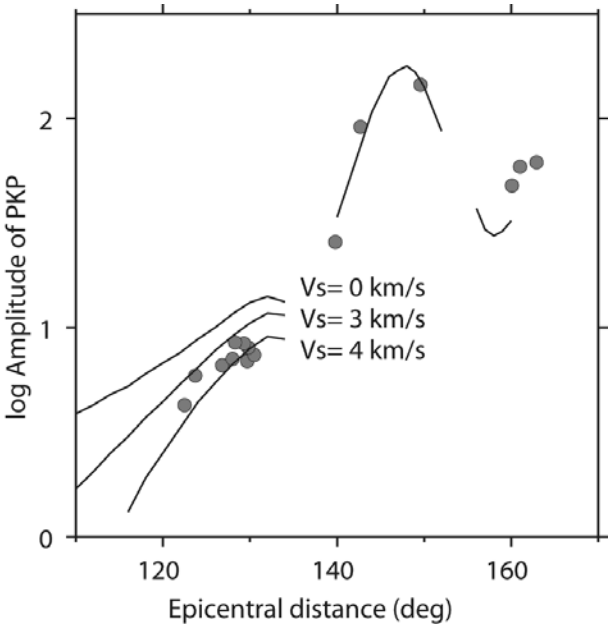

Figure 2: Determination of the S-velocity structure in the inner core. Dots: Long period PKP amplitudes observed for an Indonesian earthquake (Jan. 10, 1970). Curves: amplitudes derived from synthetic seismograms computed for a P-velocity jump at the inner core boundary of 0.6 km/s, a density jump of 1 g/cm3 and various values of the S-velocity jump. The comparison confirms the rigidity of the inner core, with an S-velocity close to 3.5 km/s (after Müller, 1973b).

The results reveal that the S-velocity below ICB is in the range 3 – 4 km/s (Fig. 2), providing a confirmation of the rigidity of the inner core from body waves observations. On the other hand, the P-velocity jump at ICB is close to 0.6 – 0.7 km/s, with a pronounced velocity gradient in the top 300 km.

In spite of the use of too a large density jump, Müller (1973b) came to a structure very close to that of model ak135 (Kennett *et al.*, 1995), which is right now the best global model for core studies. The ak135 model gives an S-velocity of 3.504 km/s below ICB and a P-velocity jump of 0.754 km/s at ICB. Only the P-velocity gradient below ICB is significantly different, but it may be poorly resolved with long period data in Müller's study.

Further investigations with a similar approach have been made later in Müller's group by Häge (1983), on the basis of an extended data set. Allowing for a larger range of ICB density jump (0 to 1.2 g/cm^3), Häge came to a P-velocity jump of 0.64 ± 0.05 km/s, and to an S-velocity of 2.5 – 3.0 km/s below ICB, with a rather steep S-velocity gradient.

On the other hand, the velocity and attenuation near the inner core boundary have been investigated by Spies (1991) from the differential travel times and amplitudes of broadband PKP(DF) and PKP(BC), for South Pacific events recorded at the Gräfenberg and NARS arrays. His study confirms the presence of a low velocity gradient at the base of the liquid core, and leads to a low P-wave quality factor (Q ~ 200) in the uppermost 200 km of the inner core, increasing to Q ~ 570 at greater depth.

The Velocity Profile in the Liquid Core

The liquid core is sampled by the three PKP phases (PKP(AB) and PKP(BC) which turn respectively in the middle and at the base of the liquid core; PKP(DF) which turns inside the inner core), but none of these phases samples the upper part of the liquid core. SKS and SKKS waves, which propagate as S waves in the mantle and as P-waves in the core, allow filling this gap. It is thus a priori interesting to use these waves to infer the velocity profile of the liquid core from CMB to ICB. In an attempt to model the SKS and SKKS waveforms of Tonga-Fiji events recorded in North America, Kind & Müller (1977) proposed a liquid core model (N20A) with a steep velocity gradient at depth ~3700 km, followed by a low gradient. This structure gives a good fit of the differential travel times and relative amplitudes of SKS and SKKS for this particular path. In addition, it shifts to large distance the interference between SKS and the $SP_{diff}KS$ / $SKP_{diff}S$ phase, a phase first discovered by Kind & Müller (1975), which has a short diffracted path as P-wave along the core mantle boundary. This small phase is however difficult to separate from SKS on

long period records (it is easily observed on broadband data, *e.g.*, Garnero *et al.*, 1998). Kind & Müller (1977) mentioned that the velocity profile they obtained, which implies a chemical stratification of the core, needed confirmation before being further interpreted. In a second study of SKS and SKKS, Schweitzer & Müller (1986) analysed a much larger data set, with worldwide-distributed paths. Their analysis revealed that smooth models as 1066B (Gilbert & Dziewonski, 1975) inferred from eigenmodes, or Hales & Roberts (1971) model deduced from body wave travel times, explained correctly both the differential travel times and amplitude ratios of SKS and SKKS, except for the path Fiji-Tonga to America, where N20A is more convenient. Because lateral heterogeneities in the liquid core are unlikely, this result suggested that deep mantle heterogeneities east of the Tonga subduction zone are the most plausible explanation for the SKS and SKKS anomalies (Schweitzer & Müller, 1986). Tomographic models confirmed this later (*e.g.*, Bijwaard *et al.*, 1998).

The Core-Mantle Boundary

Synthetic seismograms revealed to be also a very powerful tool for investigating the properties of the core-mantle boundary (CMB). An important problem was the value of the rigidity of the liquid core beneath the CMB, as a non-zero value may have important implications for the modelling of the magnetic field. Another problem was the value of the velocity gradient at the base of the mantle and the possible existence of stratification above the CMB, which had been proposed by several authors. Müller *et al.* (1977) analysed the amplitude of PcP waves, and the PcP/P amplitude ratio, for deep South American events recorded at North American long period stations. The comparison of the data with the values derived from synthetic seismograms led to reject most of the models with layering at the base of the mantle, and showed that a first order discontinuity at CMB explains correctly the data. On the other hand, the results favoured a negative velocity gradient at the base of the mantle, and a zero-rigidity at the top of the liquid core.

Later studies have shown that these results are not necessarily valid at the worldwide scale: either positive or negative velocity gradients have been found at various places in D", and the ultra-low velocity layer (ULVZ) at the base of D" also exhibits significant lateral variations (*e.g.*, Valenzuela & Wysession, 1998; Garnero *et al.*, 1998). On the other hand, a non-zero rigidity zone ("sediments") at the top of the core has been proposed to explain the shape complexity of the ScP waves reflected east of Australia (Rost & Revenaugh, 2000). However, such observations are possible only with broadband data.

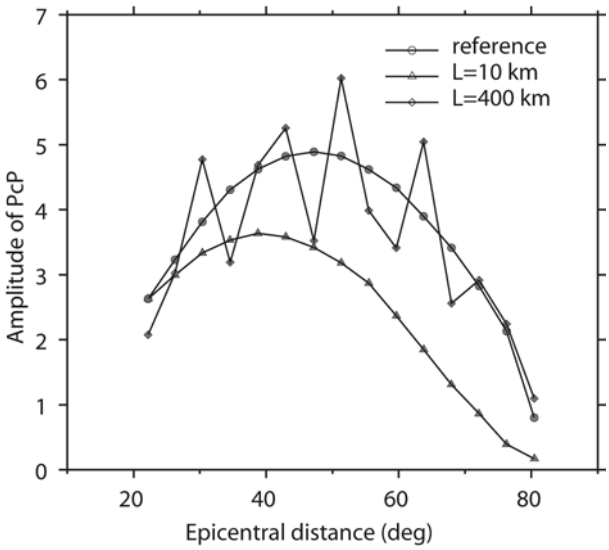

Figure 3: Theoretical values of the peak-to-peak amplitudes of PcP (in arbitrary units) as a function of distance for a 1 s period PcP pulse reflected at an undulated core-mantle boundary. Full line is for a core-mantle boundary without topography, dashed lines correspond to undulation wavelengths of 10 and 400 km with 1 km topography (after Kampfmann & Müller, 1989).

As noted by Müller *et al.* (1977), the PcP and P amplitudes for a single event exhibit similar variations as a function of distance. This suggests either that there is no significant CMB topography, or, if any, that the long period PcP waves are unable to detect it. In order to investigate if PcP is able to detect CMB topography, theoretical computations of PcP amplitudes for a CMB with sinusoidal topography have been performed using 3D Kirchoff theory (Kampfmann & Müller,

1989). Topography with wavelengths from 10 to 600 km and amplitude of 0.5 or 1 km has been considered. The results obtained for a 1s period PcP pulse reveal that there is a PcP amplitude reduction for short wavelength topography, and strong amplitude variations due to focusing and defocusing for long wavelength topography (Fig. 3). These variations may be responsible for the strong scattering observed in the PcP wave amplitudes. They also show the limitations in the use of PcP arrival times for the retrieval of the CMB topography.

The Gravitational Energy due to the Crystallization of the Inner Core

The latent heat due to iron solidification provides part of the energy necessary to maintain the geodynamo. Loper (1978) showed that the gravitational energy released by the light elements, which do not enter the inner core during crystallization, also contributes for an important part to this energy. In resolving analytically this problem, Müller & Häge (1979) showed that the densities of both light and heavy elements are sensitive parameters in the estimate of the released gravitational energy. They also estimated the gravitational energy due to the deformation of the Earth consecutive to inner core crystallization (because liquid and solid do not occupy the same volume). In the absence of chemical change at ICB, the complete solidification of the core would be associated to a 5 km decrease of the Earth's radius (Häge & Müller, 1979). It turns out that the energy released by the compression of the Earth has only a minor contribution to the global energy budget (Müller & Häge, 1979). These models assume a continuous growing of the inner core from Earth formation to present, a hypothesis which is now strongly debated (*e.g.*, Labrosse *et al.*, 2001).

Conclusion

As shown above, G. Müller and his team have made important advances concerning the structure and physics of the core. Among his main results are the demonstration of the absence of first order discontinuity (hence of chemical stratification) at the base of the liquid core, the indirect proof of the rigidity of the inner core from body waves, and the modelling of the behaviour of the waves reflected at an undulated core-mantle boundary.

The use of synthetic seismograms for modelling core phases contributes certainly to the originality of his work. But this would be of no use without a great interest in the data and a great perspicacity in the observation of the seismograms. The ability to go from the theory to the observation, and reciprocally, is undoubtedly an approach that not all scientists are able to do. It is a permanent source of new questions and new ideas, and a wonderful approach for teaching science, a domain where Gerhard Müller was also an outstanding personality.

References

Bijwaard, H., W. Spakman & E. R. Engdahl, 1998. Closing the gap between regional and global travel time tomography. J. Geophys. Res. **103**, 30 055-30 078.

Bolt, B. A., 1964. The velocity of seismic waves near the Earth's center. Bull. Seism. Soc. Am. **54**, 191-208.

Bolt, B. A., 1972. The density distribution near the base of the mantle and near the Earth's center. Phys. Earth Planet. Inter. **5**, 301-311.

Buchbinder, G. G. R., 1971. A velocity structure of the Earth's core. Bull. Seism. Soc. Am. **61**, 429-456.

Cleary, J. R. & R. A. W. Haddon, 1972. Seismic wave scattering near the core-mantle boundary: a new interpretation of precursors to PKP. Nature **240**, 549-551.

Doornbos, D. J. & N. J. Vlaar, 1973. Regions of seismic wave scattering in the Earth's mantle and precursors to PKP. Nature Phys. Sc. **243**, 58-61.

Engdahl, E. R., 1968. Core phases and the Earth's core, Ph. D. Thesis, St. Louis Univ., 197 pp.

Garnero, E. J., J. Revenaugh, Q., Williams, T. Lay & L. H. Kellog, 1998. Ultra-low velocity zone at the core-mantle boundary. In: Gurnis *et al.* (editors). The core-mantle boundary region, Am. Geophys. Un., ISBN 0-87590-530-7, 319-334.

Gilbert, J. F. & A. M. Dziewonski, 1975. An application of normal mode theory to the retrieval of structural parameters and source mechanisms from seismic spectra. Phil. Trans. R. Soc. Lond. **A 278,** 187.

Häge, H., 1983. Velocity constraints for the inner core inferred from long period PKP amplitudes, Phys. Earth Planet. Inter. **31**, 171-185.

Hales, A. L. & J. L. Roberts, 1971. The velocities in the outer core. Bull. Seism. Soc. Am. **61**, 1051-1059.

Kennett, B. L. N., E. R. Engdahl & R. Buland, 1995. Constraints on seismic velocities in the Earth from traveltimes. Geophys. J. Int. **122**, 108-124.

Labrosse, S., J.-P. Poirier & J.-L. Le Mouël, 2001. The age of the inner core. Earth Planet. Sci. Lett. **190**, 111-123.

Loper, D. E., 1978. The gravitationally powered dynamo. Geophys. J. R. astr. Soc. **54**, 389-404.

Qamar, A., 1973. Revised velocities in the Earth's core. Bull. Seism. Soc. Am. **63**, 1063-1105.

Rost, S. & J. Revenaugh, 2000. Seismic detection of rigid zones at the top of the core. Science **294**, 1911-1914.

Spies, T., 1991. Untersuchung der Struktur in der Nähe der Grenze zum inneren Kern mit PKP-Phasen. Dissertation, Universität Frankfurt, 150 pp.

Valenzuela, R. W. & M. E. Wysession, 1998. Illuminating the base of the mantle with diffracted waves. In: Gurnis *et al.* (editors). The core-mantle boundary region, Am. Geophys. Un., ISBN 0-87590-530-7, 57-72.

On Seismic Sources Volume Changes

Paul G. Richards, Columbia University, USA

Abstract

The seismic waves generated by an underground explosion can be modeled simply in terms of a point source with isotropic moment, and also by a source region that increases its volume. Müller (2001a) noted that two different formulas have been published, relating volume change to the isotropic moment, and he indicated that one of them must be incorrect. Here, it is shown that both formulas are correct. They are based on two different definitions of the equivalent volume change.

Introduction

Gerhard Müller is most well known internationally for his contributions to the reflectivity method and its applications to study Earth structure. He is also well known for an important contribution to theoretical seismology, concerning seismic sources with volume changes. During 2000 – 2001, he and I corresponded several times on this subject, and almost thirty years earlier we discussed source theory when he was a visiting scientist in the United States. In Müller (1973a) he described an elegant formula relating the isotropic moment of an explosive point source to an equivalent volume change. But then, over a twenty-five year period, a textbook (Aki & Richards, 1980) and several papers (*e.g.*, Bowers & Hudson, 1999) appeared, that seemed to give a different formula for the equivalent volume change. Müller (2001a) pointed out these differences, but did not resolve them.

Because of our correspondence, I discussed the issue in the second edition of the textbook (Aki & Richards, 2002, see Problem 3.8). In this note, I comment directly on the reason for two different formulae relating an isotropic moment to an equivalent volume change, showing that both formulae are correct. The apparent discrepancy is due to use of different definitions for the equivalent volume change.

Theoretical Framework

Seismic waves from earthquakes and explosions are initiated in the source region by a variety of phenomena, usually entailing large and suddenly changing values of stress that in general may lead to changes of state, and that are not linearly related to strain. For example, in an earthquake source region, rocks fracture and may melt. In an explosion, rocks can even be vaporized. But outside the source region it is found in practice that seismic waves propagate with small changes in stress that are easily related to small changes in strain, and the equations of linear elasticity prevail.

We may separate the two regions by specifying a source volume V, inside which there is non-linear behaviour, and outside which the waves propagate linearly. It is common practice to characterize the actual seismic source by the parameters of an equivalent seismic source that, using linear theory, generates exactly the same seismic waves in the region outside V, as the actual seismic source.

Müller's Approach in 1973

Specializing to the simple case of an explosion within an infinite homogeneous isotropic medium, specified by its mass density ρ, and Lamé moduli λ and μ, Müller (1973a) modeled the source region by a spherical volume whose radius is increased to a new value. In this note, I use V for the source volume. Initially it has radius a, increasing to a value $a + \delta a$ as a result of the explosion. The volume increase of this seismic source is therefore given by $\delta V = 4\pi a^2 \delta a$, or $\delta V = S_1 \delta a$, where S_1 can be thought of as the area of the source, which has been displaced through the distance δa.

The radius a is sufficiently large, that all the non-linear complications of processes at the source are confined to radii less than a. However, in practice for an explosion, a can still be small enough that it is much less than the wavelengths of the P-waves radiated into the far field. Such P-waves therefore can be regarded as emanating from a point source, and the question is how best to characterize such an equivalent point source.

Calculating the radiated P-wave outside V is a simple application of scalar potentials, since by symmetry no S-waves are generated. Thus, the displacement is $\mathbf{u} = \nabla\phi$ where ϕ satisfies a scalar wave equation with speed α, and $\alpha^2 = [(\lambda + 2\mu) / \rho]$. Here, $\phi = \phi(r, t)$ where r is the radius in a coordinate system of spherical polars such that the original surface of V is $r = a$. In general, ϕ is an outgoing spherically symmetric solution to $(1 / \alpha^2)(\partial^2\phi / \partial t^2) = \nabla^2\phi$, and so $\phi = -[F(t - r/\alpha)] / r$ for some function F, called the reduced displacement potential. It follows that the radial displacement is given exactly for this idealized problem by

$$u_r = \partial\phi/\partial r = [\dot{F}(t - r/\alpha)] / (\alpha r) + [F(t - r/\alpha)] / r^2 \qquad (1)$$

The first term dominates in the far field (when r is large), and the second term dominates in the near field (when r is small, for example at $r = a$).

Since $u_r = \delta a$ when $r = a$, for sufficiently long times that the final increase in radius has been attained, it follows from use of the last term in eq. (1) that $F(\infty) = a^2\delta a$. But the first term of the right-hand side of eq. (1) allows us to relate F to the strength M_1 of three mutually perpendicular dipoles. Several authors (including Love, 1944) have shown that the far field displacement for such a source is

$$u_r = [\dot{M}_1(t - r/\alpha)] / (4\pi\rho\alpha^3 r).$$

(Note that we can also express such an isotropic source by a second order moment tensor $\mathbf{M}$ with components $M_{pq}(t)$ given in terms of the Kronecker delta by $M_1(t)\,\delta_{pq}$.) The relationship between F and M_1 must therefore be

$$M_1(t) = 4\pi\rho\alpha^2 F(t).$$

These theoretical results have all been known for several decades, but Müller (1973a) was the first to put them all together to obtain (in the notation used here)

$$M_1(\infty) = (\lambda + 2\mu)\, S_1 \delta\alpha = (\lambda + 2\mu)\, \delta V. \qquad (2)$$

The first equality in eq. (2), is reminiscent of the relationship $M_0(\infty) = \mu S_0 D$ between the scalar moment M_0 of an earthquake, equal to the product of rigidity (μ), fault area (S_0), and average fault slip (D). Whereas earthquakes principally radiate S-waves (whose velocity is related to μ), explosions radiate P-waves (whose velocity is related to the combination of elastic moduli $\lambda + 2\mu$ appearing in the above equation for M_1). Müller's 1973 result is therefore an elegant extension to explosion sources, of general concepts long associated with earthquake sources.

The second relationship in eq. (2), indicates that the important physical attribute determining the strength of seismic signals from an explosion point source is the volume increase δV. Several authors have noted that this increase is an invariant of the source we have chosen to characterize in terms of an expansion from radius a to a value $a + \delta a$, because it is the combination $F(\infty) = \alpha^2\delta a$ which determines the long wavelength strength of the seismic signal. (If a is increased, then δa must decrease in such a way that the combination $a^2\delta a$ stays the same — but this means that the volume increase δV stays the same.) Note that whatever radius a is chosen, the radius increase δa and volume increase δV represent actual increases of the radius and the volume used to characterize the source.

The Approach of Aki & Richards (1980), Based on Eshelby (1957)

In contrast to Müller's (1973a) approach, the work of Eshelby (1957) described a series of thought experiments, which include (in the case of explosions) a conceptual volume increase. Aki & Richards (1980) described these thought experiments for a general volume source. Figs. 1, 2, and 3, in this note, describe them for a spherical source region that undergoes an expansion.

Thus, Fig. 1 shows the source in its original state, and the first thought experiment, in which the source material is removed from its matrix. Tractions are applied, on both the internal surface Σ^+(the hole), and the external surface Σ^- of the sphere that has been removed (the source material), in order to maintain their shapes.

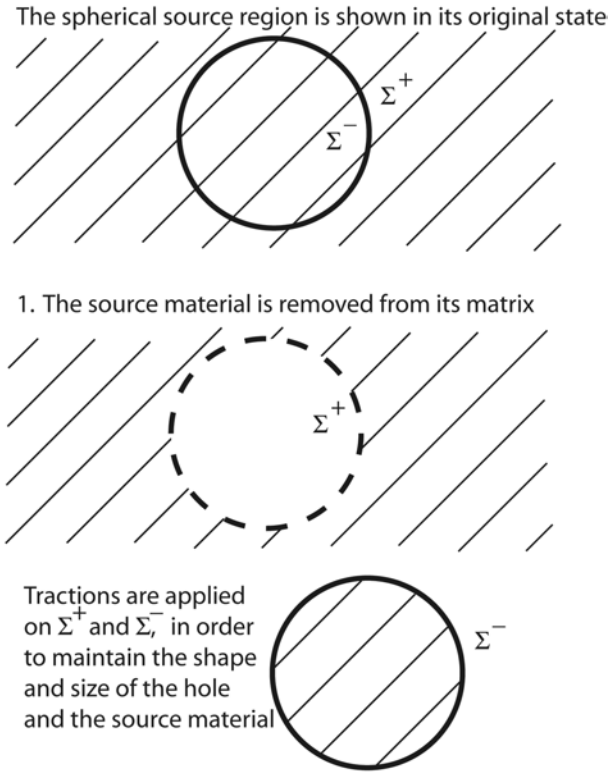

Figure 1: A spherical source region is shown in its original state, and as the result of the first of a series of thought experiments due to Eshelby (1957).

Fig. 2 shows the second and third thought experiments. In the second experiment, the source material undergoes a transformation, which does not change its stress. This is accomplished by a strain field Δe_{rs} called the stress-free strain, or the transformational strain. We use the symbol ΔV for the resulting change in the whole volume (originally V, and now $V + \Delta V$). In the present case of an isotropic expansion, $\Delta e_{rs} = (1/3)\,(\Delta V / V)\,\delta_{rs}$. The third thought experiment is to apply an additional stress field throughout the transformed volume, generated by tractions on its surface Σ^-, to return it to its original shape. A detailed examination for the spherical case we are considering, shows that to accomplish this third experiment we merely need to apply a pressure, given by $(\lambda + (2 / 3)\,\mu)\,(\Delta V / V)$, to Σ^-.

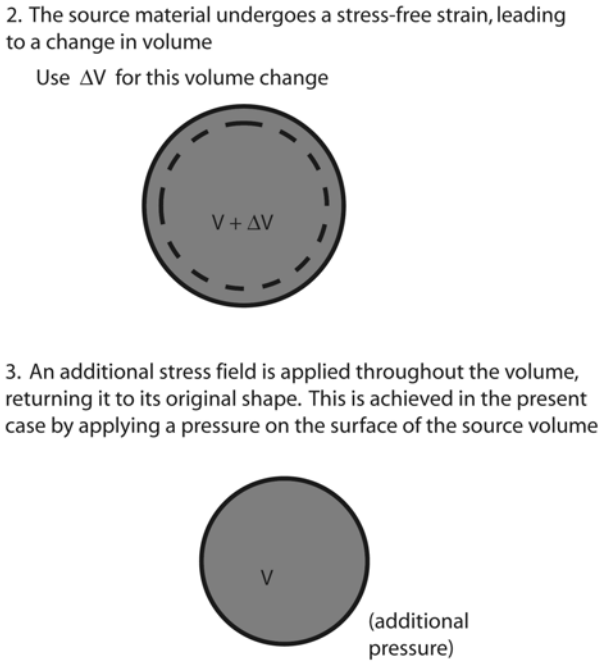

Figure 2: The second and third thought experiments are shown. The volume increase denoted as ΔV is a transformational or stress-free strain.

Fig. 3 shows the final pair of experiments. Thus, in thought experiment number four, we put the spherical source region back into its hole (noting that it has the correct shape to enable it to fit exactly), and we weld it in place so that there can be no sliding across its surface, and no development of any cavities. At this point there is still an extra traction on the surface Σ^- of the source region so that there is a traction difference between Σ^+ and Σ^-. In thought experiment number five, we

release the applied traction over Σ^-. This is equivalent to imposing a traction discontinuity across the welded interface. As a result, the source region changes it size. We denote its new volume by $V + \delta V$. Then δV is the actual volume change of Müller (1973a).

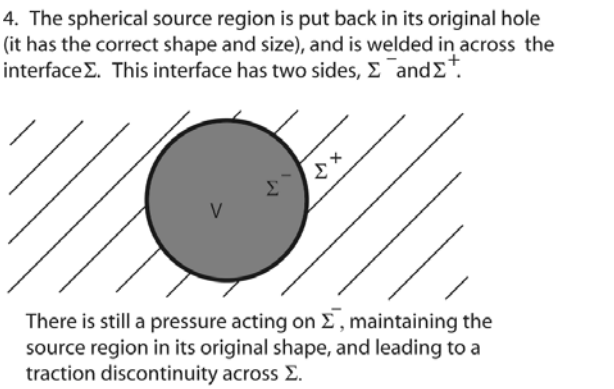

Figure 3: The fourth and fifth thought experiments are shown. δV differs from ΔV.

In effect, we can regard the volume change ΔV specified in the second thought experiment as an unconfined volume change. In the case of an explosion, ΔV will be larger than the volume change δV specified in the fifth thought experiment. The latter change, which is the actual (final) volume change, is a result of taking into account the confining effects of the surrounding medium.

Discussion

Aki & Richards (1980) showed that in terms of the stress-free volume change ΔV of Fig. 2, the isotropic moment is given by

$$M_1(\infty) = [\lambda + (2 / 3)\, \mu]\, \Delta V. \qquad (3)$$

Müller (2001a) pointed out the two different relationships, here given as eq. (2) and eq. (3), between the isotopic moment of an explosion source, and an associated volume change. But he appears to have regarded these volume changes as being the same. He wrote that "the discrepancy ... is not resolved", and thus whether eq. (2) or eq. (3) is correct, is left as a question. He noted that the derivation of eq. (2) is simpler, and that he "was unable to find the weak point in the more complicated derivation" of the alternative equation [given here by eq. (3)]. A purpose of this note is to point out that there is no discrepancy once it is realized that the two volume changes, denoted here as δV and ΔV, have different definitions. The relationships eq. (2) and eq. (3) are both valid. This point is discussed further in Aki & Richards (2002, Problem 3.8).

Several papers have chosen to summarize explosion source strength in terms of a volume change at the source. For example, Bowers & Hudson, 1999; and Dreger *et al.*, 2000. Both these papers use eq. (3) rather than eq. (2) to go from isotropic moment to volume change. Because there are two different definitions of volume change, it is important to specify which is being used.

There is still a question as to which of the two volume increases, δV or ΔV, has greater merit as a device to characterize the size of an explosive source. It would seem appropriate to make the choice, based on which of the two definitions helps us more, to build up our intuition concerning the way in which explosions generate seismic signals. In this regard, we may note that if we have a series of explosions of the same charge size (or yield), and they are set off at different depths, then for the shallower explosions there will be a smaller overburden. Therefore we can expect that the resulting "actual" volume change, δV, of the non-linear source region will be greater for the shallower explosions, because it is less confined than for deep explosions. And hence the shallower explosions will result in stronger seismic signals. (We are assuming that all explosions in the series are tamped and well-confined.)

Extensive theory and a number of observations have shown that this expectation is correct: shallower explosions generate stronger signals than deep explosions of the same charge size.

(See, for example, Mueller & Murphy, 1971.) In this case, it is intuitively clear that δV is greater for the shallower explosions. It follows that the stress-free volume change, ΔV, is also greater for the shallower explosions. However, this last conclusion, which follows from the proportionality between δV and ΔV, is not directly obvious, at least to the present author, who therefore concludes that for practical purposes the better choice of volume change is that suggested by Müller (1973a), namely, δV.

Acknowledgement

I greatly appreciate the opportunities I had from 1971 to 2001 to discuss the subject matter of this paper, and many other issues, with Prof. Gerhard Müller.
This note is Lamont-Doherty Earth Observatory contribution number 6546.

References

Aki, K. & P. G. Richards, 1980. Quantitative Seismology – Theory and Methods, volume 1, W. H. Freeman and Co., San Francisco, ISBN 0-7167-1058-7, xiv+556+16 pp.

Aki, K. & P. G. Richards, 2002, Quantitative Seismology – Theory and Methods, 2nd edition, University Science Books, Sausalito, California, ISBN 0-935702-96-2, xviii+700 pp.

Bowers, D. & J. A. Hudson, 1999, Defining the scalar moment of a seismic source with a general moment tensor. Bull. Seism. Soc. Amer. **89**, 1390-1394.

Dreger, D. S., H. Tkalčić & M. Johnston, 2000. Dilatational processes accompanying earthquakes in the Long Valley Caldera. Science, **228**, 122-125.

Eshelby, J. D., 1957. The determination of the elastic field of an ellipsoidal inclusion, and related problems, Proc. Roy. Soc. Lond. **A 241**, 376-396.

Love, A. E. H., 1944. A Treatise on the Mathematical Theory of Elasticity. 4th edition, Dover Publications, New York, xviii+643 pp.

Mueller, R. A. & J. R. Murphy, 1971. Seismic characteristics of underground nuclear detonations. Part I. Seismic spectrum scaling. Bull. Seism. Soc. Amer. **61**, 1675-1692.

Complex Earthquakes: Multiple Shock Events Reveal Rupture Propagation, Size and Duration of the Source Process

Wolfgang Brüstle, Freiburg

Abstract

From 1977 to 1985, the working group of Gerhard Müller at Karlsruhe and Frankfurt/Main universities investigated earthquake source processes resolving the spatio-temporal extent of "complex earthquakes". On the basis of long-period WWSSN and some broadband seismograms available at that time we considered the following complexities reflecting both kinematical and dynamical features of rupture:

- Ruptured area: curved fault planes, separated and eventually rotated subfaults, en-echelon-fashion faulting.
- Propagation of rupture: abrupt changes in rupture velocity – for example a sudden termination of rupture expansion.
- Dislocation of rock: rugged dislocation time function, reverse slip (overshooting), strong spatial variations in final dislocation, changes of slip direction etc.
- Source mechanism: *i.e.*, any deviation from pure shear dislocation.

We examined P-wave seismograms and true ground displacements to find prominent directivity effects of rupture propagation (for example Fig. 1) and multiple shock appearances. Among others the middle-deep to deep earthquakes in Peru-Bolivia (August 15, 1963), Romania (March 4, 1977), Kurile Islands (December 6, 1978), and Mexico (October 24, 1980) were investigated. Double-couple fault plane solutions of individual source shocks and their relative localization using the master-event technique yielded fix points of rupture history. The most striking feature frequently observed was found to be a stopping phase. We interpreted the stopping phase kinematically by abrupt termination of rupture expansion at one end of the fault. The stopping phase eventually was the key to determine total source extent in space and time, as well as mean rupture velocity. Subsequently we modelled the entire rupture process according to the dislocation theory of shear faulting. A kinematical source description proved to be well adapted to source and data characteristics. Wave propagation through the earth's mantle was treated by simple ray theory as well as by the reflectivity method. The forward modelling approach moreover yielded reliable values of seismic moment, source dimensions, mean dislocation and stress drop. Source complexities were related to unbroken fault gaps, bending of the fault plane, acceleration of rupture propagation in asperities, and, most impressive in its radiation effect, to the sudden termination of rupture in front of a barrier. All these complexities were discussed with respect to tectonic implications (for an example see Fig. 2).

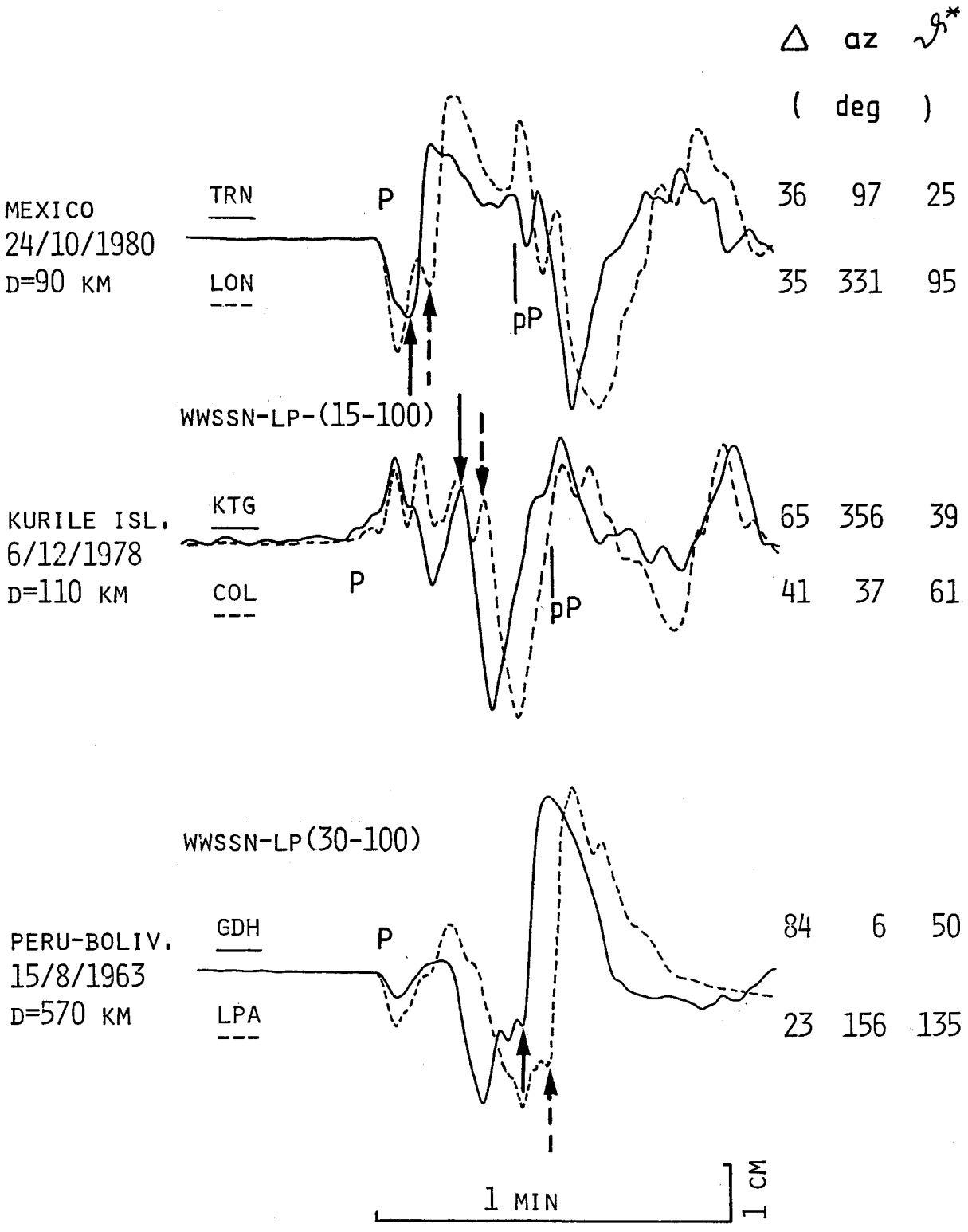

Figure 1: Rupture directivity causes different durations of P wave seismograms as demonstrated for three selected events. Arrows point to stopping phases present in these seismograms, each time at two stations with different take off angles ϑ* (angle between predominant rupture direction and ray direction). Δ is epicentral distance, az is station azimuth, D is hypocentral depth.

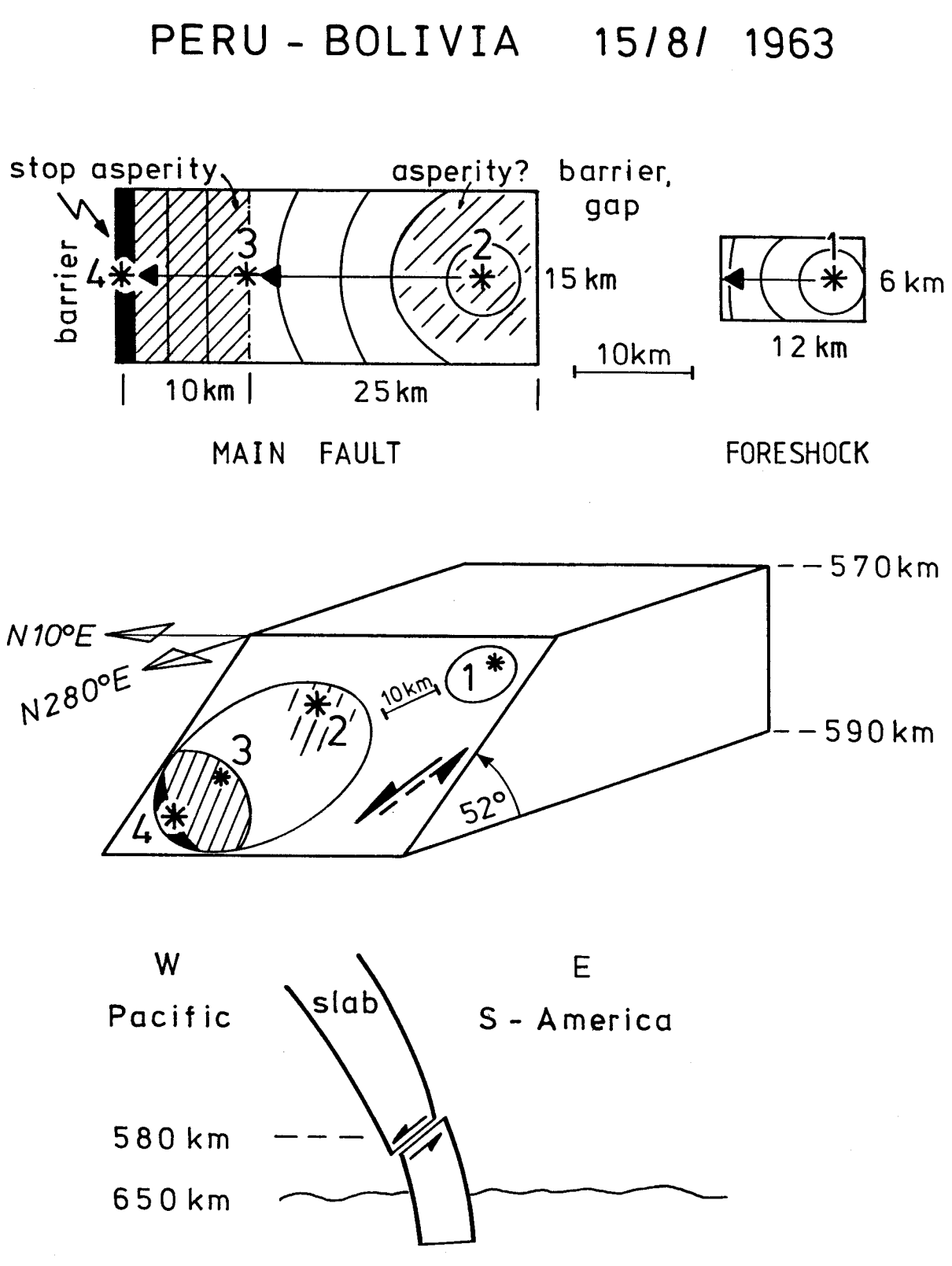

Figure 2: Favoured source history for the example of the Peru-Bolivia event of August 15, 1963. Top: Star symbols denote positions of shocks 1, 2, 3 and 4 due to foreshock, start of main event, rupture acceleration, and sudden stop of rupture propagation respectively. Arrows show predominant rupture direction into 340° azimuth and 20° down dip. Middle: Sketch in 3D view. Arrows show slip direction. Bottom: Illustration of source mechanism within the subducted plate and possible connection to resistance against slab subduction at a mantle discontinuity in 650 km depth.

Fifth-Force Experiments in Retrospect and Newton's Big G

Walter Zürn, Schiltach

Introduction

Gerhard Müller suggested to meet for lunch during the 1986 ESC / EGS meeting in Kiel. On this occasion he brought up the problem of the fifth force and suggested to test this conjecture in an experiment. Stacey had claimed to see evidence for a range dependence of Big G when he measured gravity down a mineshaft and predicted gravity did not agree with the observations. Both of us did not believe that Stacey's knowledge of density in the rocks around a mineshaft was good enough to claim new physics. Gerhard had already contemplated measuring the gravity effect of large water masses in the pumped storage reservoir at Vianden, Luxembourg. For several good reasons we decided to do it in the Southern Black Forest at the Hornberg reservoir. When we approached the responsible engineer there, he immediately asked if our measurements have to do with this fifth force, which he had read about in the newspapers. From here on it was pure fun; both for Gerhard and myself, we both felt that we worked on something fundamental in physics. After the experiment Gerhard concentrated on the data analysis and soon we were ready to publish. In this phase I could more than ever see his energy, perseverance and his strive for publishable results, and was again impressed.

Background

The Standard Model of the theory of elementary particles involves four basic interactions: the electromagnetic force, the weak force, the strong interaction and gravitation. The corresponding mediating particles (the forces are exerted by exchanging virtual particles) are the photon, the W- and Z-bosons, the gluons and the gravitons. The weak force controls radioactive decay and the strong force holds the nuclei and quarks together. The larger the mass of the exchange particles the smaller the range of the force, so since photons have zero mass, the electromagnetic force has infinite range.
Theoretical physicists would like to unite all four interactions into a single one and they were successful with the first two (the electroweak force), and quite confident with the third one (quantum chromodynamics), but gravitation so far defies these attempts. Some supersymmetric and string theories, trying to achieve such a unification, predict new forces (or particles) with macroscopic ranges (Franklin, 1993) and therefore two kinds of experimental results were making headlines: the reanalysis of the classic Eötvös experiment and the measurement of gravity down a mineshaft (*e.g.*, Fischbach & Talmadge, 1999). The first indicated a weak material dependence of big G, the second a range dependence of gravity or deviation from the inverse-square law, both possibly expressions of an additional interaction, a fifth force. One possibility to describe a range-dependent interaction with finite range (or finite mass of the mediating particle) is the Yukawa-Potential; so the gravitational potential would be modified as follows:

$$W(r) = G \cdot \frac{M_1 \cdot M_2}{r} \cdot \left[1 + \alpha \cdot e^{-\frac{r}{\lambda}} \right]$$

where r is mass separation distance, G the gravitational constant at infinity, M_1 and M_2 the interacting masses, α the relative strength and λ the range of the fifth force. Fig. 1 shows two curves of this type in terms of an apparent gravitational constant.
The first experiments around the beginning of the 1980s were followed by a flurry of activity among physicists, geophysicists and geodesists. Tests for the existence of deviations from Newtonian gravity fall basically into four categories: composition-dependent experiments and tests of the

inverse-square law, both either with terrestrial or laboratory/controlled sources.

The Hornberg Hydroelectric Lake Experiment

The experiment and its results are described in Müller *et al.* (1989, 1990). This reservoir, completely artificial, looks like a track-and-field stadium with a length of almost 700 m and a width of 265 m. We recorded for 22 days continuously the water level in the lake, gravity variations with six LaCoste-Romberg field gravimeters at two positions above and below the water level in a tower inside the lake and barometric pressure variations, all digitally with a sampling rate of 1 / minute. Proper analog antialias-filtering was necessary because of the clear gravity signal from the seiches excited by hydroelectric activities and wind. Daily variations of the water level were between 5 and 22 m. The gravimeters were calibrated immediately before and after the experiment on the vertical calibration line at the Institut für Erdmessung in Hannover.

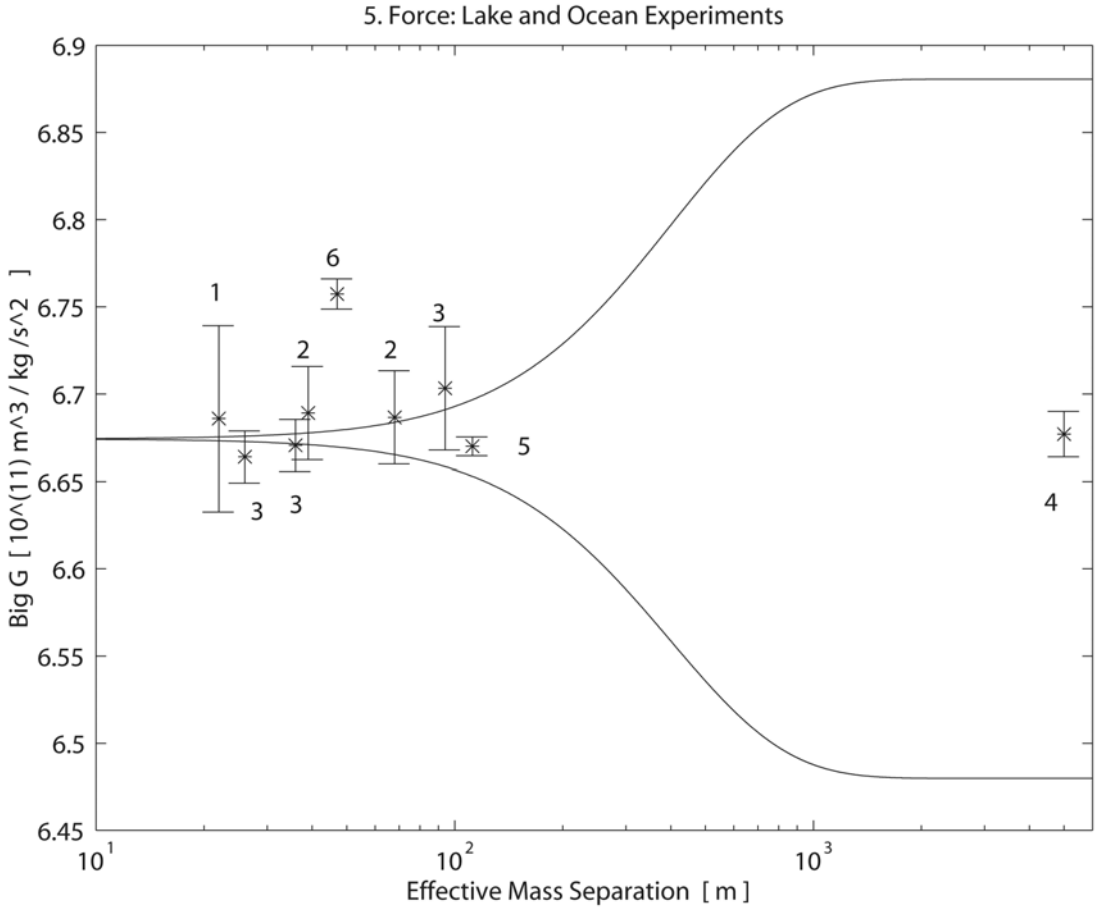

Figure 1: Newton's gravitational constant G measured by lake and ocean experiments as a function of effective mass separation. Solid lines: range dependence for repulsive (top) and attractive (bottom) fifth force with a relative strength of $\alpha = 0.03$ and a range $\lambda = 200$ m. Observations from: 1 – Moore *et al.* (1988), 2 – Müller *et al.* (1989), 3 – Oldham *et al.* (1993), 4 – Zumberge *et al.* (1991), 5 – Cornaz *et al.* (1994), 6 – Achilli *et al.* (1997). The lab reference value is from Luther & Towler (1982). Note the outlier 6, probably due to instrument calibration errors (Casula, pers. comm., 2000).

Many auxiliary measurements like water densities and temperatures as functions of water depth, levelling along the tunnel under the lake at different water levels (loading of the crust) among others were also made. The gravity signal from the water in the lake was about 320 nm/s^2/m, maximally more than 7000 nm/s^2, the earth tide was maximally 2300 nm/s^2 and the air pressure effect is roughly 4 nm/s^2/hPa. No significant deviation from the

lab value of the gravitational constant at effective distances of 39 and 68 m could be detected with an uncertainty of about 0.4 percent. This uncertainty was larger than originally expected and was caused by the uncertainty in the gravimeter calibration. This cause could be identified by the use of three gravimeters at the same position, which should have shown signals with smaller deviations between them. The results are shown in Fig. 1 together with other results from lakes.

This experiment was used to determine the gravitational constant at a certain mass separation. However, if differences would have been observed, they could also be blamed to a material dependence: water and tungsten, as compared to the materials involved in the reference value. Last not least the test presents an independent check for the Hannover calibration line.

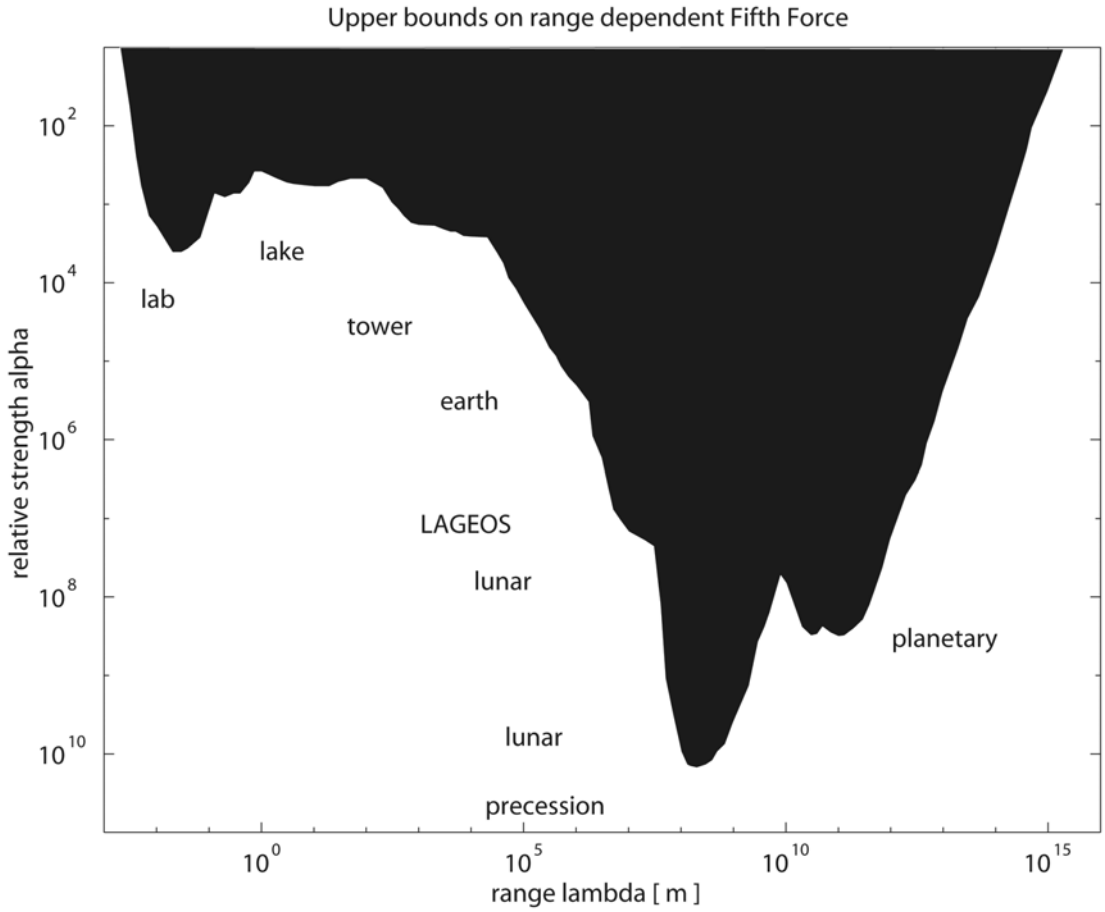

Figure 2: Field (black) of experimentally excluded values for relative strength α and range λ for the fifth force (adopted from Fischbach & Talmadge, 1999). Type of test is indicated near the boundary curve.

Retrospect

By 1994 the vast majority of all experiments had shown that no deviation from the inverse-square law or from the universality of free fall (material dependence) could be detected (with uncertainties, of course). A few deviatoric results had been reexamined and found to be at fault. Very few other deviatoric findings remain unexplained still today, but are heavily contradicted by all other experiments and thus infected by some unidentified systematic error with rather high probability. Fig. 1 shows all results (known to me) except one obtained by experiments using pumped-storage reservoirs and an important result obtained in the ocean (Zumberge *et al.*, 1991). One of the still deviatoric examples is also from a lake. Achilli

et al. (1997) have performed a very careful experiment and analysis, but were obviously fooled by a systematic error. According to one of the authors gravimeter calibration could be at fault (Casula, pers. comm. 2000). The one lake experiment not included in Fig. 1 was resulting in a deviation of G from the reference value by 7 percent due to lake water penetrating and leaving the ground directly under the gravimeter (Edge & Oldham, 1991). Clearly the most restrictive result is from Zumberge *et al.* (1991). This experiment in the ocean was orders of magnitude more elaborate and expensive than all the lake tests and the results were published after our own experiment and publication. Franklin (1993) and Fischbach & Talmadge (1999) have written excellent monographs on these experiments, their background and the history.

Despite the failure to detect a fifth force, these experiments were useful in gravity research. Fig. 2 shows the parameter space explored for a possible Yukawa term in the gravitational potential. Before all these experiments, the upper bound for the relative strength at distances between 10 and 5000 m would lie above the upper limit of the plot. Of course, it is possible that deviatoric effects exist below the boundary curve between explored and unexplored regions. Gillies (1987) lists a whole series of effects on gravitation not included in General Relativity which have been suggested, experimentally investigated or theoretically predicted. Experiments are able to provide upper bounds for such effects, just like the solid curve in Fig. 2. To help lower these boundaries is fundamental research and this is why many of the fifth force experiments were important contributions.

The search for deviations from Newton's law of gravitation (as a special case of General Relativity) continues. New experiments are performed to look for deviations from the inverse-square law at the sub-millimeter scale, because some string theories suggest that some additional dimensions might cause measurable effects at these ranges, so far with negative results. At the cosmic range in recent years the detection that neutrinos possess mass (not yet measured) sheds new light on the enigma of the Dark Matter in the universe. Also recently it was found by studying distant supernovae that the expansion of the universe accelerated and the so-called Dark Energy is invoked to have a name for this new mysterious force. Both phenomena are not really understood. In popular journals (DER SPIEGEL **8, 2002**) one could find news, that both PIONEER 10 and 11 spacecraft that left the solar system on opposite sides are braked by some small force which is not understood. All these effects have to do with interactions of masses, so the search for deviatoric behaviour and the quest for understanding the observations is not over.

Big G

The high experimental activity in the search for the fifth force led to renewed interest in the physics community for more accurate determinations of the gravitational constant in the lab. As a matter of fact, some of the groups involved in the fifth force problem became involved in measurements of Big G. Big G is the most inaccurately known fundamental constant today (Mohr & Taylor, 2002). New measurements with improved apparatus were performed with much smaller uncertainties than before. Fig. 3 plots several new measurements with different methods versus time since 1994 (Varga, pers. comm. 2003), all in the laboratory. The formal uncertainties do not always overlap, because unidentified systematic errors are lurking everywhere. One highly respected experiment in Germany deviates by more than half a percent from the other modern measurements, but systematic effects causing this could not be identified.

Acknowledgements

Discussions with Peter Varga and his compilation of G-measurements are gratefully acknowledged. Thomas Forbriger and Rudolf Widmer-Schnidrig critically read the manuscript.

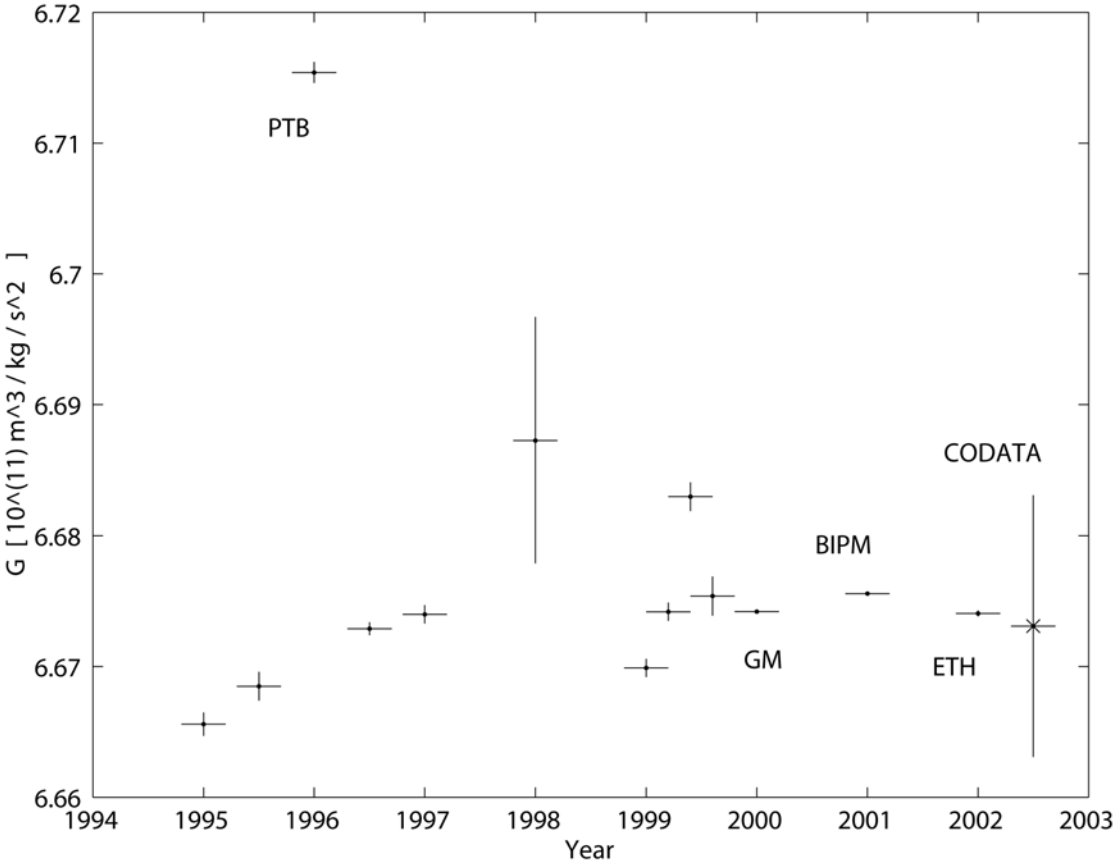

Figure 3: Measurements of Newton's gravitational constant G versus time. A few values are identified: PTB – Michaelis *et al.* (1995), GM – Gundlach & Merkowitz (2000), BIPM – Quinn *et al.* (2001), ETH – Schlamminger *et al.* (2002). CODATA is the adopted mean value by Mohr & Taylor (2002).

References

Achilli, V., P. Baldi, G. Casula, M. Errani, S. Focardi, F. Palmonari & F. Pedrielli, 1997. A geophysical experiment on Newton's inverse-square law. Il Nuovo Cimento **112 B**, 775-804.

Cornaz, A., B. Hubler & W. Kündig, 1994. Determination of the gravitational constant at an effective interaction distance of 112 m. Phys. Rev. Lett. **72**, 1152-1155.

Edge, R. J. & M. Oldham, 1991. The investigation of gravity variations near a pumped-storage reservoir in North Wales. In: J. Kakkuri (ed.). Proceedings of the 11th international symposium on earth tides, Helsinki, July 31 – August 5, 1989. Schweizerbart, Stuttgart, ISBN 3-510-65148-0, 662 pp., 415-424.

Fischbach, E. & C. L. Talmadge, 1999. The search for non-Newtonian gravitation. Springer, New York, ISBN 0-387-98490-9, xvii+305 pp.

Franklin, A., 1993. The rise and fall of the fifth force. American Institute of Physics, New York, ISBN 1-563-96119-9, 141 pp.

Gillies, G. T., 1987. The Newtonian gravitational constant. Metrologia **24**, 1-56.

Gundlach, J. H. & S. M. Merkovitz, 2000. Measurement of Newton's constant using a torsion balance with angular acceleration feedback. Phys. Rev. Lett. **85**, 2869.

Luther, G. B. & W. L. Towler, 1982. Redetermination of the Newtonian gravitational constant G. Phys. Rev. Lett. **48**, 121-123.

Michaelis, W., H. Haars & R. Augustin, 1995/6. A new precise determination of Newton's gravitational constant. Metrologia **32**, 267-276.

Mohr, P. J. & B. N. Taylor, 2002. The fundamental physical constants. Physics Today **2002-8**, BG6-BG9.

Moore, G. I., F. D. Stacey, G. J. Tuck & B. D. Goodwin, 1988. Determination of the gravitational constant at an effective mass separation of 22 m. Phys. Rev. **D 38**, 1023-1029.

Oldham, M., F. J. Lowes & R. J. Edge, 1993. A decametric scale investigation of the gravitational constant. Geophys. J. Int. **113**, 83-94.

Quinn T. J., C. C. Speake, S. J. Richman, R. S. Davis & A. Picard 2001, A new determination of G using two methods. Phys. Rev. Lett. **87**, article 111101.

Schlamminger, S., E. Holzschuh, E. & W. Kündig, 2002. Determination of the gravitational constant with a beam balance. Phys. Rev. Lett. **89**, article 161102.

Zumberge, M. A., J. A. Hildebrand, J. M. Stevenson, R. L. Parker, A. D. Chave, M. A. Ander & F. N. Spiess, 1991. Submarine measurement of the Newtonian gravitational constant. Phys. Rev. Lett. **67**, 3051-3054.

Gerhard Müller's "Experiments in the Kitchen"

Torsten Dahm, Hamburg

Introduction

In the second half of 1996, Gerhard Müller presented in the weekly seminar of his working group, in which I was participating, first examples and specimens of starch layers dried by air. The layers had been formed just by chance in his kitchen, as he said. He pointed us to the interesting patterns of cracks and joints that had formed. In the following weeks and months, possibly stimulated by plans in the department to apply for an interdisciplinary research program on (crack) patterns in geosystems, he began to repeat and improve his simple experiments with starch layers systematically. Nearly every week new results and insights were discussed in the seminar. During the first weeks, I and maybe most of the present students were a bit confused by this development. In our group of theoretical seismology and mathematical geophysics we were usually involved in theoretical problems of wave propagation or numerical simulation. We had some contact with fracture mechanics and the numerical simulation of cracks and crack propagation, but not with analogue experiments "in the kitchen". But it seems to me that Gerhard Müller had a similar feeling at the beginning.

In one of his first publications on this subject he explained why he started these starch experiments (Müller, 1997); analogue experiments are useful to study fundamental complex processes, especially when realistic computer simulations are not yet possible. The problems of crack formation, crack propagation and crack interaction are such very complex processes.

The research during his last years concentrated on two specific crack-problems: (1) the generation and interpretation of morphological structures on joints and (2) the formation of columnar joints.

Morphological structures on cracks and joints are often observed in glass and ceramics, but also in rocks. These structures reflect the fracture process, and their study may reveal the space and time dependence of the fracturing process, as well as the stress of the material before and during rupture. Plumose lines or structures radiate from the rupture nucleation point. It was well known that their orthogonal trajectories are the rupture fronts and that by drawing them the evolution of the rupture can be visualized. Gerhard's contribution was the experimental generation of plumose structures and the simultaneous observation of the surface rupture velocity and direction. Encouraged by his observations, he introduced an analogy between plumose lines and seismic rays, and was thus able to develop and verify a first quantitative inversion scheme of plumose lines to rupture velocity (Müller & Dahm, 2000). He further showed that large amplitude structures, so-called fringe zones, could be associated with slow and quasi-static rupture propagation (Müller & Dahm, 2000; Müller, 2001). This does not confirm the usual view that slow rupture produces smooth and fast rupture rugged crack faces (*e.g.*, Engelder & Fischer, 1996, pp. 259-261); it rather points to the opposite.

Columnar joints with polygonal cross sections are well known to form in cooling basalt layers. Their formation has interested scientists for about 300 years, but has been understood only qualitatively. Different controversial hypotheses had been developed to explain the initial phase of the column formation, ranging from dynamic horizontal crack propagation and bifurcation, over convection hypotheses, to quasi-static vertical fracture growths (see Müller, 1998). Gerhard Müller was able to generate columnar joints in drying starch-water layers under controlled conditions and to observe their formation velocity. They grow quasi-static in vertical direction. By studying their growth rate and cross-sectional shape as a function of layer thickness, column length and drying rate, he formulated a first experimentally based, quantitative model for their generation. He showed how to transfer

the starch-column model to explain the formation of basalt columns (Müller, 1998a; 1998b; 1999).

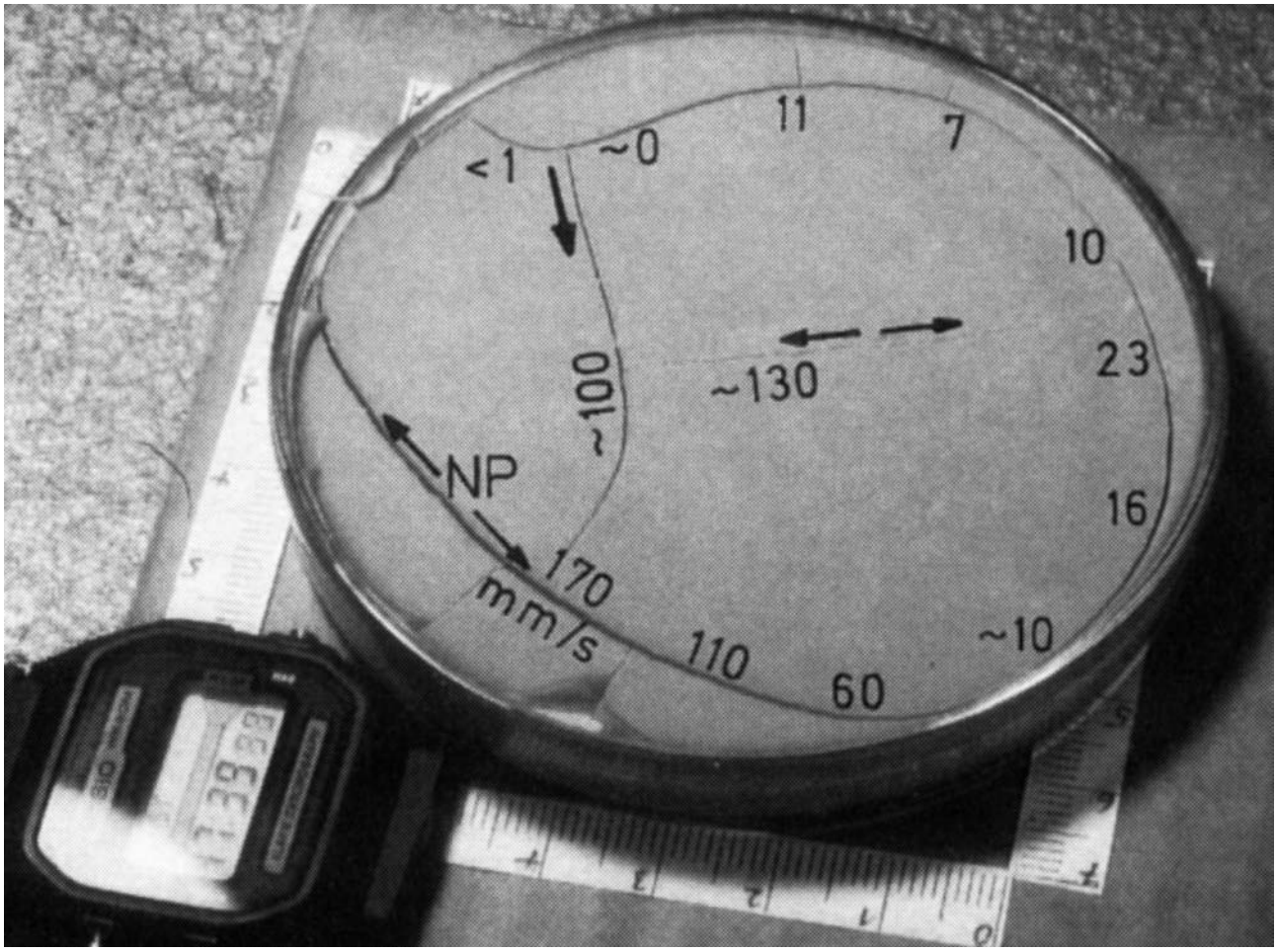

Figure 1: First generation tensile cracks in cornstarch. Rupture in horizontal direction is partly dynamic, partly quasi-static; with crack tip velocities in the order of cm/s (see numbers). NP indicates the nucleation point of the rupture; the arrows give the rupture direction.

Experimental Set-up and Observations

Most conclusions have been derived from one type of experiment, as described in detail in Müller (1997; 1998) and in Müller & Dahm (2000). The desiccation experiments were performed in glass vessels with vertical walls and cylindrical or rectangular cross sections; diameters vary from 50 to 100 mm, and depth vary from 10 to 45 mm. Desiccation was controlled mainly by a lamp (60 or 75 W) in fixed distance. In some cases a hair dryer had been used. The desiccation and crack formation was observed by video and additional photographing. During the experiment he continuously measured the weight and volume decrease of the probes (depth measurements). Some of his specimens have been analysed in detail after the experiment; either by photo to study the morphology on single joints, or, in the case of the columnar joints, by X-ray tomographic studies. He also applied active sound penetration experiments with piezo sensors to measure the elastic properties of starch-water layers.

Gerhard observed two types of desiccation cracks:

(1) Cracks of the first generation that propagated in sub-horizontal direction with quasi-static velocities in the range of 10 mm/min to dynamic velocities up to 100 mm/s. First generation cracks ruptured the whole layer, although the rupture front was curved and not necessarily vertical. Uni- as well as bi-

lateral rupture occurred, and the joints formed a rectangular angle when approaching already existing joints. The rupture morphology and plumose lines could not be observed directly during the experiment, but afterwards when preparing the specimen to photograph the rupture plane.

(2) Cracks of the second generation that propagated slowly in vertical direction from top to bottom in a quasi-static manner. They filled the unbroken regions surrounded by cracks of the first generation. Their pattern at the surface of the specimen was irregular. However, it became more and more regular during vertical growth. Polygonal columns developed with increasing columns length, and the cross-sectional thickness of the columns changed depending on the drying rate. The starch column with a typical diameter of millimeter looks very similar to basalt columns observed in nature, although their typical diameter is in the order of decimeter and thus much larger.

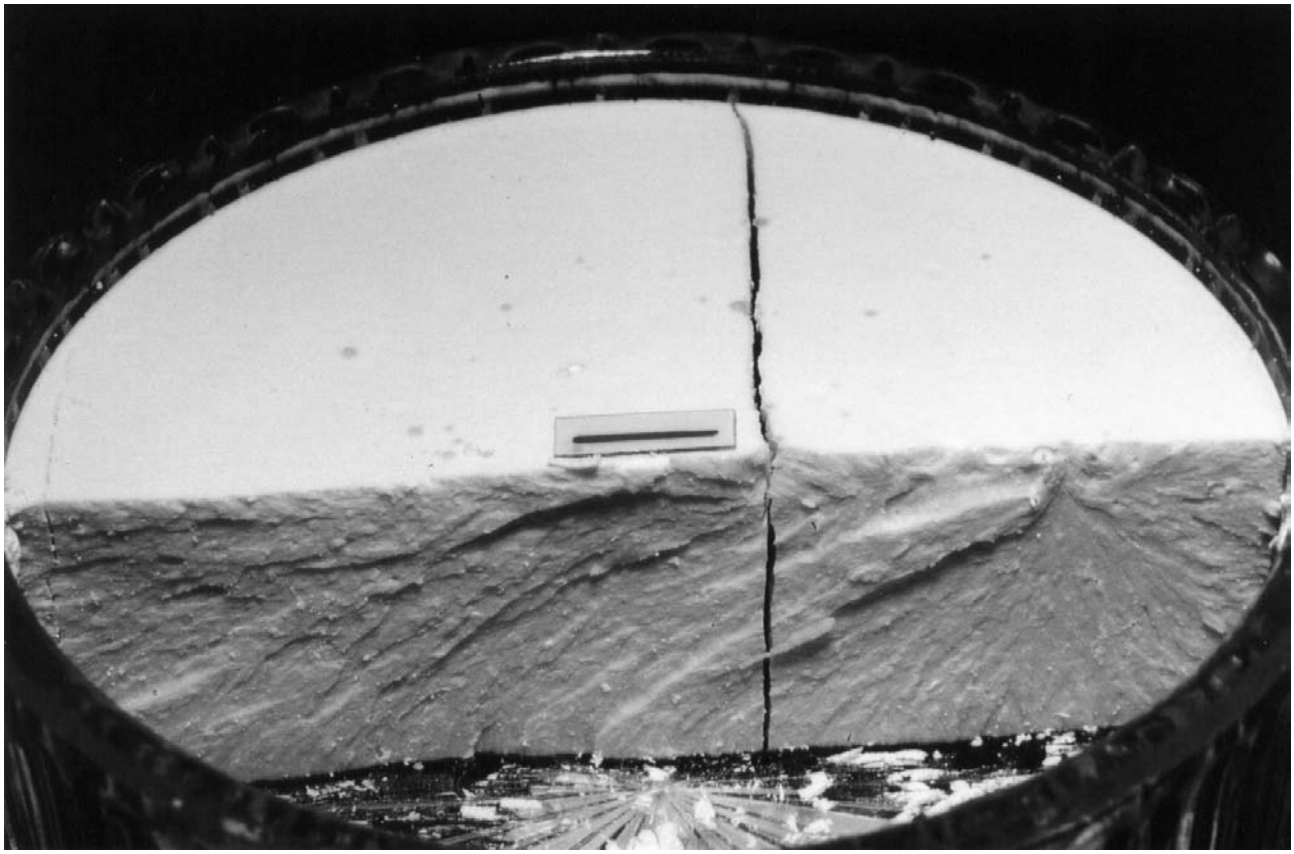

Figure 2: Plumose morphology indicates rupture direction. Rupture fronts are orthogonal to plumose lines. Rupture velocity was quasi-static in the range of 10 mm/min. The black line indicates 10 mm.

Tensile Crack Morphology and Rupture Velocity

Figure 1 shows first generation tensile cracks in cornstarch. The nucleation points are indicated by points from which arrows start; and the numbers indicate the rupture velocity in horizontal direction. They were partly dynamic and partly quasi-static. After the desiccation experiment, the probes were prepared to analyse the morphological structures on the rupture plane. An example is given in Fig. 2. Plumose lines converge at the nucleation point. They indicate the local direction of the rupture front, which is perpendicular to the plumose lines. Other examples of observed plumose lines and morphological structures on rupture planes are given in Müller & Dahm (2000); Müller (2001). Gerhard Müller suggested the approximate analogy between plumose lines and rupture fronts to seismic ray trajectories

and wave fronts to model plumose lines. A simple, analytical example of constructed plumose lines and rupture fronts is given in Fig. 3 (from Müller & Dahm, 2000). In Müller & Dahm (2000) it is further shown that a more complex rupture velocity can be resolved by means of a conjugate gradient inversion of plumose lines. It is the first example of a quantitative inversion of plumose lines. The approach has potential applications. It may be used to study sedimentary joints, but also other fracture mechanical problems and to analyse laboratory experiments.

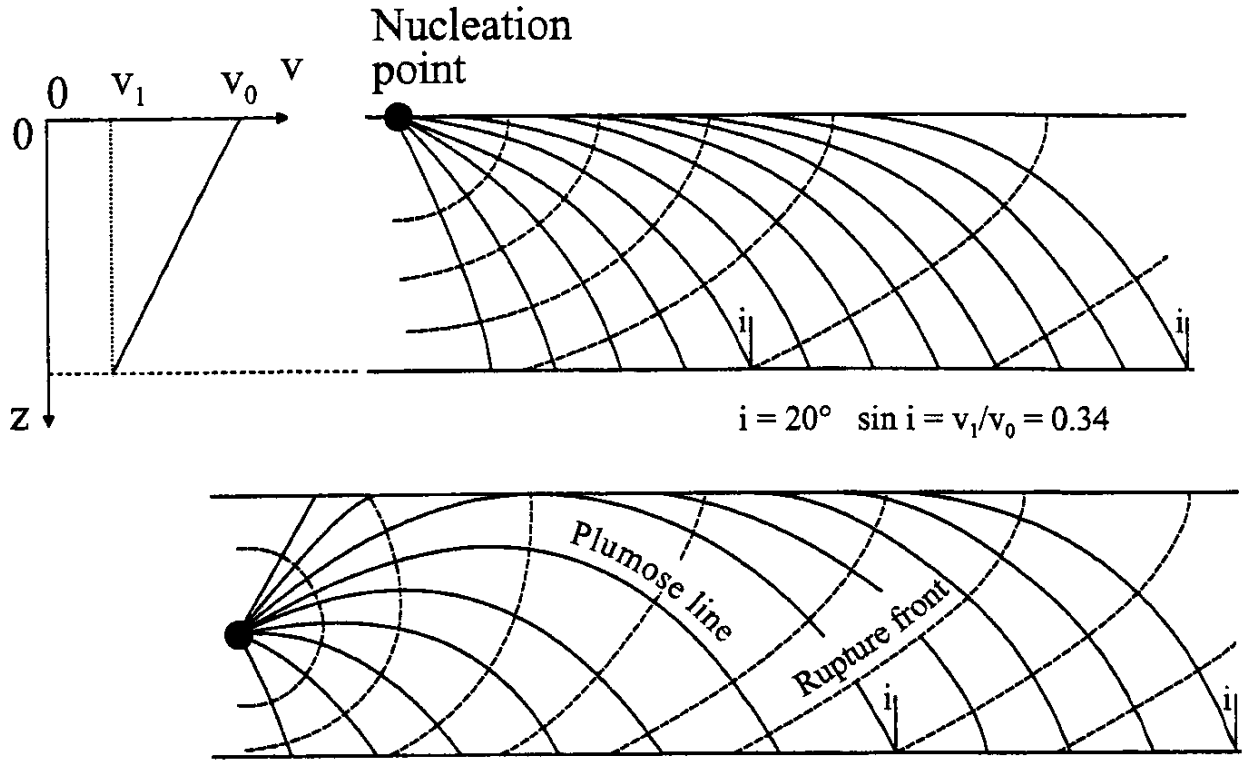

Figure 3: Plumose lines and rupture fronts are constructed by seismic ray-tracing methods. In this example the rupture velocity linearly decreases with depth.

Columnar Jointing in Drying Starch Layers

The cracks of the second generation start to develop several hours after the formation of first generation cracks in the so far unbroken regions (Fig. 4). They appear first on the free surface of the specimen. Gerhard could show that these cracks grow slowly in vertical direction, and that their irregular pattern at the free surface becomes more and more regular. Typically, hexagonal or pentagonal column cross sections develop (Fig. 5). The cell diameter is controlled by the vertical concentration gradient of the water content. A high gradient is connected with thin starch columns. By analogy, Gerhard proposed that the diameter of basalt columns is controlled by the temperature gradient at the crack front in the basalt layer, and not, as sometimes assumed, by the cooling rate. The two orders of magnitude difference in the column diameter in starch and basalt can be explained by the difference in crack front speed in both cases, which itself depends on the hydraulic diffusivity of starch or the thermal diffusivity of magma, respectively. Gerhard was thus able to provide a first model on the generation of basalt columns based on controlled laboratory experiments and giving important insights in the physical understanding of the processes involved.

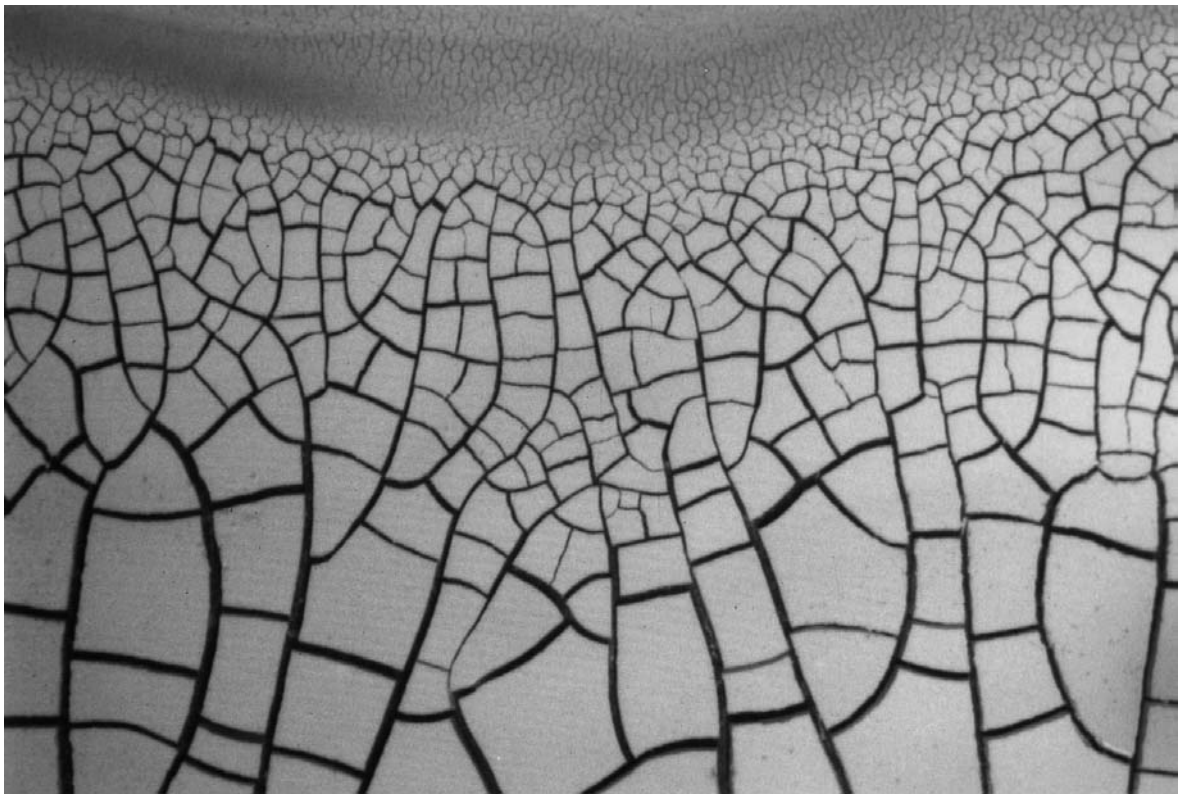

Figure 4: First and second-generation cracks as seen at the surface of a starch layer. The thickness of the starch layer increases from the upper to the lower boundary of the figure. The formation process for second-generation cracks has already started in the upper region of the figure, while mostly first generation cracks are visible in the lower region of the figure.

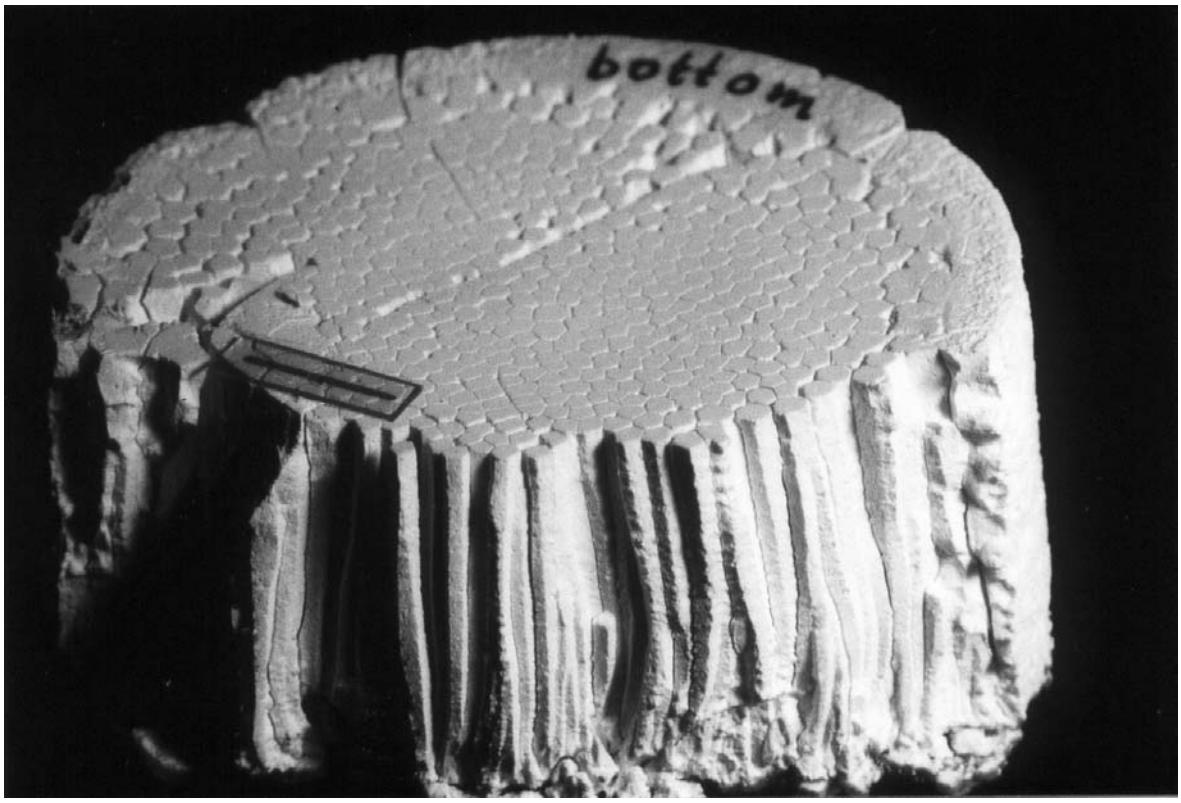

Figure 5: Example of Gerhard Müller's starch columns. The specimen is up-side down, the black line indicates 10 mm. Polygonal (mostly hexagonal) cross sectional shapes have developed during the slow vertical growth of the second-generation cracks.

Acknowledgements

This contribution is dedicated to Gerhard Müller. I had the luck to work with him in Frankfurt as his scientific assistant during 1994 to 2000. He was an excellent scientist, supervisor and teacher, and additionally a very fair and friendly personality. Even during his last years, when he was suffering on very serious health decease, he was working harder and more efficiently than everybody in his group. With his enthusiasm for solving problems, with his persistent and efficient way of doing research, with his astuteness and his broad knowledge, he always provided us with inspiration and a good example.

References

Engelder, T. & M. P. Fischer, 1996. Loading configurations and driving mechanisms for joints based on the Griffith energy-balance concept. Tectonophysics **256**, 253-277.

The Reflectivity Method – a Success Story

Dedicated to Gerhard Müller (+) on his Symposium

Karl Fuchs, Karlsruhe

Opening

All who knew Gerhard would agree that he would not have liked this title! I am sure, he even would not have liked the title of this symposium.
Nevertheless the academic marriage between two persons, each with its own abilities and its different characters and methods changed the world of Deep Seismic Sounding (DSS) not only in the crust and lithosphere, even down to the inner core from the previous inversion of mainly travel times to that of the full wavefield. It was very timely, spread like fire throughout the scientific community and therefore it was a success story! Gerhard, sorry to say so and you played a key role in this marriage! He would admit this!

Towards the Reflectivity Method

Two young scientists met during the 1960s, pursuing to different avenues to numerically synthesize wave propagation in realistic media. In the beginning they worked separately at different places. They had different and common forerunners and academic teachers (Table 1).

Table 1: Forerunners.

	Ray-Theoretical Method *Gerhard Müller*	Reflectivity Method *Karl Fuchs*
Forerunners	Cagniard, 1932 Pekeris 1955, 1960 de Hoop, 1958 Cerveny, 1961 to 1966 and more Pekeris, Alterman, Abramovici, Jarosch 1965 Spencer, 1965 Bortfeld, 1964, 1967 Helmberger 1968	Thompson, 1950 Haskell, 1953 Keilis-Borok, 1953 Brekhovskikh, 1960 Cerveny, 1961 Harkrider, 1964 Nuttli, 1964 Phinney, 1965 Cooley & Tukey, 1965: FFT
Joint Forerunners (academic teachers)	Heinz Menzel & Otto Rosenbach, 1958. The influence of a layer with a complying with a linear velocity law on the shape of the on the shape of the seismic pulses. Geoph. Prosp. **6**, 408-432 *(both Mathematicians from Königsberg Unversity, both formerly at PRAKLA; both at TU Clausthal (Bergakademie))*	

In 1969 they decided to join their efforts at the Geophysical Institute of Karlsruhe University. The timetable (Table 2) of their cooperation shows how the fundaments were prepared separately and then within a very short time span the development of the reflectivity method was finalized. It became rapidly known throughout the Deep Seismic Sounding community and beyond.

Table 2: Merging two different approaches – timetable.

	Ray-Theoretical Method *Gerhard Müller*	Reflectivity Method *Karl Fuchs*	
1963		Clausthal, PhD Thesis: Wave propagation in wedge-shaped media	1963
1964	Mainz, Diploma Thesis: Elastische Kugelwellen und ihre Reflexion und Brechung an der ebenen Trennfläche zwischen zwei homogenen, isotropen Halbräumen	St. Louis University: P-waves transfer function for a system consisting of a point source in a layered medium	1964
1965	Clausthal: Scientific Assistent	South West Center for Advanced Studies, Plano, Texas: Plane wave reflectivity of layered medium.	1965
1966	First personal contacts		1966
		Geophysical Kolloquium Clausthal-Zellerfeld: Reflection seismic images of the earth crust and its boundaries	
1967	Clausthal, PhD Thesis: Theoretische Seismogramme für Punktquellen in geschichteten Medien		1967
1968	Theoretical seismograms for some types of point-sources in layered media. Part I: Theory; Part II: Numerical Calculations. Z. Geophys. **34**	1) Karlsruhe, Habilitation Thesis: Die Reflexion von Kugelwellen an inhomogenen Übergangszonen mit beliebiger Tiefenverteilung der elastischen Moduln und der Dichte. (Still with the method of stationary phase.) 2) Successful direct integration over angle of incidences: Presentation at Symposium on Mathematical Geophysics, Tokyo/Kyoto: The reflection of spherical waves from transition zones with arbitrary depth-dependent elastic moduli and density. J. Physics Earth **16**, Special Issue, 1968	1968
1969	Gerhard moves from Clausthal to Karlsruhe	The method of stationary phase as a diagnostic aid in estimating the field pattern of body waves reflected from transition zones. Z. Geophys. **35**	1969
1969/ 1970	Integration of ray theoretical part through layered overburden on top of reflective zone, influence of free surface		1969/ 1970
1970	Exact ray theory and its application to the reflection of elastic waves from vertically inhomogeneous media. Geophys. J. R. astr. Soc. **21**	Visit to Ottawa/Mike Berry First application to interpretation of system Grenville record sections with reflectivity method. ---------- Program description and all commentaries translated from German into English.	1970

1971	K. Fuchs and G. Müller Computation of Synthetic Seismograms with the Reflectivity Method and Comparison with Observations. Geophys. J. R. astr. Soc. **23**		1971
1971	IBM Watson Lab and Lamont Doherty, Columbia University: Approximate treatment of elastic body waves in media with spherical symmetry. Geophys. J. R. astr. Soc. **23**	The method of stationary phase applied to the reflection of spherical waves from transition zones with arbitrary depth-dependent elastic moduli and density. Z. Geophys. **37**	1971
1972	Development of Flat Earth Approximation, integration into Reflectivity Program, application to inner core reflections		1972
1973	Amplitude studies of core phases. J. Geophys. Res. **78**		1973
1974	Karlsruhe, cumulative Habilitation Thesis: Flat Earth Approximation and inner core amplitudes		1974

What Caused the Success of the Reflectivity Method?

Of course, the Reflectivity Method was timely in the scientific scenery!
But, lest we forget, let me take a few minutes to remind all of us about some historic background, which might otherwise become forgotten.
In Germany after World War II it was a coincidence of scientists with strategic thinking and willingness to cooperate, as well as the exciting development in the computer industry. All this generated a climate of research opportunities for the young generation.
The leading generation of the post-war Geophysicists in Germany had a very clear primary focus: to generate a climate of cooperation between the many small Earth science institutes or departments in Germany and to return to international cooperation. They convinced the **Deutsche Forschungs-gemeinschaft** (DFG) to install a series of large scale research programs in the Earth sciences: *e.g.*, "Exploration of the Deep Structure of the Earth Crust in Central Europe" with a strong component of international cooperation.
In these early years the DFG (*Waldemar Heitz* and later *Franz Goerlich*) literally forced upon the Geophysical Institutes an institution, which would today be called a Research Consortium (FKPE = Forschungskollegium Physik des Erdkörpers).
Heinz Menzel at Clausthal and *Otto Rosenbach* at Mainz belonged to the young driving forces in this cooperation of Earth Sciences including geophysics institutions in Germany. They had both studied mathematics and physics at Königsberg University before and during World War II. After the war they had begun their professional career with PRAKLA at Hannover in the exploration industry.
In seismology and DSS the other driving force was located in Stuttgart with *Wilhelm Hiller* and the even younger generation with international contacts to Lamont: *Hans Berckhemer* and *Stephan Müller*.
Gerhard Müller and Karl Fuchs profited directly from this stimulating spirit of national, international and interdisciplinary spirit prevailing throughout the western part of Germany.
The DSS-part of these programs generated the refraction/wide-angle reflection observations in high quality and growing and dense quantities. The young generation of scientists felt very soon, that the previous methods of interpretation, based primarily on travel times, were inadequate to the richness of information

in the new data. This was the primary motivation for both Gerhard Müller and Karl Fuchs to start to develop methods to calculate synthetic seismograms.
The revolution in the computer industry was another timely incentive for both of us to achieve our ideas. In a very short time we went from machineries like ZUSE 23, IBM 1620 to IBM 7094, from punched tapes, punched cards to magnetic tapes, and in language from machine language, ALGOL to FORTRAN.
The coincidence of all these developments and circumstances were very fortunate. But all this is worthless if you do not meet the right persons to share your ideas and to work together. The chemistry was alright (as one would say today). This was the basis for a very frank, sometimes controversial interaction.

Open Unconditional International Cooperation

After our presentations on various conferences and workshops we received numerous requests for the FORTRAN code of our Reflectivity program. We both were determined from the beginning that we would share our program unconditionally with any reasonable request. This was not completely unselfish: we hoped and experienced that this free communication helped tremendously to detect hidden bugs, to improve the program and to develop new ideas.

Conclusions

This Academic Marriage had its up and downs. As in every marriage this happens and is the power of every successful marriage. The characters were clearly very different.
It was sheer luck for both of us to have met each other during this time. In spite of the difference in characters, the chemistry was alright and helped to overcome differences in opinion.
It was personally luck for Karl Fuchs, to have Gerhard Müller at Karlsruhe when he returned from Lamont. In his quiet, inconspicuous and yet ambitious manner he helped very much to keep Geophysics at Karlsruhe in the right balance between experiment and theory, between teaching and research.
When Gerhard went to start his new carrier on the Chair of "Mathematical Geophysics" at Frankfurt the marriage, after separation, converted into friendship between Karl and Gerhard, from SIE to DU. I still appreciate when Gerhard attended my 70 years symposium in April last year obviously with physical difficulties. He asked me on the stairs to go forward, he would follow. Now he went ahead!

Thanks Gerhard, for this fruitful Academic Marriage and Friendship!

Mantle Heterogeneity

Brian L. N. Kennett, RSES, Canberra

Introduction – Tomography as a Forensic Tool

Tomographic inversions for a single wavetype control the spectrum of heterogeneity, but do not give any direct information on underlying causes. It is only when multiple sources of information are brought to bear on the 3-D structure that we can pass from images to assessment of processes.

There has been recent progress in a number of areas towards the development of multiple images of the mantle at comparable resolution. Kennett *et al.* (1998) have used the arrival times of P and S waves in a joint inversion to extract information on the distribution of bulk-sound and shear wavespeed in the mantle with resolution at a 2 x 2º level, where ray coverage is available. Masters *et al.* (2000) use a wide range of different P and S body wave and surface wave information spanning a large range of frequencies to produce whole mantle images of bulk-sound, shear and P wavespeed with moderate resolution.

The use of bulk-sound and shear wavespeeds as proxies for the bulk modulus and shear modulus provides a link to laboratory experiments and *ab initio* calculations, but highlights the limitations imposed by our relatively weak knowledge of the variations in density within the Earth.

The relative behaviour of the two classes of wavespeeds can provide clues to the nature of the process occurring within the earth. Where the variation of the bulk-sound speed and shear wavespeed are comparable in behaviour a thermal origin is likely, but when the two wavespeeds are anti-correlated some alternative hypothesis needs to be sought. At shallow depths some infusion of volatiles or melt could have a profound influence on shear wavespeed with less effect on bulk-sound speed, alternatively chemical heterogeneity may play a role.

The images of subduction related structures show a relatively complex pattern of variation in the upper mantle, but it would appear that there is a stronger shear component for older subducted lithosphere. The stagnant slab material in the transition zone, most likely emplaced by slab roll-back, has a stronger bulk-sound speed signal possibly because the shear differences are annealed more quickly by the influence of the external temperatures.

Although there are distinct bulk-sound signatures in subduction penetrating into the top of the lower mantle, below about 1000 km the dominant signal in deep slabs is in shear wavespeed variation and this dominates the P wavespeed images.

Joint Tomography

Although body wave sampling of the mantle is restricted because of the available source and receiver locations, relatively high resolution can be achieved for about half of the mantle using tomographic inversion of P and S arrival times.

P and S times from the Engdahl *et al.* (1998) reprocessing of the catalogue of the International Seismological Centre have been used with some supplementations. Only uphase times where both P and S times are available for the same source and receiver pair are utilised. Although the S waves generally have somewhat lower frequency than for P, the sampling wavelength will be comparable and so we are able to extract a consistent set of tomographic images.

The *ak135* model of Kennett *et al.* (1995) has been used as the initial reference and arrival times are selected whose residuals lie within 7 s of the predictions of the *ak135* model for P and residuals within 25 s for S. The large span for S is designed to cope with the well-recognized fast S wavespeeds in shields near the surface and the presence of zones of depressed S wavespeed towards the base of the mantle. Because of the large range of residuals

we undertake inversion of the arrival times with 3-D ray tracing.

The joint inversion of the P and S times to extract the bulk-sound speed and shear wavespeed is based on the work Kennett et al. (1998), with a number of improvements made to the algorithm. The initial approach is to undertake separate P and S wavespeed inversion using a linearized algorithm and then employ these 3-D models as the basis for 3-D ray tracing in the joint inversion which uses a multiply iterative scheme as developed by Kennett *et al*. (1998). The iterative updates allow cross-interaction between the two wavespeed distributions and make an efficient use of memory.

Masters *et al.* (2000) point out that the absolute level of heterogeneity derived from body wave inversions using catalogue data is lower than that from waveform analysis and the use of times of longer period phases. Such an effect is an inevitable consequence of the significant noise in the data set (especially for S). However, by choosing a restricted data set with comparable paths for P and S we should have good control on the relative amplitude of the variations of bulk-sound and shear wavespeed even if the absolute level is not well constrained.

Slab Heterogeneity

Both global inversions and regional tomographic inversions have been undertaken to understand the characteristics of the wavespeed variations associated with subduction. In the regional inversions a 19 layer model is employed down to 1500 km with 1x1º cells in the region of interest embedded in a coarser global model with 5x5º cells. Separate regional inversions have been undertaken for the northwest and southwest Pacific subduction zones. In the global inversions 2x2º cells are used with 18 layers through the mantle (as in the study by Kennett *et al.*, 1998).

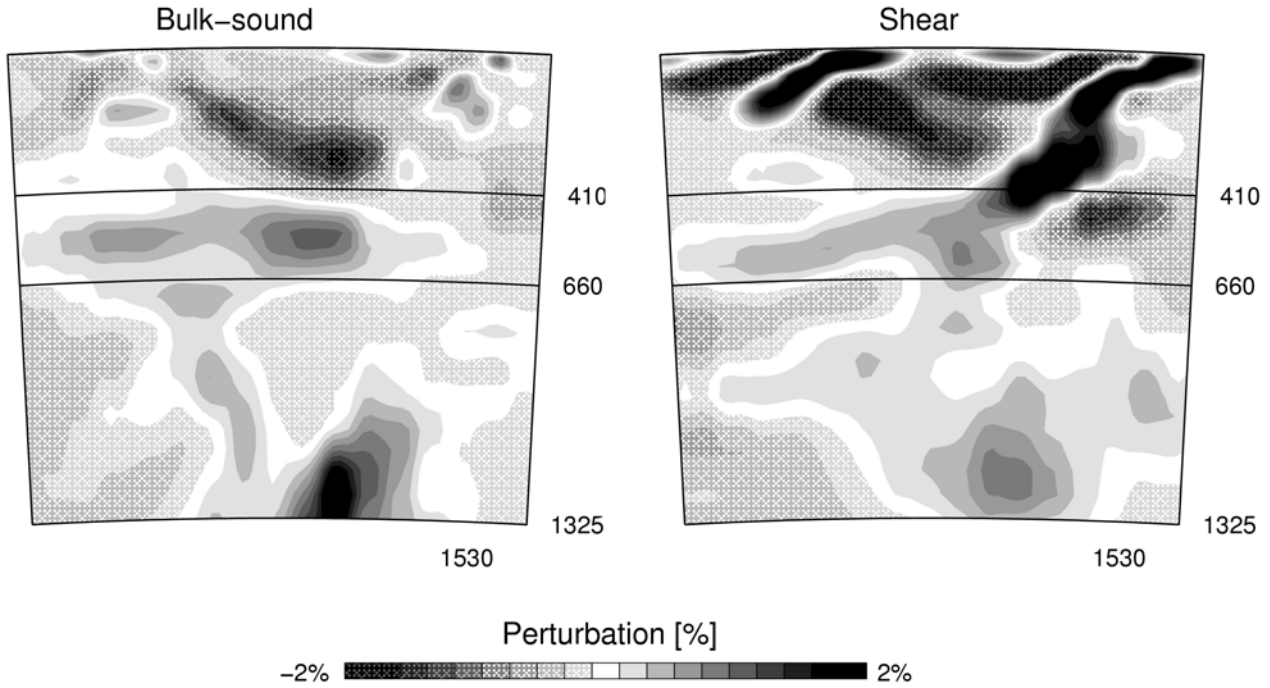

Figure 1: Vertical cross-section through regional joint tomographic model for the northwest Pacific passing through the Ryukyu and Izu-Bonin arcs along the line of section of Widyantoro *et al.* (1999). The perturbations are plotted relative to the *ak135* model.

The differences in character of bulk-sound and shear images in the upper part of the mantle are illustrated in a cross section across the Ryukyu and Izu-Bonin arcs in Fig. 1. As noted by Widiyantoro *et al.* (1999) there are significant differences in the P and S tomographic images for this region, particularly for the recumbent slab in the transition zone, which lies on top of the 660 km discontinuity. The two subduction zones

show up very clearly in the shear wavespeed images but have a rather weak expression in bulk-sound. However, the stagnant slab, that was mostly likely laid down during slab roll-back, is at least as marked in bulk-sound as in shear. There is a suggestion that there may be some degree of penetration of the slab into the lower mantle in the image but interpretation is complicated by the presence of the strong lower mantle anomaly below 1000 km depth. Although the images in Fig. 1 are plotted relative to the *ak135* model, the tomographic inversion was fully nonlinear with 3-D ray tracing.

The strong shear wavespeed contrasts seen in Fig. 1 seem to be characteristic of the subduction of older lithosphere, but where younger oceanic lithosphere is being subducted as, *e.g.*, in many of the southwest Pacific subduction zones the bulk-sound variation is more pronounced than for shear. Horizontal features lying on top of the 660 km discontinuity display a marked bulk-sound speed anomaly and it is possible that this configuration is more favourable for thermal annealing of the shear wave variations.

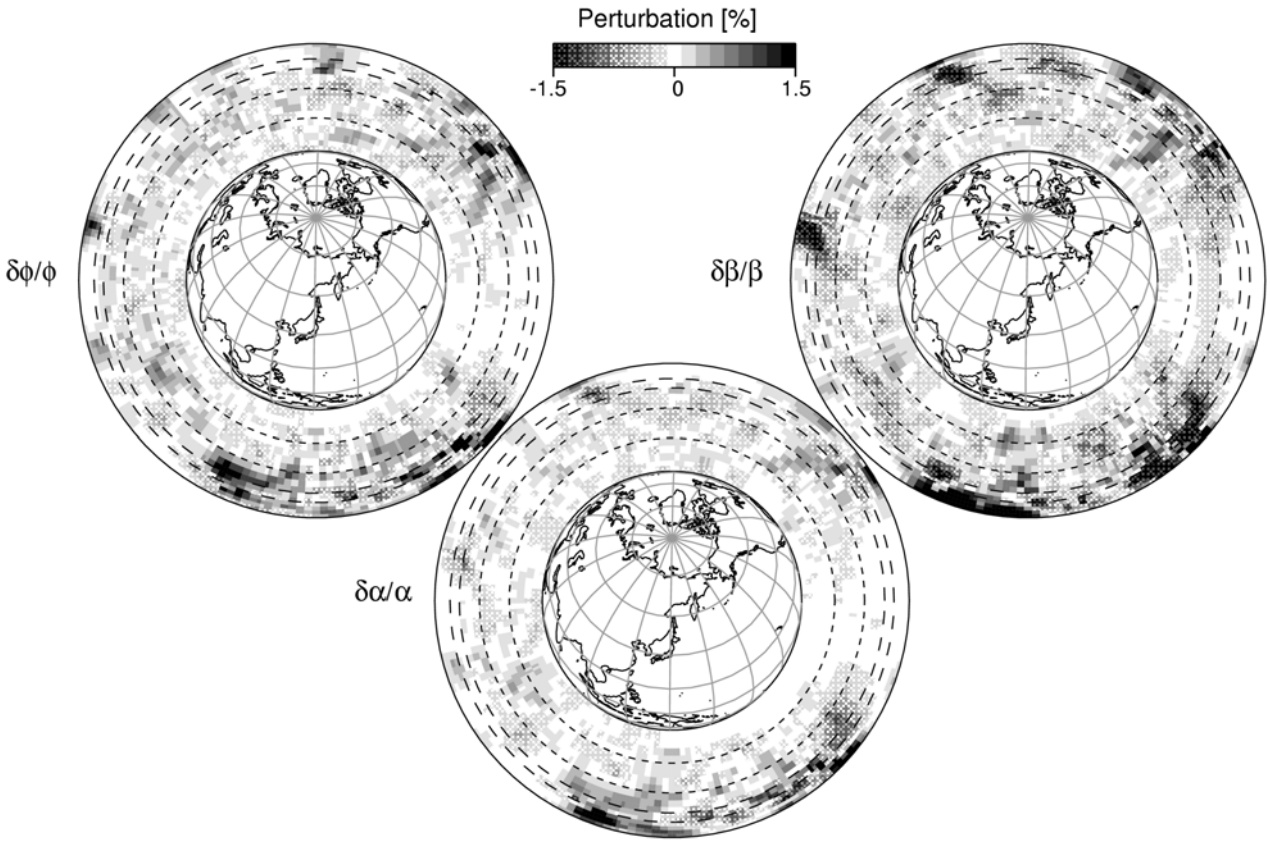

Figure 2: Great-circle through the global joint tomographic model cutting through the Farallon feature below central America, the Fiji region with a stagnant slab section and a deep shear anomaly beneath Australia. The perturbations are plotted relative to the *ak135* model.

In the lower mantle, the narrow zones of high wavespeed which have been associated with past subduction of the Farallon plate under theAmericas and at the northern edge of the Tethys ocean have by far their strongest expression in shear. Most of the P wavespeed anomalies come from the variation of the shear wavespeed. Although such features are particularly prominent in the depth range from 900-1500 km, they are by no means the only anomalies in the lower mantle. Cross-sections through the globe passing through Central America, the Fiji region and Australia are displayed in Fig. 2. The Fiji subduction appears as a prominent feature in the bulk-sound image $\delta\Phi / \Phi$ lying above the 660 km discontinuity. Further to the west under Australia there is a strong shear feature

($\delta\beta / \beta$) associated with the fast cratonic lithosphere but also a steep wavespeed anomaly extending from just below the 660 km discontinuity to below 2000 km depth. This is present but less marked in the resultant P wavespeed image $\delta\alpha / \alpha$) reconstituted from the bulk-sound and shear contributions.

Beneath Central America there is a strong shear wavespeed feature, which does not reach all the way to the surface, probably because the subducted slab is quite young; instead the shallow portion is better represented in bulk-sound. Despite the strength of the shear anomaly the P wavespeed feature has a slightly different dip introduced by the interaction of the shear and bulk-speed contributions. It is almost as if different components of the deep slab carry different physical signatures as they interact with the surrounding lower mantle.

Discussion

What then are the likely causes of S wave dominance in the many of the images of deep slabs? We need to find a way to maintain contrast in the shear wavespeed structure as the material is thrust deep in the mantle. Ultimately we would expect thermal equilibration with the surroundings, but this could be substantially delayed if the slab material remains chemically distinct from its surroundings. The retention of anisotropic fabric in the slab might also serve to reinforce the S signal.

In the deeper parts of the mantle the anomalies that we might associate with remnant subduction are not significantly larger than many other shear anomalies. These features could have arisen from incomplete mixing in prior iterations of the geodynamic cycle. There is a feature beneath Australia in the deep mantle possibly related to 300 Ma subduction that is of comparable size to that inferred to arise from the subduction of the Farallon plate. Other enigmatic anomalies are to be found beneath South America and under Asia.

Many of these objects are too small to be resolved in the studies using whole mantle sampling with lower frequency waves but there is a good correlation with the general patterns found in the work of Masters *et al.* (2000) in those regions of common coverage.

The joint exploitation of P and S wave information has begun to reveal new facets of mantle heterogeneity and we can anticipate more surprises as we learn to exploit more of the information in seismograms.

Acknowledgement

I would like to thank Alexei Gorbatov for his efforts in the development of nonlinear tomographic routines for joint inversion and in the construction of the tomographic models.

References

Engdahl, E. R., R. D. van der Hilst, & R. Buland, 1998. Global teleseismic earthquake relocation with improved travel times and procedures for depth determination. Bull. Seism. Soc. Am **88**, 722-743.

Kennett, B. L. N., E. R. Engdahl & R. Buland, 1995. Constraints on the velocity structure in the Earth from travel times. Geophys. J. Int. **122**, 108-124.

Kennett, B. L. N., S. Widiyantoro & R. D. van der Hilst, 1998. Joint seismic tomography for bulk-sound and shear wavespeed in the Earth's mantle. J. Geophys. Res. **103**, 12469-12493.

Masters, G., G. Laske, H. Bolton & A. Dziewonski, 2000. The relative behaviour of shear velocity, bulk sound speed, and compressional velocity in the mantle: implications for chemical and thermal structure. In: Shun-Ichiro Karato *et al.* (eds.). Earth's deep interior: mineral physics and tomography from the atomic to the Global Scale, AGU Geophysical Monograph **117**, ISBN 0-87590-975-2, 63-87.

Widiyantoro, S., B. L. N. Kennett & R. D. van der Hilst, 1999. Seismic tomography with P and S data reveals lateral variations in the rigidity of deep slabs. Earth. Planet. Sci. Lett. **173**, 91-100.

Amplitude Study of Core Phases: Spectral Decay Constants of $PKP(BC)_{diff}$

Jörg Schlittenhardt, BGR, Hannover

Abstract

Traditional Earth models of the outer core show a smooth increase in *P* velocity with depth down to the inner core boundary (ICB). However, there is also evidence for the existence of a zone with constant or reduced velocity gradient in a 100 – 200 km thick layer above the ICB (as expressed in models AK135 (Kennett *et al.*, 1995) and IASP91 (Kennett & Engdahl, 1991) in Fig. 1, for example). Such seismic models are in agreement with the hypothesis of an increase in the diameter of the inner core due to slow cooling and crystallization of the iron alloy at the base of the outer core, where lighter core material is accreted above the ICB. Such zones with an enrichment of lighter core material could possibly be recognized by the manner in which the *P*-wave velocity increases with depth. To tackle the problem of the nature of the velocity gradients at the base of the outer core spectral decay constants $\gamma(\omega)$ of $PKP(BC)_{diff}$ were calculated for both earthquakes from the Tonga Fiji region recorded by the stations of the GRSN (German Regional Seismological Network) and from theoretical seismograms calculated with the reflectivity method (Müller, 1985). The model calculations demonstrated that the $PKP(BC)_{diff}$ amplitudes are very sensitive to the velocity gradient above the ICB: increasing the velocity gradient results in a stronger attenuation of $PKP(BC)_{diff}$ which in turn increases the decay constant (Schlittenhardt *et al.*, 2002). This is clearly demonstrated in Fig. 2 where the theoretical decay spectra for the three reference Earth models of Fig. 1 are shown. Additional comparison of the theoretical $\gamma(\omega)$ values with those determined from GRSN data indicates the existence of reduced velocity gradients at the base of the outer core. A modified PREM model (Dziewonski & Anderson, 1981) with a 150-km-thick zone of constant velocity above the ICB gives the best fit to the observed $\gamma(\omega)$ (Wolf, 2002).

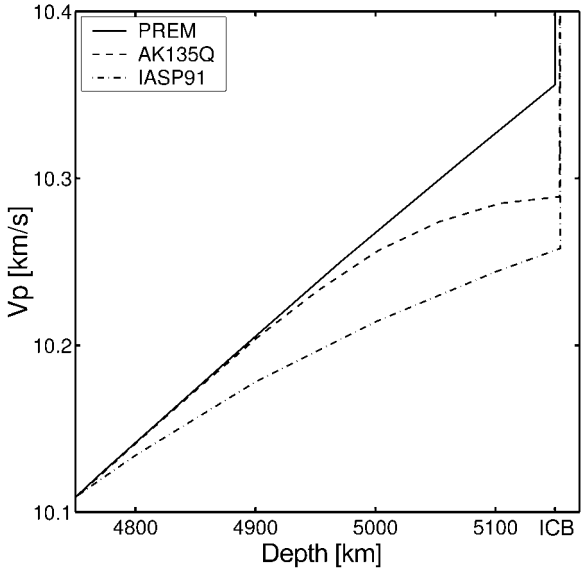

Figure 1: Velocity-depth functions for the Earth models PREM, AK135 and IASP91 for the depth range above the inner core boundary (ICB). P-wave velocity gradients vary in a zone approximately 200 km thick at the base of the outer core.

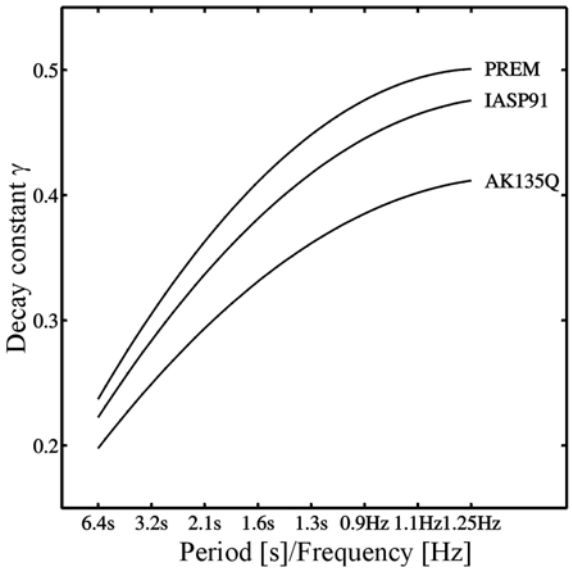

Figure 2: Theoretical decay spectra γ of the Earth models PREM, IASP91 and AK135 as shown in Fig. 1. Note the increased decay constants for models with increasing velocity gradient above the ICB.

References

Dziewonski, A. M. & D. L. Anderson, 1981. Preliminary reference Earth model. Phys. Earth Planet. Inter. **25**, 297-356.

Kennett, B. L. N., E. R. Engdahl, 1991. Traveltimes for global earthquake location and phase identification. Geophys. J. Int. **105**, 429-465.

Kennett, B. L. N., E. R. Engdahl & R. Buland, 1995. Constraints on seismic velocities in the Earth from traveltimes. Geophys. J. Int. **122**, 108-124.

Schlittenhardt, J., M. Wolf, M. Weber & F. Scherbaum, 2002. Amplitude study of core phases using data of the German Regional Seismological Network (GRSN). In: Korn, M. (ed.). Ten years of German Regional Seismological Network (GRSN)). Deutsche Forschungs-gemeinschaft (DFG), Senate Commission for Geosciences, Report **25**, Wiley-VCH, Weinheim, ISBN 3-527-27514-2, 178-191.

Wolf, M. D. C. 2002. Amplituden der Kernphasen im Bereich der Kaustik B und Untersuchung der Struktur der Übergangszone zum inneren Erdkern mit spektralen Amplituden der diffraktierten Phase PKP(BC). Dissertation, Universität Potsdam, 107 pp. (http://deposit.ddb.de/cgi-bin/dokserv?idn=964730642).

Seismic Reflections at the KTB Site in Germany

Matthias Zillmer, GEOMAR, Kiel

ISO-89 3-D reflection Seismic Survey

The goal of this study was to determine the reflection strength of structures in the Earth's crust at the KTB area (Zillmer *et al.*, 2002; see also Müller & Zillmer 2002).
The KTB (German continental deep drilling program) was preceded by the ISO-89 seismic survey. The largest experiment was a 3-D reflection survey, which covered an area of 20 x 20 km with the KTB site at its centre. 3300 shots were performed, and each shot was recorded by 478 geophones on 10 parallel lines with a maximum source-receiver offset of 6.2 km. A vibroseis source with a frequency range 12 – 48 Hz was used.
The two most important reflecting structures in the depth range 2-15 km are the Erbendorf body (EB), a high-velocity structure, and the steep event 1 (SE1), a fault-like continuation of the Franconian Lineament (FL) to depth. The FL separates sediments in the SW from crystalline rocks in the NE. Images of the subsurface obtained by migration methods have shown that the SE1 dips steeply to the northeast at an angle of approximately 55 degree (Harjes *et al.*, 1997; Körbe *et al.*, 1997; Buske 1999). A refracted wave from the EB was recorded in a wide-angle seismic experiment (DEKORP, 1988; Gebrande *et al.*, 1989).
1800 single shots northeast of the FL were investigated. Reflection signals from the SE1 and EB were found in 80 and 70 shots, respectively. The SE1 reflections are located in the following regions: at 6 km southeast of the KTB (3.8 – 5.4 km depth), at 3.5 km south (4.3 – 5.2 km depth), and at 8 km northwest (5.1 – 6.4 km depth). The G, B and R10 reflections at 10, 11 and 15 km depth and the R1 reflector are considered to be part of the EB. The R1 reflector is located at 7 km southeast of the KTB in 8.4 – 11.5 km depth.
Reflection coefficients of the SE1 and EB were obtained by comparing the measured amplitude ratios SE1/Pg and EB/Pg with the corresponding ratios in synthetic seismograms. The Pg wave was used as a reference wave. It is the first arriving wave, which propagates in the upper crystalline crust. The thickness of the SE1 and EB is constrained by the time length of their reflection signal, which does not exceed the pulse duration of the Pg wave. For the SE1 a thickness between 50 and 300 m is concluded from the time length of the signal, and an upper limit of 350 m thickness is estimated for the EB. The steep-angle ISO-89 3-D measurements have only detected the top of the EB, otherwise its refracted wave would not have been observed for tens of kilometres in wide-angle measurements. In the interior of the EB, a smooth decrease in velocity is compatible with the interpretation of the wide-angle measurements, *i.e.*, a high-velocity zone on top of rocks with more normal crustal velocities.

Modelling of Wave Propagation

Short-profile refraction measurements have shown that there are high velocities of 5 km/s close to the surface in the area northeast of the FL. From borehole logs it is known that Vp values of 6 and 6.3 km/s are reached at 1 and 3 km depth, respectively. For greater depth the velocity is varying around the average value 6.3 km/s. The Sg wave can be occasionally seen in single-shot sections, and a value of Vs = Vp / $\sqrt{3}$ is confirmed by the borehole logs. The density is determined by the Nafe-Drake relation for crustal rocks, rho = 1.8 + 0.15 Vp. Attenuation is described by a frequency independent Qp factor in the range between 250 and infinity. An exception is the first kilometre depth were the strong amplitude decay of the Pg wave can only be explained by very low Qp values smaller than 100. Qs is set to 4/9 Qp.
Synthetic seismograms are computed with the ray method and with the reflectivity method for a 1-D velocity-depth model. Dynamic ray tracing is performed by solving a set of

ordinary differential equations for the travel time and the amplitude of the seismic ray. The radiation pattern and the free-surface conversion are included in the computations. The reflectors are dipping planes with a complicated internal 1-D structure. A frequency-dependent reflection coefficient for a stack of layers is computed.

A detailed comparison of observed and computed pulse forms is difficult due to scattering and noise in the data. The polarity of the reflections could also not be determined. The amplitude ratios SE1/Pg and EB/Pg in the data are compared to the amplitude ratios in synthetic seismograms. For the SE1 a velocity decrease was used based on the assumption that the SE1 is a fault zone; the velocity increases at the boundary to the EB, which is known as a high-velocity body. The reflector-zone model for both the SE1 and the EB (R1) must have pronounced parameter contrasts in order to explain the observed amplitude ratios. The size of the velocity jumps and reflection coefficients varies with the assumption about the damping. It also varies with the type of discontinuity: A first-order discontinuity describes the case of the strongest velocity jump. A thin layer with a thickness of the quarter of a wavelength leads to constructive interference and therefore describes the smallest velocity jump. For the thin layer case and Qp = 500 at depths greater than 1 km, velocity changes from 6.3 to 5.4 km/s at the SE1 and from 6.3 to 7.4 km/s for the EB (R1) explain the amplitude relations SE1/Pg and EB/Pg in the data. For the model of a first-order discontinuity we obtain reflection coefficients of -0.11 and +0.09 for the SE1 and EB(R1), respectively. The angles of incidence are smaller than 15 degree. In the case of the EB there are also less reflecting parts B, G and R10 with velocity jumps from 6.3 to 6.8 km/s for the first-order discontinuity models.

Conclusions

The SE1 results of this study quantitatively support the view that it is a cataclastic thrust-fault zone, which continues the FL into the crust. The EB reflector has a cataclastic top zone with a thickness of a few hundred meters. Such a zone could possibly be the result of sill-like intrusion of the high-velocity body into the crust.

References

Buske, S., 1999. Three-dimensional pre-stack Kirchhoff migration of deep seismic reflection data. Geophys. J. Int. **137**, 243-260.

DEKORP Research Group, 1988. Results of the DEKORP4/KTB Oberpfalz deep seismic reflection investigations. J. Geophys. **62**, 69-101.

Gebrande, H., M. Bopp & T. Schmidt, 1989. Crustal structure in the surroundings of the KTB drill site as derived from refraction and wide-angle seismic observations. In: Emmermann, R. & J. Wohlenberg (eds.). The German continental deep drilling program. Springer, Berlin, ISBN 3-540-50922-4, 151-176.

Harjes H.-P., K. Brahm, H.-J. Dürbaum, H. Gebrande, G. Hirschmann, M. Janik, M. Klöckner, E. Lüschen, W. Rabbel, M. Simon, R. Thomas, J. Tormann & F. Wenzel, 1997. Origin and nature of crustal reflections: Results from integrated seismic measurements at the KTB superdeep drilling site. J. Geophys. Res. **102**, 18267-18288.

Körbe, M., M. Stiller, H. Horstmeyer & T. Rühl, 1997. Migration of the 3-D deep-seismic reflection survey at the KTB location, Oberpfalz, Germany. Tectonophysics **271**, 135-156.

Seismology on a Small Scale: Acoustic Emission Measurements in Rock Mechanics

Thomas Spies, BGR, Hannover
Jürgen Hesser, BGR, Hannover
Jürgen Eisenblätter, GmuG, Ober-Mörlen

Abstract

The application of acoustic emission (AE) measurements in rock mechanics is outlined. Results of the operation of an AE network in a mine are presented which provide a contribution for the evaluation of the hydraulic integrity of the rock and the stability of the cavities. The locations of AE events and their magnitudes were determined using a network of 24 sensors. High AE activity was found between the closely spaced rooms. The exact location of a small drift connecting two rooms in the level of their roofs could be reconstructed by the AE activity around its contour.

Introduction

Seismology and acoustic emission measurements (AE) are related fields, which use the phenomenon that in case of sudden fracturing in a rigid body, stored elastic energy is released in form of seismic waves. The sources of AE basically show the same properties as earthquakes but on a much smaller scale. Because there is a large difference in source dimension, which can be hundredths of kilometres in case of an earthquake and millimetres in case of a microcrack, the frequency content of the seismic waves released by the different facture processes is also very different. The investigated range of frequency of AE measurements in non-destructive inspection and in laboratory measurements with rock samples is between 5 kHz and about 1 MHz whereas in case of AE measurements in the field it is between about 1 kHz to 100 kHz. Many methods of data evaluation have been transferred from seismology to AE measurements to derive the location, magnitude, seismic energy as well the source mechanism and orientation of AE events (*e.g.*, Ohtsu, 2000; Niitsuma, 2000; Manthei *et al.*, 2000).

In rock mechanics AE measurements are applied in the laboratory and in the field, mainly in mining, as they provide unique information on microfracturing in the rock. In case of mining, *e.g.*, for mineral extraction and in case of the disposal of wastes underground, the hydraulic and the mechanical integrity of the rock are necessary requirements for the safe and economic operation and for the long-term safety. They have to be evaluated and monitored. Changes of the permeability of the rock and of the stability of cavities result from the formation of micro- and macrocracks while and after the driving of the cavities. In the laboratory AE measurements are applied in basic investigations of the relations between microcracking, material damage, permeability change and macroscopic failure of the rock (Spies *et al.*, 2000). In the mines the results of AE monitoring provide the identification of regions in which microfracturing takes place and in which changes of permeability and stability have to be expected (*e.g.*, Spies *et al.*, 2002). AE measurements were conducted with salt rocks and granite rocks in context with the research for the disposal of radioactive waste underground (*e.g.*, Falls & Young, 1998; Manthei *et al.*, 2000; Spies & Eisenblätter, 2001; Spies, 2001).

As an example for the application of AE methods in rock mechanics, results of an operation in a salt mine are presented in this paper. The mine of Morsleben located between the towns of Braunschweig and Magdeburg in northern Germany is used as a repository for low-level radioactive waste since 1978. It is a salt deposit with thick folded strata of rock salt in succession with strata of anhydrite, potash

and salt clay (Behlau & Mingerzahn, 2001). The waste is disposed of in large rooms mainly in rock salt. In specific segments of the mine geomechanical investigations are performed to characterize the rock behavior by strain and stress measurements, hydraulic measurements and AE measurements.

AE Measurements in a Salt Mine

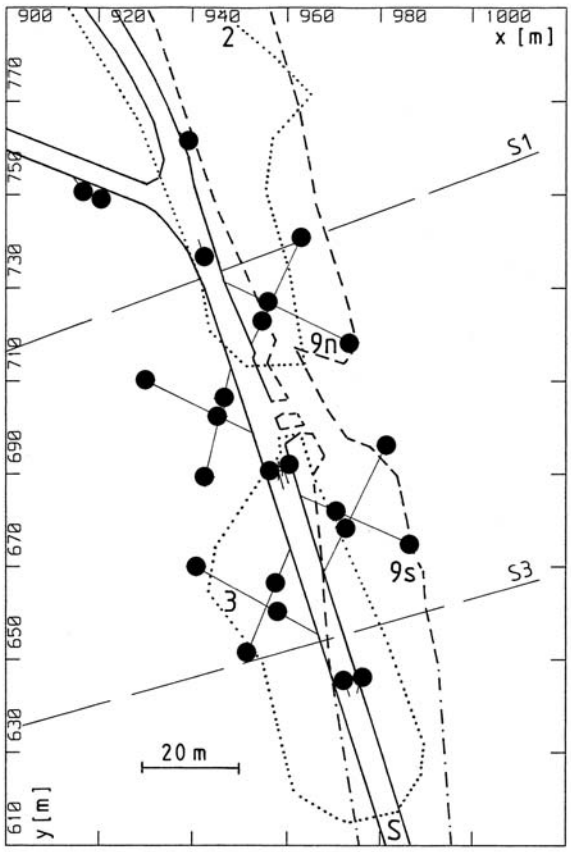

Figure 1: Plan view of the monitored region with the projection of three levels plotted one upon another: upper level in dashed lines (Rooms 9n and 9s), intermediate level in solid lines (Drift S), lower level in dotted lines (Rooms 2 and 3). The AE sensors in the boreholes are denoted by the black dots. The profile lines of the vertical cross sections S1 and S3 through the cavities are indicated (see Figs. 2 and 3).

Description of Operational Site

Fig. 1 displays a segment of the Morsleben mine in a plan view (horizontal projection) where cavities with close spacing were mined in rock salt about 70 years ago. The orientation of the y-axis is south to north and of the x-axis west to east. In this plan view three different levels are displayed one upon another in a rather complex arrangement: the Rooms 9n and 9s at the upper level in dashed lines, the drift S at the intermediate level in solid lines and the Rooms 2 and 3 at the lower level in dotted lines. To clarify this complex figure, the vertical cross section along the profile line S1 shown in Fig. 2 can be used. In Fig. 2 the large Room 9n at the upper level, the drift S at the intermediate level and the large Room 2 at the lower level are displayed using the same signatures as in Fig. 1. The vertical section of profile line S3 exhibits a similar arrangement for the southern vertical row of cavities in Fig 1. The average depth level of the cavities displayed is 500 m. In the drift of the intermediate level fissures in the walls and floor heave were observed. The opening of the fissures is controlled by strain measurements, which resulted in opening rates of 0.2 mm/a.

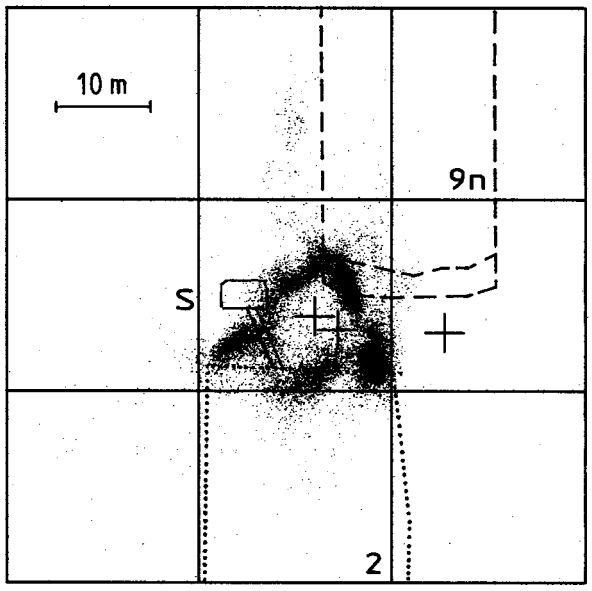

Figure 2: Cavities in the vertical cross section S1 and locations of AE with magnitudes M > 0 dB as dots (data of one month, 17,241 events).

Measuring Principle and Methods

To monitor the situation displayed in Fig. 1 an AE network is used. The piezoelectric sensors were installed in boreholes of 3 to 30 m length. The locations of the sensors are denoted by the black dots. The deeper boreholes are equipped with two sensors. All boreholes were drilled from the drift, as the large rooms are not accessible with drilling equipment. So only AE events in the region between the large rooms can be located. From the geomechanical

point of view this is no disadvantage as the stress concentrations are expected between the large rooms.

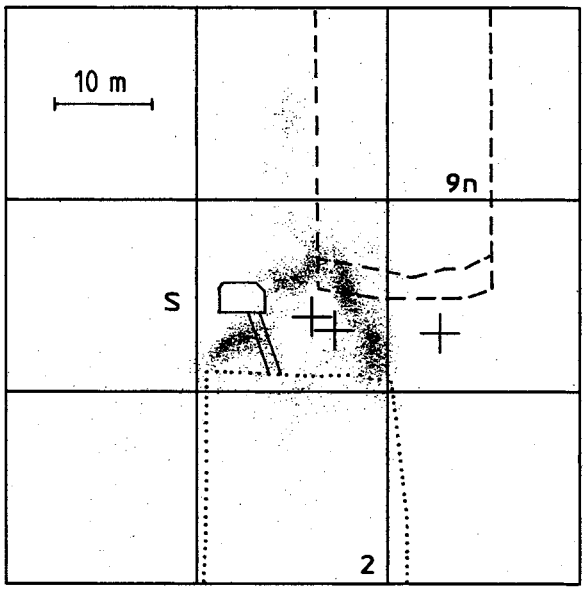

Figure 3: Cavities in the vertical cross section S1 and locations of AE with magnitudes M > 40 dB as dots (data of one month, 3320 events).

The seismic signals are recorded in the frequency range from 1 to 100 kHz. Using this range, a high sensitivity and a location accuracy of about 1 m is achieved in distances up to 50 m from the sensor network. The locations of AE events are determined automatically on site by inversion of the travel times of P-waves and S-waves, which are extracted from the signals. A measure of strength analogue to the magnitude in seismology is determined on site, too. The maximum amplitudes of the 24 sensor signals and the distances of the AE source from the sensors are used to this end. We define the mean amplitude at a reference distance of 50 m from the source as the AE magnitude of the source specified in dB. Typical waveforms of an AE event, here of 12 of the 24 sensors, are shown in Fig. 4.

Results

As examples for the obtained AE locations, Figs. 2 and 3 show data of a spatial interval with a thickness of 20 m in the direction perpendicular to profile S1. The data of this interval are projected into the vertical cross section S1. Fig. 2 contains all events regardless of magnitude whereas in Fig. 3 only larger events with magnitudes M > 40 dB are included. Some of the microcracks seem to be located inside the openings. At one hand this can be explained by variations of the geometry of the rooms perpendicular to the profile line S1. In this 20 m horizontal interval the level of the floor of Room 9n is varying as indicated by the two lines in Figs. 2 and 3. Furthermore Room 2 has a more irregular shape of the roof compared to the information provided by standard mine survey. The crosses in Figs. 2 and 3 denote the locations of sensors in the horizontal interval.

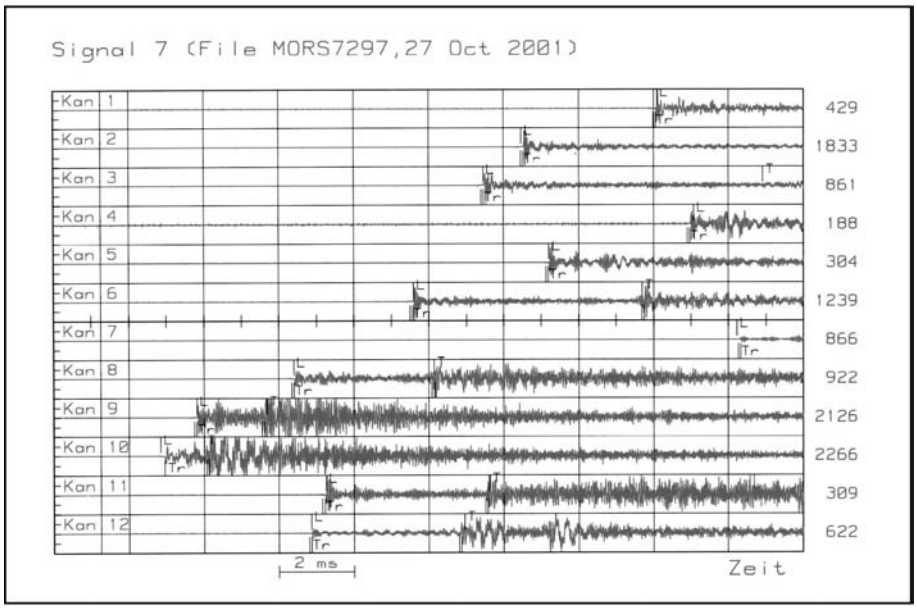

Figure 4: Section of signals of an acoustic emission event recorded by 12 of the 24 sensors. Time interval 2 ms, displayed is a time window of 20 ms, whole record length 40 ms. Peak amplitude in mV is shown at the end of each track. Tr: triggered P wave onset. L, T: calculated onset times of P and S waves, respectively.

The locations in Figs. 2 and 3 show dense accumulations between the edges of the rooms. Especially in case of the larger events with magnitudes M > 40 dB in Fig. 3 narrow bands of AE events can be recognized. The density of locations indicates a high geomechanical load in these so-called shear bands. The reason for the microcrack generation are high stresses around the cavities leading to creep deformation of the rock salt accompanied by dilatancy (Hunsche & Hampel, 1999). One distinct difference between the distributions of locations of events with lower magnitudes M < 40 dB in Fig. 2 and those with larger magnitudes M > 40 dB in Fig. 3 is found. Above the roof of Room 2 at the lower level only events with lower magnitudes M < 40 dB occur.

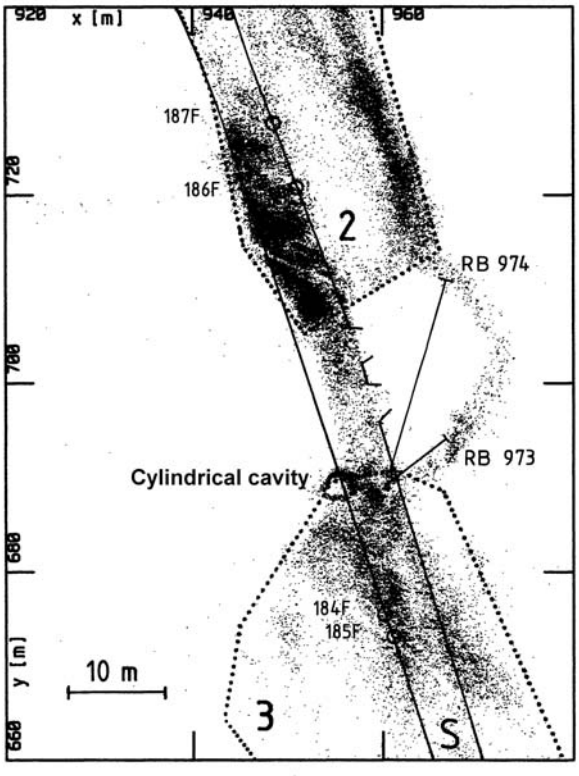

Figure 5: Plan view of intermediate level (Drift S) and lower level (Rooms 2 and 3). The AE locations of a 2 m thick depth interval between the floor of the intermediate level and the roof of the lower level are displayed (data of one year, 72,902 events). Two boreholes were drilled from the drift to verify the existence of the bow shaped small drift. Small circles mark strain measurements at fissures in the walls.

The AE locations were compared to results of geomechanical model calculations providing the distributions of stresses and deformations around the cavities (static calculations). Deviatoric stresses and deformations, characterizing the shear loading of the rock, are found to be high between the edges of the openings and they show the same band-like spatial distribution as the stronger AE events in Fig. 3. On the other hand it was found that tensile stresses exist above the roof of Room 2 where the weak AE events of Fig. 2 occur. So the comparison of locations of AE events and the results of geomechanical model calculations showed close agreement in their spatial distributions and it allowed to draw conclusions on the source mechanism of the located microcracks.

Fig. 5 is a plan view showing AE locations in a 2 m thick vertical interval in the middle between the roofs of Rooms 2 and 3 and the floor of Drift S. Here only the contours of the drift at the intermediate level in solid lines and the Rooms 2 and 3 at the lower level in dotted lines are given. The contours have been revised in comparison with the results of standard mine survey (see Fig. 1) to be consistent with the observed spatial distribution of AE. Again it can be seen that the AE activity is limited to the rock directly above the roof of the lower rooms. The AE locations also map smaller loaded elements of the arrangement of cavities indicating the achieved accuracy of location of less than 1 m. For instance, a roughly cylindrical cavity with a vertical axis and with a diameter of 2 m can be recognized as a ring of AE (see notation in Fig. 5). This cavity is a vertical connection from the floor of drift S down to the roof of Room 3. Furthermore specific activity outside the cavities which were documented in the mine's maps, in the shape of a bow is observed connecting the corners of Rooms 2 and 3. From detailed analysis of the locations it was concluded that there could be another small drift causing this unexpected activity. As the lower rooms are not accessible to look for such a feature this had to be proofed by two boreholes (see notation RB 973 and RB974 in Fig. 5). The boreholes reached the proposed drift in the predicted locations within accuracy better than 1 m.

Summary

In rock mechanics AE measurements are used in the laboratory and in the field as they provide unique information on the generation of microfracturing in rocks. They contribute to the evaluation of hydraulic and mechanical integrity in rock engineering projects, for instance in mining. As an example, an application of AE measurements in a mine is presented. They were carried out to monitor microcrack generation between closely spaced cavities in an underground repository for low level radioactive waste. The locations of AE events and their magnitudes were determined. Regarding the density of events high AE activity was found between the large rooms. By comparison of the AE results with the results of geomechanical model calculations a differentiation of microcracks with shear mechanisms and those with tensile mechanisms could be performed. The exact location of a small drift connecting two rooms in the level of their roof could be reconstructed by the AE activity around its contour. From the obtained results on the microcrack generation and from other geomechanical investigations not discussed in this paper, it was concluded that permeability had increased between the large rooms and it will further increase due to continuing microcracking. It was also concluded that the roofs of Rooms 2 and 3 should be supported to preserve their stability permanently, *e.g.*, by backfilling of the rooms.

References

Behlau, J. & G. Mingerzahn, 2001. Geological and tectonic investigations in the former Morsleben salt mine (Germany) as a basis for the safety assessment of a radioactive waste repository. Engineering Geology **61**, 83-98.

Falls, S. D. & R. P. Young, 1998. Acoustic emission and ultrasonic-velocity methods used to characterise the excavation disturbance associated with deep tunnels in hard rock. Tectonophysics **289**, 1-16.

Hunsche, U. & A. Hampel, 1999. Rock salt – the mechanical properties of the host rock material for a radioactive waste repository. Engineering Geology **52**, 271-291.

Manthei, G., J. Eisenblätter, & T. Spies, 2000. Acoustic emission in rock mechanics studies. In: Kishi, T., M. Ohtsu, S. Yuyama, (eds.). Acoustic emission – beyond the millenium. Elsevier, Oxford, ISBN 0-08-043851-2, 127-144.

Niitsuma, H., 2000. Acoustic emission / microseismic technique: review of research in the 20th century. In: Kishi, T., M. Ohtsu, S. Yuyama, (eds.). Acoustic emission – beyond the millenium. Elsevier, Oxford, ISBN 0-08-043851-2, 109-126.

Ohtsu, M. (2000): Moment tensor analysis of AE and SiGMA Code. In: Kishi, T., M. Ohtsu, S. Yuyama, (eds.). Acoustic emission – beyond the millenium. Elsevier, Oxford, ISBN 0-08-043851-2, 19-34.

Spies, T., H.-J. Alheid & O. Schulze, 2000. Einsatz ultraschallseismischer Verfahren zur Untersuchung der hydraulischen Integrität des Gebirges. Felsbau **18(5)**, 119-126.

Spies, T. & J. Eisenblätter, 2001. Acoustic emission investigation of microcrack generation at geological boundaries. Engineering Geology **61**, 181-188.

Spies, T., 2001. Comprehensive study of microfracturing in salt rock. In: Aswegen, G. van, R. J. Durrheim, W. D. Ortlepp (eds.). Proc. V. International Symposium on Rockbursts and Seismicity in Mines (RaSiM5), Magaliesberg, Südafrika. The South African Institute of Mining and Metallurgy, Johannesburg, Symposium Series **27**, 167-172.

Spies, T., J. Eisenblätter & G. Manthei, 2002. Neue Entwicklungen in der Mikroakustik am Beispiel von Messungen im Endlager Morsleben. Z. Angew. Geol. **2002(2)**, 30-37.

Automatic Monitoring of Induced Seismicity

Michael Roth, NORSAR
Volker Oye, NORSAR

The production of hydrocarbon reservoirs, the exploitation of hydrothermal fields and mining activity in general are associated with microseismicity. Changes in the local stress field and pore pressure can initiate sudden movements along existing faults or can generate new fractures which in turn results in the emission of seismic energy. Hence, the monitoring and analysis of microseismic events has the potential to delineate the internal structure of the subsurface, to get information on present stress conditions and to image dynamic processes like subsidence and fluid flow.

We have developed a software system for the automatic monitoring of microseismic data recorded by a vertical 3C geophone string deployed in an observation well. The system facilitates the interactive input of geophone positions, data formats, seismic velocities and technical parameters for the individual processing steps. Additionally it provides an interactive module to determine the orientation of the geophones.

The key elements of the automatic data processing are detection, phase picking, polarization analysis and the localization. Our detection algorithm is based on the continuous evaluation of the signal-to-noise ratio (SNR) at each individual geophone. To be considered as seismic event, the seismic signals must exceed a certain SNR threshold at a specified number of geophones. Once detected, the P- and S-wave onsets are picked automatically using an autoregressive method (Leonard & Kennett, 1999; Akaike, 1973). The direction of the incoming wave field (azimuth and incidence) is determined from the P-wave polarization analysis (*e.g.*, Vidale, 1986). In the final step the processing results (P-, S-wave arrival times, azimuth and incidence angles) are inverted for the event hypocenter. Depending on the velocity model we use a linearized master event technique (homogeneous model) or a directed grid search (arbitrary 3D velocity model) using tabulated wave field parameters computed with NORSAR's 3D ray tracing software.

In a first application we processed a microseismic data set that was acquired during a hydrofracturing experiment. The data were continuously recorded with twelve 3C geophones deployed in an observation well close to the injection well. During the 1-hour period of the experiment about 4000 microseismic events occurred.

Before we started the automatic processing we calibrated the receiver string in order to obtain a consistent geophone orientation (usually in borehole deployments the orientation of the geophones is not known). To this end we determined the P-wave polarization and thus the direction of the incoming wave field for a small number of selected high-quality events. For an individual event the orientation from one geophone to the other varied up to 20º. For a specific geophone the orientation varied up to 10º for different events. We averaged the deviations at the individual geophones over all events and used these values to rotate the seismic data into a common coordinate system.

Out of the 4000 events, about 1000 passed our threshold criterion of a SNR better than 3 at at least 9 geophones, and were automatically processed and located. The localization was based on the assumption of a homogeneous P- and S-wave velocity model, because detailed information on the small-scale velocity structure was not available. Fig. 1 shows north of the geophone string a well-defined cluster of about 300 events with a relative location error (normalized by the epicentral distance) smaller than 5%. The events scattered in the westerly direction are mislocated events. A closer inspection of the waveform data showed that for those events the P-wave arrivals were very weak and that the automatic phase picker took the S-wave signal instead. In fact these events occurred also within the cluster in the

north, but due to the 90 deg rotated S-wave polarization the locations were mapped to the west. The cluster of well-located events occurs on a more or less vertical plane (about 100 x 100 m) with a distinct northeasterly strike (Fig. 1).

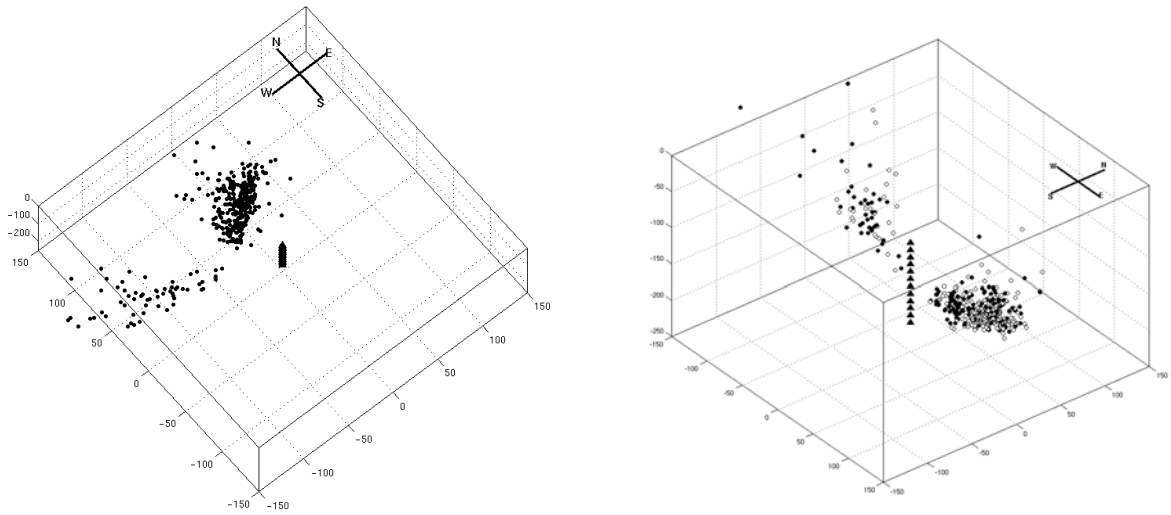

Figure 1: Microseismicity induced by hydrofracturing. The seismic data were acquired with twelve 3C geophones (triangles) deployed in an observation well. Left: Top view from SW. Right: View from SE.

The location error depends on the accuracy of the velocity model and the accuracy of the wave field parameters determined by the automatic processing. Our experience with several data sets shows that the automatic picking of the P- and S-wave arrivals works relatively well. For reasonable SNRs (> 3) the P-wave could be picked with an accuracy of 1 to 2 samples, the S-onset usually is associated with a somewhat larger uncertainty of 2 to 4 samples, because of the interfering P-wave coda. For our applications those errors roughly result in a location uncertainty of a few meters.

More critical and significant are uncertainties of the azimuth and incidence angle, which are determined from the P-wave polarization analysis. Uncertainties already arise from the determination of the geophone orientation, since this requires a detailed velocity model. In our applications the uncertainties for azimuth and incidence angle were typically 5 – 10º and 10 – 15º, respectively. For the borehole configuration large errors of the incidence angle can be compensated by the more accurate phase arrival times, since the P- and S-wave move-out also contains the information on the incidence angle. However, due to the cylindrical symmetry of the configuration the azimuths are essential for the localization, and especially for larger distances their uncertainties dominate the location errors. A combination of multiple boreholes or the instrumentation of deviated observation well would break the cylindrical symmetry and generally will improve the location accuracy.

References

Akaike, H., 1973. Information theory and an extension of the maximum likelihood principle. In: Petrov, B. N. & F. Csáki (eds.). 2nd International Symposium on Information Theory, Tsahkadsor, Armenia, USSR, September 2-8, 1971. Akadémiai Kiadó, Budapest, 267-281.

Leonard, M. & B. L. N. Kennett, 1999. Multi-component autoregressive techniques for the analysis of seismograms. Phys. Earth Planet. Int. **113**, 247-263.

Vidale, J. E., 1986. Complex polarization analysis of particle motion. Bull. Seism. Soc. Am. **76**, 1393-1405.

On the Relationship Between Seismic Moment and Source Volume

Erhard Wielandt, Stuttgart

Summary

A nonzero isotropic moment of a seismic source does not by itself indicate a change of the source volume, nor does its absence indicate a constant volume. Any isotropic moment may be associated with any positive or negative volume change of the source itself. A definite and general relationship exists however between the isotropic moment and the volume displaced through spherical surfaces enclosing the source.

The Problem

Gerhard Müller (2001a) has noted an apparent inconsistency between two relationships used to calculate the volume change δV of a seismic source from the isotropic part of its moment-tensor representation. The diagonal elements M of the isotropic tensor $\mathbf{M}_{iso}$ are one-third of the trace of the original moment tensor $\mathbf{M} = (m_{ij})$ each. The relationships in question are

$$M = (\lambda + 2\mu / 3)\, \Delta V \qquad (1)$$

following Bowers & Hudson (1999) and others (for references see Müller, 2001a), and

$$M = (\lambda + 2\mu)\, \delta V \qquad (2)$$

following Müller (1973a) and equivalent formulae for the seismic far-field derived by Wielandt (1972, 1975). Both formulae have been applied to spherical sources; however for $\mu > 0$ eq. (1) gives a larger source volume than eq. (2). The apparent inconsistency has not fully been resolved in Müller's note; he shows however that eq. (1) applies to the moment-tensor equivalent of a plane or curved crack and eq. (2) to the moment-tensor equivalent of a spherical explosive source. Aki & Richards (1980) show in the first edition of their textbook that ΔV in eq. (1) generally specifies the 'transformational', *i.e.*, hypothetical isobaric, volume change of the material in the source. We reserve the symbol ΔV to this definition. In the case of cracks, ΔV is also the actual change, but this is not generally true for other sources. The second edition (Aki & Richards, 2002) clarifies that the actual volume change of a spherical source is δV as obtained from eq. (2). It is smaller than ΔV because the expansion of the source is not isobaric but constrained by the surrounding material. What the moment-to-volume relationship might be for other source geometries has remained open. In the present note we find that the ratio between the isotropic moment and the volume change can have any positive or negative value, depending on how the source volume itself is defined. Eq. (2) is however generally valid if we understand δV as the volume displaced through a spherical surface enclosing the source.

The Volume Change of General Sources

We consider only the permanent displacement field associated with the final value of the moment tensor in unbounded, homogeneous and isotropic media.

Spherically expanding sources are exceptional in that their outer displacement field is divergence-free; their change of volume can be measured over any closed surface containing the source. In general, the displacement field of a seismic source has a nonzero divergence outside the source, and the volume change depends on the surface over which we measure it. As the interface between the "source" and the "medium" is to some extent arbitrary, so is the volume change. As will be shown below, uniqueness can be restored by restricting the interface to a spherical shape.

As an extreme, although seismologically unrealistic, example let us consider the displacement field of a linear vector dipole (LVD) in the z direction, represented by a moment tensor in which m_{zz} is the only nonzero element. Its divergence has the

mathematical form of a quadrupole potential: it is proportional to $P_2(\cos\theta) / r^3$, where P_2 is the Legendre polynomial of degree 2, θ the co-latitude and r the distance from the source. The integral of the divergence, taken over a cone either in the polar or in the equatorial direction, diverges logarithmically to minus or plus infinity. Thus, by adding part of such a cone to the original source volume, we can mathematically construct a source whose volume change for a given moment has a predefined negative or positive value. Obviously, any statement on the volume change without a detailed definition of the source volume itself would be meaningless.

More realistic, consider a situation where incompressible magma is stored in a spherical chamber and then injected into a dike. The total volume of the cavities remains constant. When a volume δV migrates from the chamber into the dike, the isotropic moment of the chamber decreases by $M = (\lambda + 2\mu)\,\delta V$ while the isotropic moment of the dike, idealized as a crack, increases by $M = (\lambda + 2\mu / 3)\,\delta V$. An isotropic moment $M = (4\mu / 3)\,\delta V$ disappears in the process. This quantity would be inferred from seismic observations as the isotropic moment of the composite source, and a conventional interpretation would suggest a reduction of the magma volume, yet actually the volume reduction has occurred in the surrounding medium. The walls of the dike, which are not part of the source, were compressed while the walls of the spherical chamber retained their volume. Alternatively, we may consider the case that the magma is compressible, and expands in the process so that the compression of the dike walls is made up. Despite this expansion of the source, the overall volume is constant and the isotropic moment is zero. Intermediate between the two cases we find expanding sources whose isotropic moment is negative. This example does not appear to be far-fetched, and should caution against an uncritical application of any moment-to-volume relationship.

In heterogeneous or anisotropic media, even a purely deviatoric moment tensor will in general be associated with a net change of volume, which might then be misinterpreted as indicating an isotropic moment. Since the source geometry of tectonic earthquakes is often well constrained, its uncertainty may be of secondary importance as compared to the effects of heterogeneity or anisotropy. The fundamental consideration remains however the same: large, mathematically infinite volume changes occur outside any source with a deviatoric moment; far-field observations cannot distinguish them from those of the source itself.

The Volume Displaced Through Spherical Surfaces

It can be shown that a source with the isotropic moment M displaces the volume

$$\delta V = M / (\lambda + 2\mu) \qquad (3)$$

through any spherical surface that encloses the source. This result is obtained in four steps.

1 – The displacement field of a linear vector dipole can be calculated analytically. The radial component of the displacement can then be integrated over the surface of a sphere centered at the source. The result is given by eq. (3), independent of the radius of the sphere. The derivation is based on formulae for the displacement field of a point force taken from Gerhard Müller's lecture notes on the theory of elastic waves (1986), and was double-checked with the computer-algebra system MuPAD Pro 2.5 (2002).

2 – The result can be generalized to spherical surfaces that are not centered around the point source but enclose it. The result is the same as for centered spheres. The mathematical proof is simple but not given here.

3 – Eq. (3) being true for any position of a point source within a given sphere, it remains valid for distributed sources.

4 – An arbitrary moment tensor is the combination of three LVDs along its principal axes, so eq. (3) is valid for any moment-tensor source.

Equation (3) appears to be the most general moment-to-volume relationship that can be derived without a detailed knowledge of the source geometry. It retains its physical

meaning for point sources, for which a volume change is otherwise difficult to define.

Acknowledgments

Most of this work was done while I was Green scholar at the Institute of Geophysics and Planetary Physics of the Scripps Institution of Oceanography, University of California at San Diego, an opportunity for which I am deeply grateful. Discussions with Gerhard Müller, Paul Richards and Torsten Dahm are gratefully acknowledged.

References

Aki, K. & P. G. Richards, 1980. Quantitative Seismology — Theory and Methods, volume 1, W. H. Freeman and Co., San Francisco, ISBN 0-7167-1058-7, xiv+556+16 pp.

Aki, K. & P. G. Richards, 2002, Quantitative Seismology — Theory and Methods, 2nd edition, University Science Books, Sausalito, California, ISBN 0-935702-96-2, xviii+700 pp.

Bowers, D. & J. A. Hudson, 1999. Defining the scalar moment of a seismic source with a general moment tensor, Bull. Seism. Soc. Am. **89**, 1390-1394.

MuPAD Pro 2.5, 2002. www.sciface.com or www.additive-net.de

Wielandt, E., 1972. Anregung seismischer Wellen durch Unterwasserexplosionen, Dissertation, Universität Karlsruhe, 120 pp.

Wielandt, E., 1975. Generation of seismic waves by underwater explosions, Geophys. J. R. astron. Soc. **40**, 421-439.

Mapping Upper Mantle Structure Using Waveform Diffractography

Wolfgang Friederich, Frankfurt

Abstract

A brief review of a diffractographic approach to waveform inversion is given. It takes into account wave phenomena like wavefront healing, off-path sensitivity and Fresnel zones, which are ignored in ray-theoretical and path-integral methods. Basic building blocks are the use of exact sensitivity kernels in the inversion and an accurate modelling of wave propagation with a coupled-mode, multiple forward scattering algorithm. The method is applied to a set of 1600 regional long-period seismic shear and surface waveforms recorded in East Asia and a 3D model of S-velocity in the upper mantle is derived. Horizontal resolution is 400 km throughout the upper mantle with an improved resolution of 200 km in the upper 200 km. The 3D S-velocity model clearly maps the slabs in the West Pacific subduction zones, which appear to stagnate around the 660 km discontinuity. Other features are low velocities in the backarc region, a plume beneath the SW of the Baikal rift and colliding Indian and Asian lithosphere under Tibet.

Introduction

Seismic travel time tomography is based on the assumption that the sensitivity of travel time to Earth structure is confined to the geometrical ray path of the considered wave. Similarly, many waveform tomographic approaches (Woodhouse & Dziewonski, 1984, Nolet, 1990) assume that differences between observed and synthetic seismograms can be expressed by integrals over velocity perturbations taken along the great circle paths from sources to receivers. However, due to the finite wavelength of seismic waves sensitivity is spread around the geometrical ray path and may even alternate in sign as one moves away from the ray. In particular, it has been shown that the sensitivity of travel times to structural perturbations essentially vanishes along the ray (Marquering *et al.*, 1999). The reason for these phenomena is the existence of diffracted wave energy not following the ray path, which may strongly contribute to the observed signal. Diffraction also causes a decay of structural information in the waveforms by a mechanism called wavefront healing (Wielandt, 1987). Perturbations of structure larger than predicted by ray theoretical approaches are needed to produce a given change of the waveform or travel time. Thus, accounting for diffraction effects allows for a more realistic assessment of the amplitude of structural perturbations. Moreover, by using correct sensitivities in an inversion, the heterogeneities are placed at the right locations. Inferred structures are naturally smoothed due to the spatial extension of sensitivity. Inconsistencies caused by inaccurate predictions of waveform or travel time changes are avoided. Taken together, for a given set of data, these benefits lead to better Earth models compared to ray theoretical approaches.

In the following I give a brief account of a diffractographic approach to the inversion of long-period seismic shear waves and surface waves (Friederich, 2003). In addition to employing correct sensitivities, the propagation of the waves through the 3D-upper mantle is accurately modelled using a coupled-mode, multiple forward scattering approach (Friederich, 1999). The true misfit between observed and synthetic waveforms is calculated and the inversion is carried through several 3D-models. I start with an introduction to waveform sensitivity kernels, then sketch the basic idea of waveform diffractography, discuss resolution for a data set covering East Asia and finally show some sections through the 3D mantle model obtained for this region.

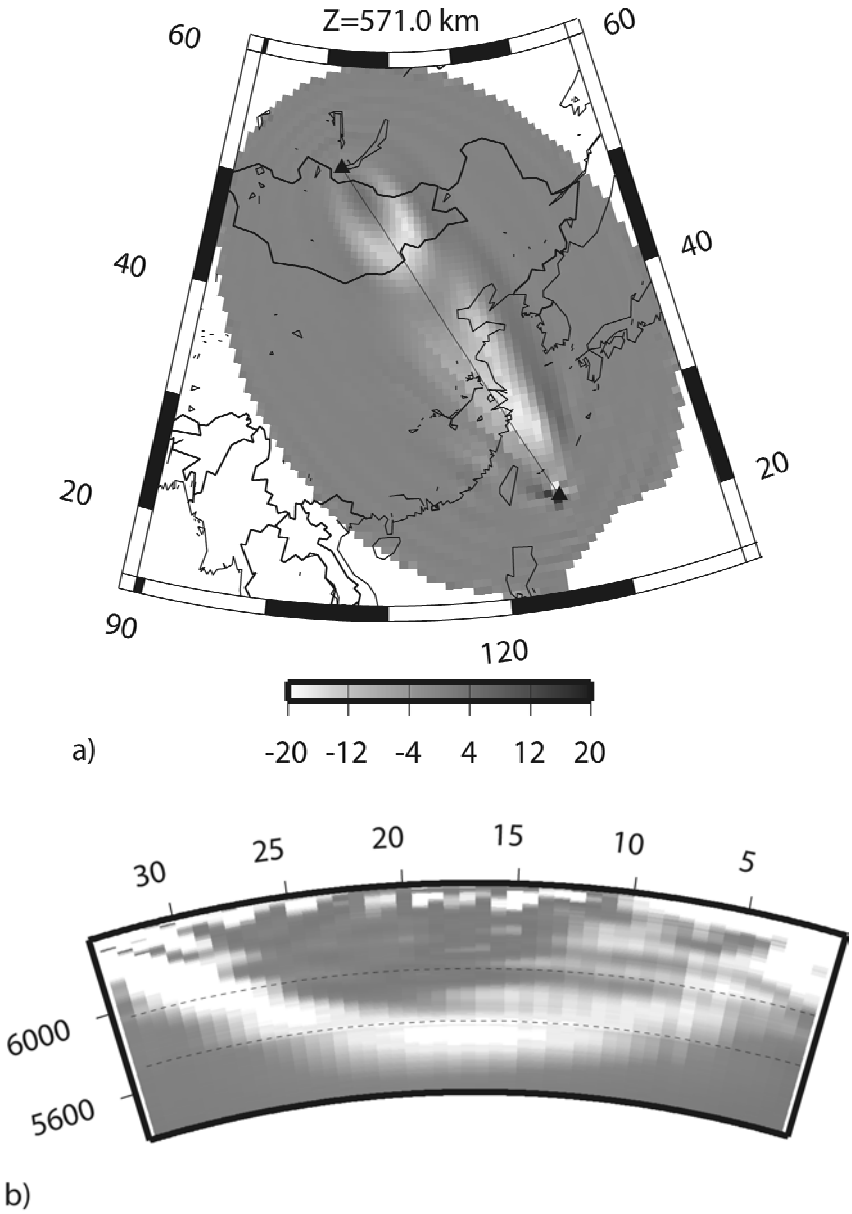

Figure 1: a) Horizontal cross-section through the sensitivity kernel at 571 km depth for an instant in the time window of the direct S wave. Scattered signal from bright areas contribute with a negative sign to the reference seismogram, the signal from dark areas contributes with a positive sign at the selected time instant. b) Vertical cross section through the same sensitivity kernel. Dark areas align with the geometric ray path of the direct S-wave. The dashed lines indicate the 410 and 660 km discontinuities.

Waveform Sensitivity Kernels

The partial derivatives of the synthetic seismograms with respect to changes of Earth structure are some times called sensitivity seismograms. If one plots the value of the sensitivity seismogram at a fixed time instant as a function of location in the Earth model one obtains a sensitivity kernel. A horizontal section through such a kernel for an earthquake close to Taiwan and a receiver near Lake Baikal at 571 km depth is shown in Figure 1a. The snapshot is taken in the time window of the direct S-wave. Positive perturbations of S-velocity located in the dark areas will produce a positive contribution to the synthetic seismogram at the selected time instant but a negative one if they are located in the bright regions. Note the asymmetry of the kernel with respect to the great circle path connecting source and receiver caused by the radiation pattern of the source. Note also the uneven distribution of sensitivity along the path. This can be understood by looking at a

vertical cross section through the same sensitivity kernel (source is on the right and receiver on the left), Fig. 1b. Again, positive perturbations of S-velocity in the bright regions will contribute negatively to the seismogram at the selected time instant. Apparently, only perturbations located in the neighbourhood of the geometric path of the direct S-wave have a significant influence on the synthetic seismogram. The bright patches in the horizontal cross section mark the penetration points of the geometric S-wave path through a spherical shell at 571 km depth. Sensitivity kernels are essential for a waveform inversion since they tell us where to place model perturbations to reduce misfit between synthetic and observed seismograms. Erroneous sensitivity kernels will cheat an inversion procedure into placing perturbations at the wrong locations. So, besides accurate synthetic seismograms, correct sensitivity kernels in accord with wave theory are an important ingredient for unbiased and realistically resolved Earth models.

Waveform Diffractography

Waveform diffractography differs in two major aspects from classical seismic tomography. First, it performs an accurate forward modelling of the seismic wavefield in accord with elastic wave theory, and second, it employs exact sensitivity kernels, which reflect the distributed nature of sensitivity, the existence of Fresnel zones and other wave phenomena like wavefront healing. The waveform inversion builds upon a linearized relation, which equates the difference between observed and synthetic seismogram to an integral over space of sensitivity kernel and velocity perturbations. All equations associated with the observed seismograms and their time samples are collected into a large system of equations which is solved in a least squares sense subject to additional smoothing constraints. Since the sensitivity kernels are spatially extended the system matrix is not as sparse as it would be in a tomographic inversion. For the data set of 1600 seismograms described below we obtained 36000 equations for 46000 velocity parameters. The system matrix had 400 million non-vanishing elements.

In the first iteration of the inversion, the velocity perturbations appearing in the linearized relations refer to one-dimensional, purely depth-dependent models specifically constructed for each observed seismogram by waveform inversion. In the following iterations they always refer to the previously obtained 3D-model. After each iteration step, synthetic seismograms and sensitivity kernels are updated. The model shown below was obtained after carrying the inversion through 4 iterations.

Data Set and Resolution

The waveform diffractography was applied to a data set of 1600 regional long-period shear and surface waveforms recorded in East Asia (Fig. 2). To assess the potential of a data set for mapping 3D-structures resolution tests are usually performed. However, their ability to tell which features of a model are real and which ones are artefacts is limited. There are several reasons for this fact:

- Systematic errors in the data and input parameters (hypocenter locations, moment tensors),
- Approximations in the physical theory by which the measured data are predicted, and
- The representation of true Earth structure by a finite number of parameters in the tomographic model.

If we assume that Earth structure is described by continuous functions of space the 3rd point implies that the tomographic inverse problem is generally underdetermined. It follows, that even for error-free data an infinite number of models exist which explain the data perfectly. For linear inverse problems (the predicted data depend linearly on the model), we can separate the space of model functions in two parts: model functions, which have an effect on the predicted data and those, which do not. The space of the no-effect model functions is often called the null-space. We can add any function from the null-space to a model without affecting the predicted data and therefore the fit to the observed data.

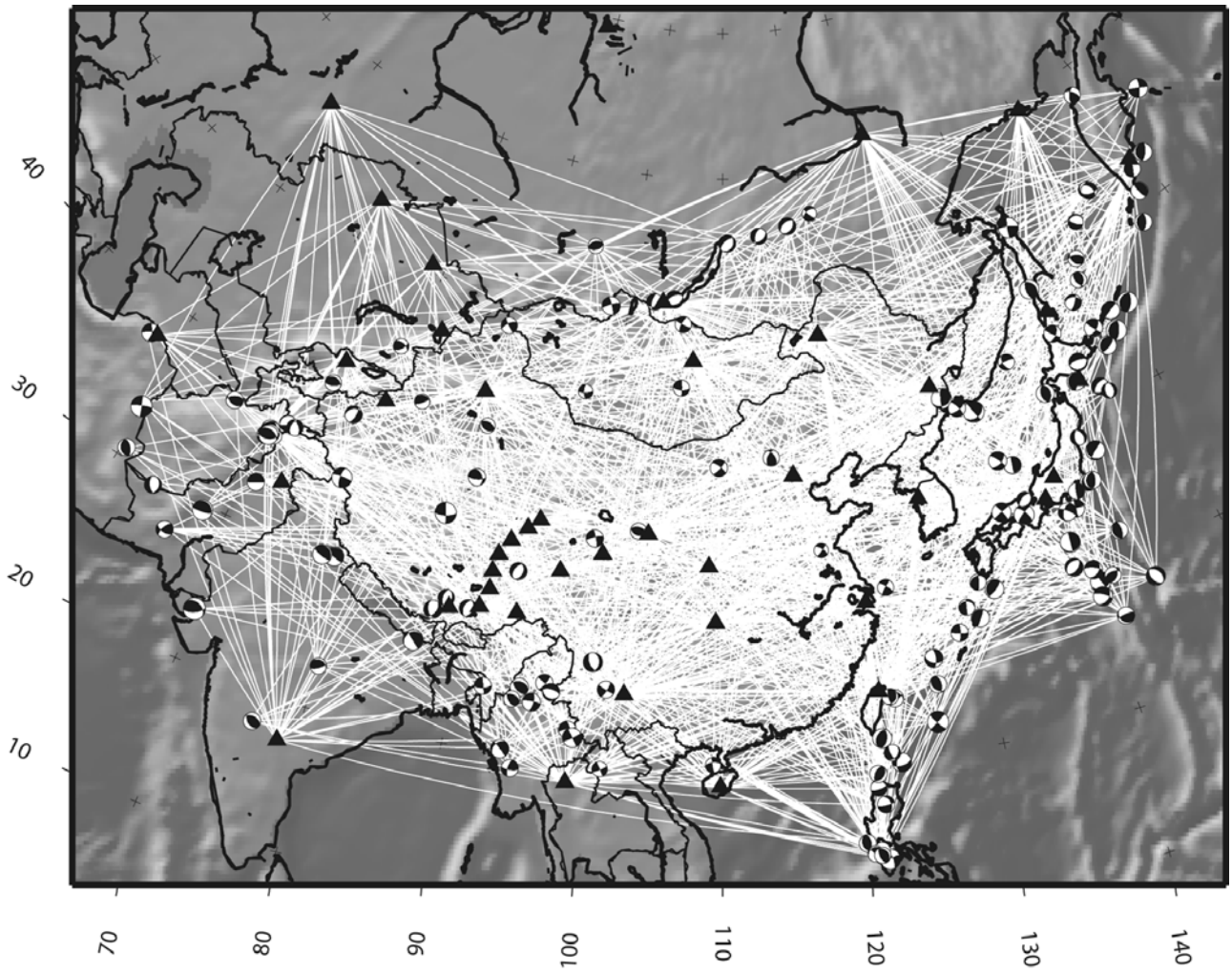

Figure 2: Station locations (black triangles), earthquake epicentres (beach balls) and all great-circle paths (white lines) for which a seismogram has been included into the data set.

Thus, basically tomographic models will never tell us how the Earth really looks like. And one might prematurely conclude that tomographic images are no good at all. Experience has proven the opposite. The model functions from the null-space mostly add detail to the tomographic models we are often not interested in. Hence, the common strategy is to search for large-scale features, which strongly influence the predicted data and explicitly suppress small-scale anomalies in the tomographic images. The resulting models fit very well into the framework of independent observations like surface geology, plate tectonics, earthquake locations and also make sense when put into dynamic calculations that predict convective motions in the Earth.

If one accepts this argument, it remains to find out what is large-scale and what is small-scale. This is called a resolution analysis. The answer depends on the data set and on the severity of the approximations in the physical theory by which we predict the data. Since often one single physical theory is available to researchers, most resolution analyses are carried out under the assumption that the theory is exact. This may lead to an overestimation of resolution. For example, ray theory ignores the fact that the travel time of seismic waves is influenced by the average structure within their first Fresnel zone and not just the structure on the ray path. A high density of crossing ray paths may suggest an unjustified sensitivity for small-scale structures. In reality, the travel times are fairly independent of the small-scale structure inside the first Fresnel zone. In other words the apparent null-space predicted by ray theory is smaller than the true null-space predicted by wave theory.

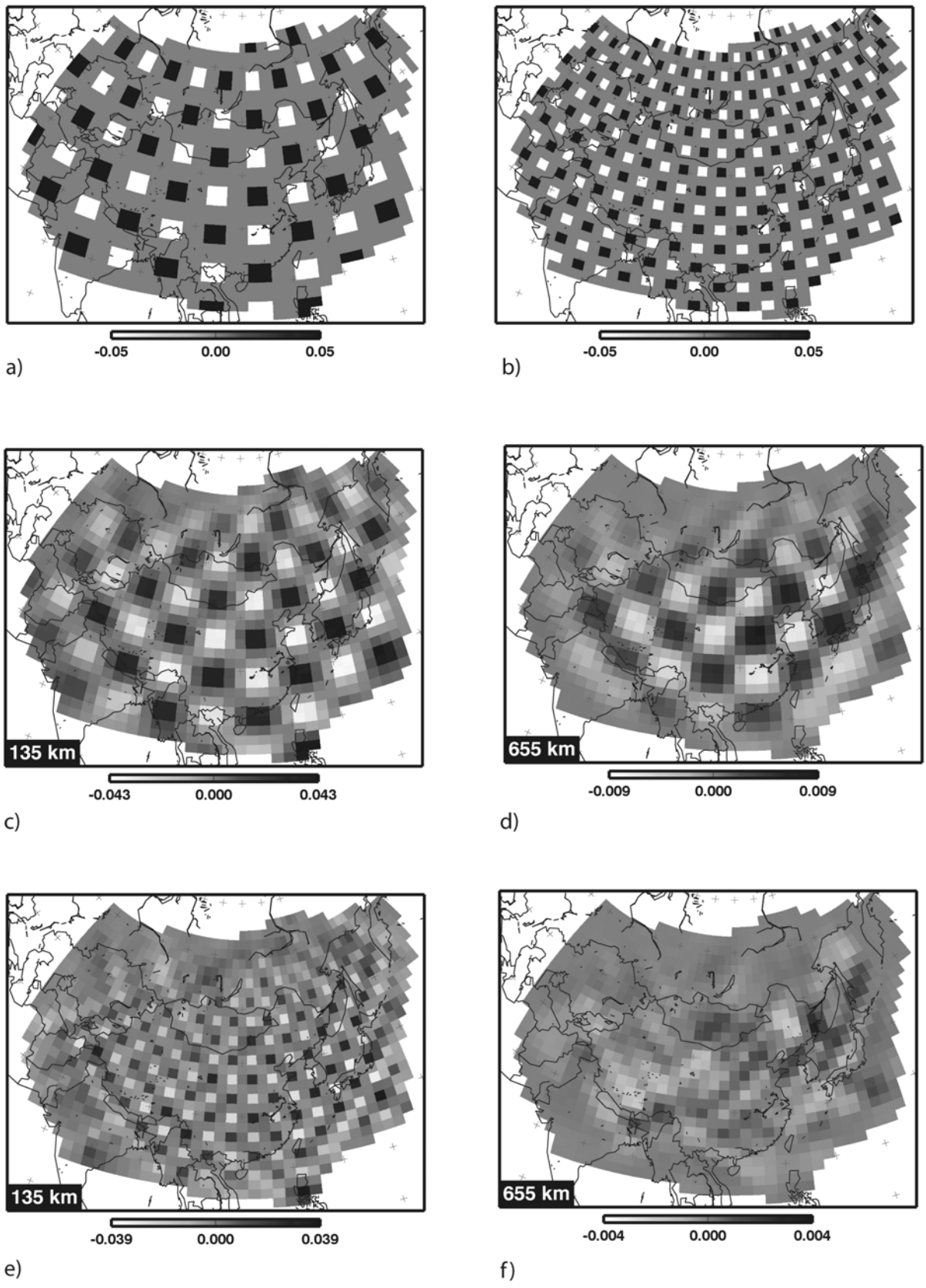

Figure 3: Resolution test with different test structures. Test structures are emplaced at two selected depths and the reconstructions are shown at the depths of emplacement. a) Test structure with blocks of 4º x 4º x 90 km; b) test structure with blocks of 2º x 2º x 90 km, reconstructions of a) at 135 km (c) and 655 km (d) depth; reconstructions of b) at 135 km (e) and 655 km (f) depth.

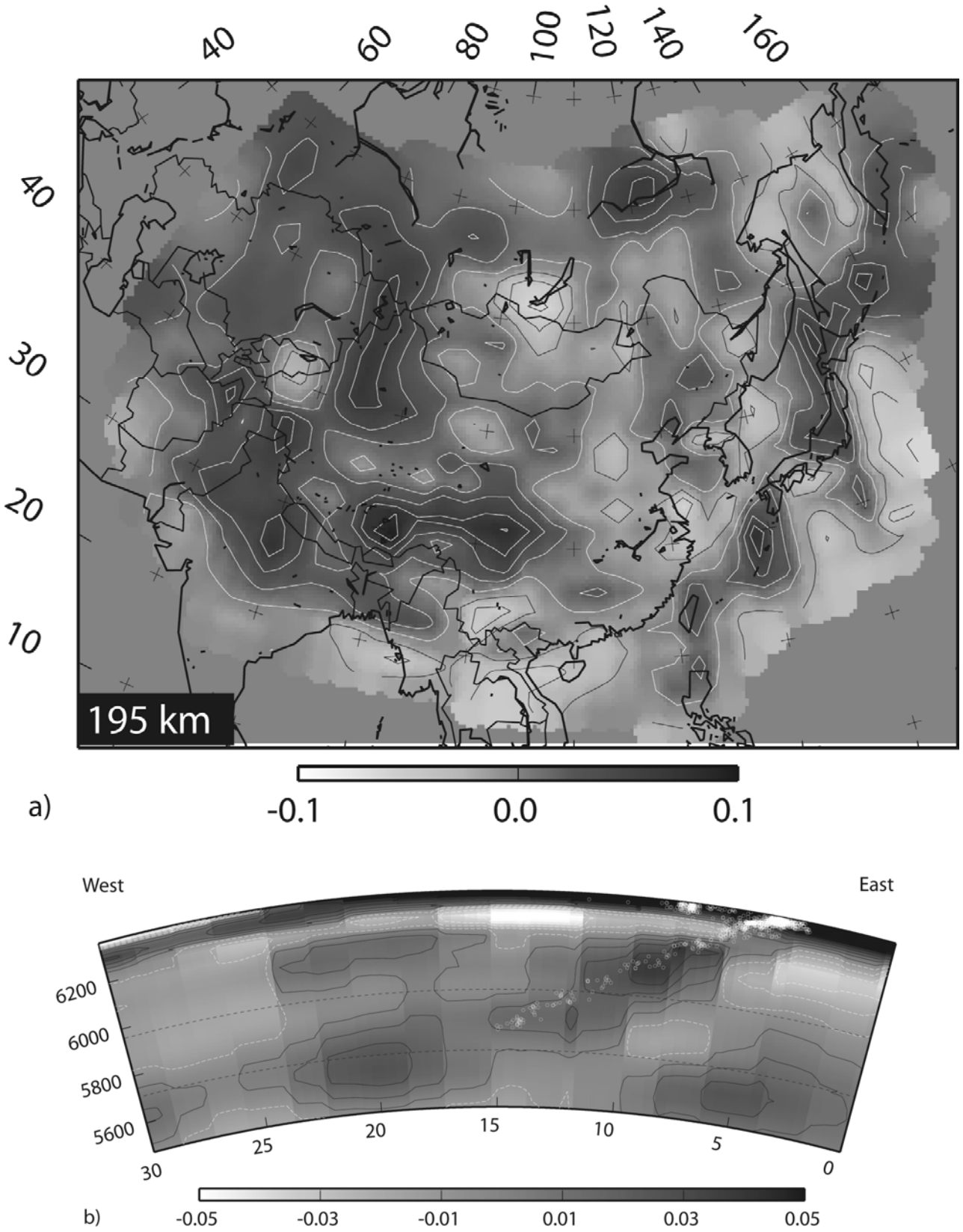

Figure 4: a) Horizontal cross section through 3D-mantle model at 195 km depth. Shown is fractional perturbation of S-velocity with respect to a 1D background model of East Asia.
b) Vertical section through the model along a great circle across the Japanese subduction zone from West to East. Small white circles indicate earthquake hypocenters. The dashed lines mark the 410 and 660 km discontinuities.

In praxis, the resolution of the data set is determined by computing a synthetic data set for test models of increasingly finer scale. The synthetic data set is inverted in exactly the same manner as the real data. The smallest structure that can be acceptably reconstructed indicates the resolution of the data set. To determine the resolution of the East Asia data set, I use block-shaped anomalies of alternating sign separated by areas with zero anomaly as shown in Fig. 3a, where block size is 4º x 4º x 90 km and Fig. 3b, where block size is 2º x 2º x 90 km. The test structures are emplaced at several depths and in Fig. 3c-f, I show horizontal sections through the reconstructed model at the depth of emplacement.

The East Asia data set can resolve structures of size 4º x 4º x 90 km throughout the mantle. At shallow depths, it can even resolve structures of smaller scale: blocks of size 2º x 2º x 90 km. In the core region of the study area, which is well covered with paths this small-scale structure is well reproduced. Thus horizontal resolution is about 200 km. Not so at 655 km depth where not much reminds of the test structure.

3D S-Velocity Model of the East Asian Upper Mantle

Here, I show some highlights of the 3D S-velocity model obtained from the data set using the waveform diffractography (Friederich, 2003). I plot fractional perturbation of S-velocity relative to an average 1D-model representative of whole East Asia.

The major features of the model can be seen in Fig. 4a: a narrow, linear high velocity feature which follows the Western Pacific subduction zones and agrees very well with earthquake hypocenters, still low velocities in the backarc regions (though the lowest velocities are attained at 80 km depth), a concentrated low velocity anomaly beneath the SW of the Baikal rift and high velocity Indian and Asian lithosphere under Tibet. Remarkably, the two lithospheres are separated by a narrow zone of average velocity and only join in the western corner of Tibet beneath the Karakorum.

Fig. 4b shows vertical cross sections across the Japan subduction zone. The slab is clearly visible as descending high velocity anomaly which correlates extremely well with hypocenter locations. Note the shallow, low-velocity backarc to the west. The slabs appear to stagnate at the bottom of the upper mantle and extend far to the west.

Conclusions

Waveform diffractography without resort to severe approximations in forward computation and inversion is feasible though the numerical effort is much greater than for ray theoretical or path-integral approaches. As a reward, high-resolution models of the upper mantle can be obtained from a relatively “small” number of long-period seismograms if path coverage is sufficient. Since wavefront healing is taken into account, the amplitudes of velocity perturbations are larger than in classical tomographic models although the model is naturally smoothed by the spatial extension of the sensitivity kernels. The models are detailed enough to be useful for tectonic and geodynamic interpretations.

References

Friederich, W., 1999. Propagation of seismic shear and surface waves in a laterally heterogeneous mantle by multiple forward scattering. Geophys. J. Int. **136**, 180-204.

Friederich, W., 2003. The S-velocity structure of the East Asian mantle from inversion of shear and surface waveforms, Geophys. J. Int. **153**, 88-102.

Marquering, H., F. A. Dahlen & G. Nolet, 1999. Three-dimensional sensitivity kernels for finite-frequency travel times: the banana-doughnut paradox, Geophys. J. Int. **137**, 805-815.

Nolet, G., 1990. Partitioned waveform inversion and two-dimensional structure under the network of autonomously recording seismographs. J. Geophys. Res. **95**, 8499-8512.

Wielandt, E., 1987. On the validity of the ray approximation for interpreting delay times. In: Nolet, G. (ed.). Seismic tomography with applications in global seismology and exploration geophysics. Reidel, Dordrecht, ISBN 90-277-2521-7, 85-98.

Woodhouse, J. H. & A. M. Dziewonski, 1984. Mapping the upper mantle: three-dimensional modelling of Earth structure by inversion of seismic waveforms, J. Geophys. Res. **89**, 5953-5986.

The Swabian Meteorite 2002/07/16 – Acoustic Point or Line Source?

Stefan Stange, Freiburg

Shortly before midnight on 2002/07/16 many people in Reutlingen (S of Stuttgart, Germany) were startled by a loud detonation or boom and heavily rattling windows. According to the European Macroseismic Scale this could be assigned an intensity of 4 (Fig. 1). The next day Sabine Lohr of the Schwäbisches Tagblatt compiled all available reports, ranging over 50 km to the South of Reutlingen (assigned intensities of 3 and less). Ground shaking was not percepted while there were a few eyewitness reports of sky illumination in spite of bad weather.

Inquiries at the weather survey and the air traffic control could exclude a thunderbolt or a supersonic plane as the source of the phenomenon. Läslo Evers with the Deelen Infrasound Array (DIA) performed a sound source localisation by analysing infrasound data from DIA and IS26 (Bavarian Forest) and taking a cross bearing (Fig. 1). At this time the event was already assumed to be a meteorite exploding in the atmosphere.

The event was also recorded at several seismograph stations of the State Earthquake Survey of Baden-Württemberg (LED), of the Swiss Seismological Service, and of the German Regional Seismic Network. In the seismograms one can distinguish ground coupled energy and an "air slap" (Fig. 2). Stations south of Lake Constance (*e.g.*, WIL and KAMOR) showed no signals above noise level.

Onset-time differences between stations more or less excluded an earthquake or an impact. A proper localisation with a constant-velocity model (v = 0.33 km/s) resulted in the epicentre marked in Fig. 1, which corresponds nicely with the infrasound solution.

The time tag of a light-curve, recorded in the Czech Republic by Pavel Spurny (Astronomical Observatory Ondrejov), could limit the trade off between height and source time. This is noteworthy since in seismology the source time of an event is nearly never known beforehand. A light-curve denotes sky illumination with a dominant sensitivity in the near infrared. In this case the intensity increase – lasting for about 2 seconds – was peaked by 4 distinct spikes (flares). This is unequivocally the signature of a fireball or bolide rushing through the atmosphere and blowing up.

Inspection of travel times (*c.f.*, Qamar, 1995) for a constant velocity model of the atmosphere exhibits that in the present case one cannot distinguish between a point explosion and a steeply descending supersonic source within reasonable confidence limits.

For a dynamic evaluation of the acoustic wave propagation a detailed velocity model of the atmosphere is needed. In the lower part of the atmosphere sound velocity is mainly controlled by the temperature which is measured up to an altitude of about 30 km by means of a radio balloon launched by the German Weather Survey (DWD) every 6 hours from Stuttgart and other locations. A sound-velocity model with a pronounced low-velocity channel in the tropopause was calculated from the data of the launch 3 hours before the occurrence of the meteorite. Temperatures up to 50 km were taken from ECMWF-data for grid point 47º N / 10.5º E.

The reflectivity method (Fuchs & Müller, 1971; Müller, 1985) was used to compute theoretical seismograms for the atmospheric model. The code – based on a program by Gerhard Müller – was not exactly suited for this kind of model but gave a very good idea about relative amplitudes. 80 small explosions ripple-fired from 50 km through 30 km height represented the meteorite on its supersonic flight. A flight path of 20° from vertical and a speed of 10 km/s were simulated.

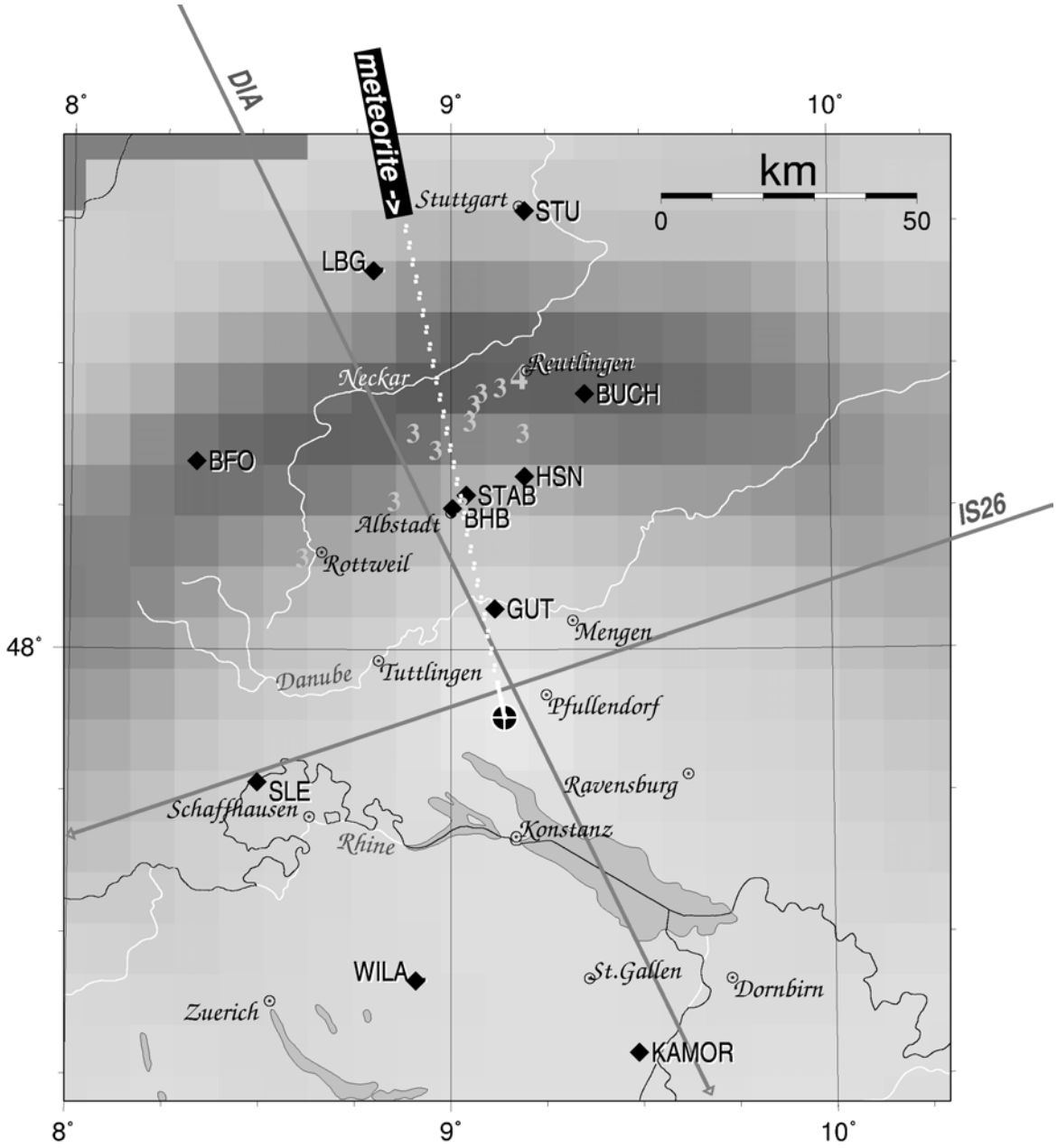

Figure 1: The area in SW-Germany where the acoustic event was observed (numbers represent EMS intensities) and recorded (diamonds are seismic stations). ⊕ is the seismological epicenter (supposed end of the supersonic flight through disintegration), which is close to the wind-corrected result of the infrasound cross-bearing. The gray shading denotes synthetic amplitudes of the sonic boom for a meteorite with the indicated flight path. Note that only the last 8 kilometers (horizontal) contribute to the sonic boom.

Fig. 1 shows the geographical distribution of synthetic maximum amplitudes around the epicentre of the end of the supersonic flight (the flight azimuth is 169º). The distribution compares nicely with the observations: the loudest boom was heard around Reutlingen, station GUT recorded only a tiny signal, and S of Lake Constance as well as N of Stuttgart there was nothing to be detected. An explosion would of course produce a point symmetric pattern of amplitudes.

Hence, it can be concluded that this simple model of a finite supersonic line source explains the observations quite well. Moreover, amplitude distribution requires that the meteorite came in from N or NNW.

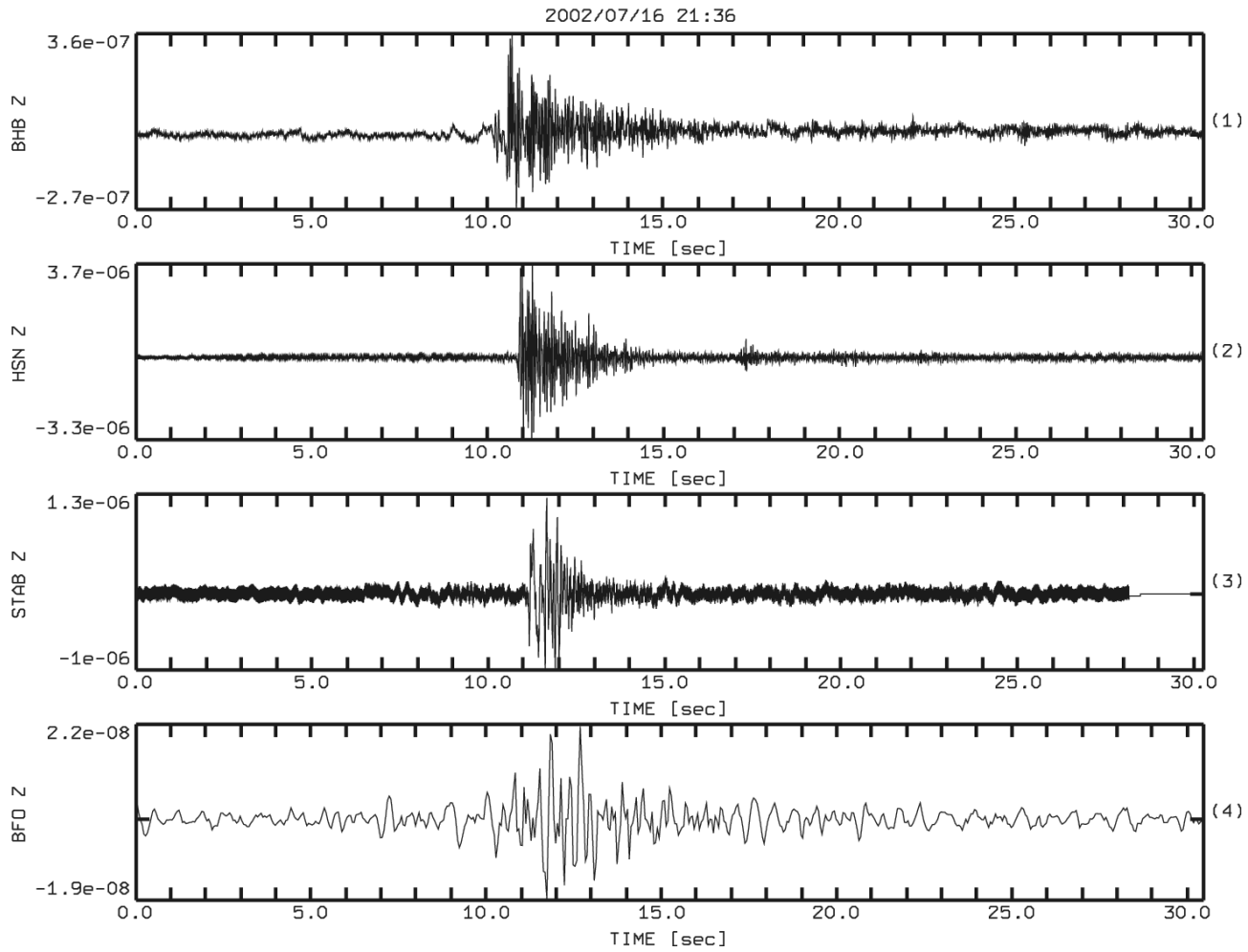

Figure 2: Selected seismograms of the meteoritic event over Baden-Württemberg; shown are vertical components of ground velocity.

The conclusion of this study is that a steeply descending supersonic fireball may well be mistaken for an earthquake or surface explosion at first sight. However, combined utilization of data from seismological and infrasound recordings as well as optical and acoustic observations reveals the true origin of the phenomenon. Modelling of acoustic seismograms from a supersonic moving source (a line source of 20 km length) in the atmosphere complements the sparse arrival-time data and fits the entire set of observations much better than a point source (explosion) can do.

Acknowledgement

Data and much advice were provided by L. Ceranna, N. Deichmann, L. Evers, B. Muehr, B. Naujokat, and P. Spurny. W. Brüstle read the manuscript and helped through many discussions. Thanks to them all.

References

Qamar, A.,1995. Space shuttle and meteoroid – tracking supersonic objects in the atmosphere with seismographs. Seism. Res. Lett. **66 (5)**, 6-12, 1995.

The complete poster is available under: http://www.lgrb.uni-freiburg.de/d/fach/led/led.htm

Dynamics of the Hammer Blow

Thomas Forbriger, Schiltach

Introduction

Shallow seismic record sections are not just the impulse-response of the subsurface. Filters in the recorder, the geophone response, also influence the waveforms and, in particular, the unknown force time-function of the hammer blow. By fitting a trial function to the data, I show that half a period of a sine-function of finite duration may serve well as force time-function in modeling recorded data by synthetic seismograms.

Modeling Shallow Seismic Record Sections

The data quality we can obtain with simple hammer blows in shallow seismics is often underestimated. Fig. 1 shows two field examples. The seismograms are recorded in an offset range of a few decameters and are displayed on a reduced time-scale. The large amplitude signal in the center of each plot is the dispersed Rayleigh wavetrain with multiple modes contributing to the signal. Clearly these waveforms contain valuable information about subsurface structure.

In recent years we learned how to deal with these multimode datasets (Forbriger, 2001) and how to infer subsurface properties by modeling the field data in the frequency and phase-slowness domain using the reflectivity method (Fuchs & Müller, 1971). The resulting models can be used to model full seismograms quantitatively, although no waveform modeling took place in the inversion.

Synthetic seismograms for both datasets are shown in Figs. 2a and 2b. They are calculated for the subsurface models obtained from the frequency and phase slowness wavefield-coefficients. In the plot they are compared to the recorded seismograms. The amplitudes are scaled by an offset-dependent factor. The synthetics fit the data already quite well. There are, however, still residuals. In particular in Fig. 2b (BERKHEIM) dissipation in the model is still too weak for high frequencies.

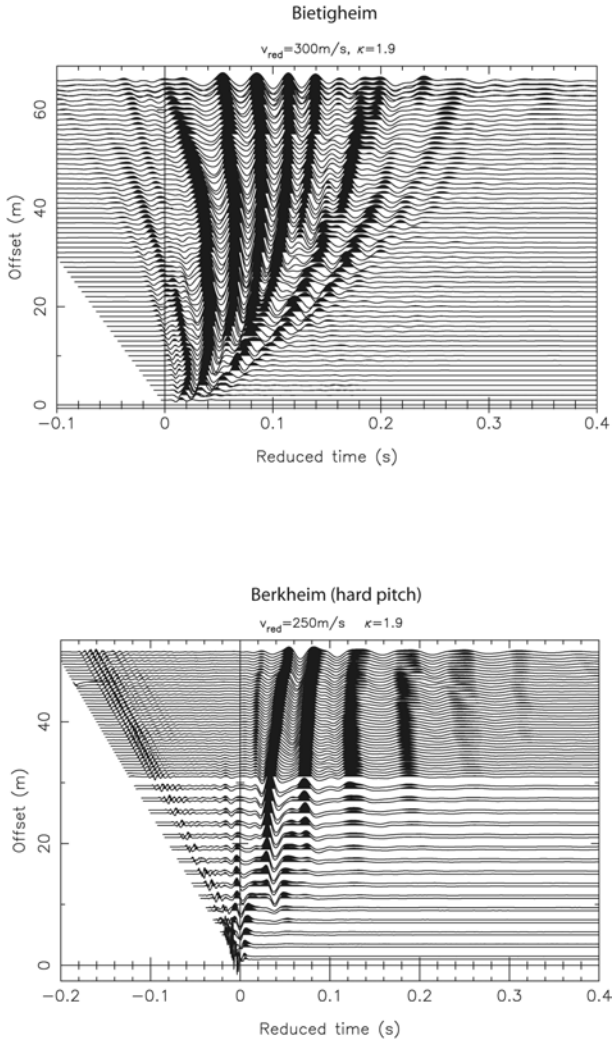

Figure 1: Two examples of shallow seismic field data. The seismograms are excited by a hammer blow and are recorded by vertical geophones. In both cases multiple modes are interfering in the Rayleigh wavetrain.

Preliminary results show, that we can obtain significant constraints on the *Q*-model by a subsequent inversion of full seismograms. The waveform fit is clearly improved at large offsets in Fig. 2c and the amplitudes at near offsets now almost equal the data.

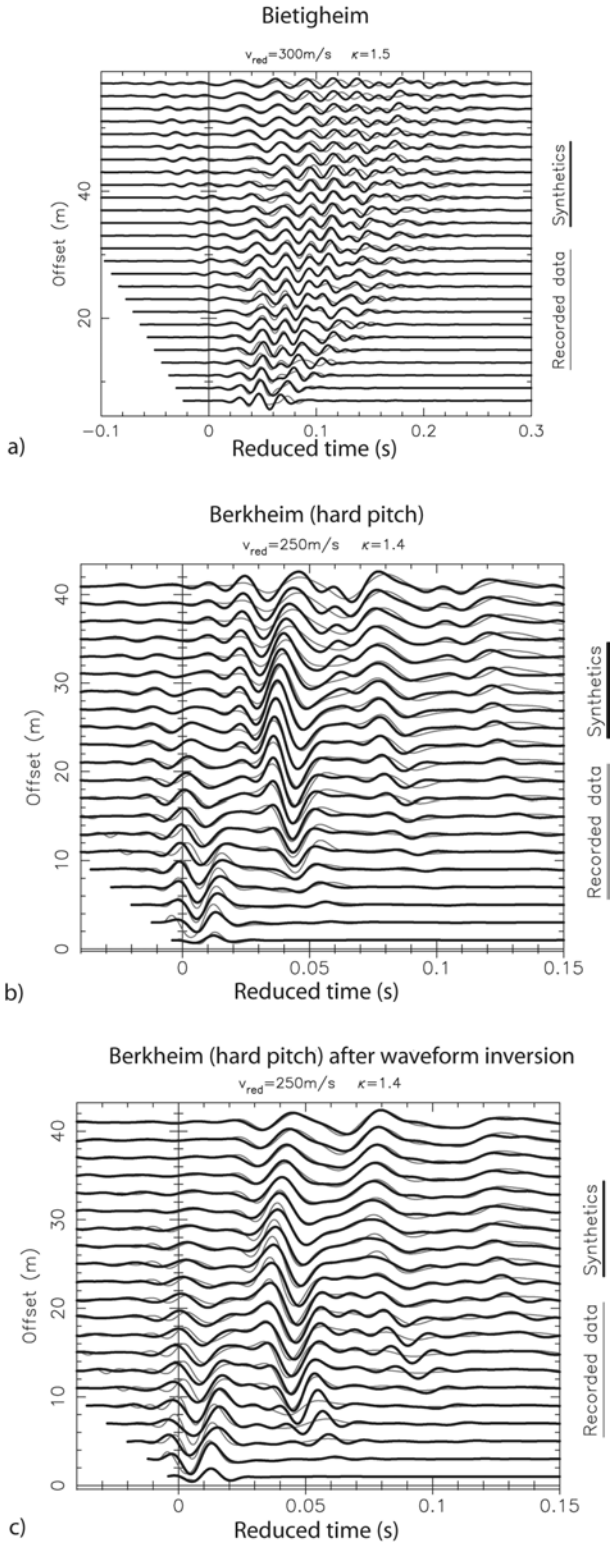

Figure 2: (a) and (b): Synthetic seismograms (thick lines) are compared with recorded waveforms (thin gray lines). Traces are scaled by an offset dependent factor. Absolute amplitudes are compared. The seismograms already fit quite well although no waveform fitting was involved in deriving the underlying subsurface models. In (b) dissipation is still too weak at high frequencies. (c) shows synthetics for an improved subsurface model obtained from subsequent waveform inversion.

Waveform inversion introduces extra complications. The recorded waveform is not only the impulse response of the subsurface but also contains the response of all field instruments. While the filters in the recording system and the geophone response are known, we do not know the force time-function of the hammer blow. The latter has a time constant within the recorded period range and strongly influences the waveform. Thus, we have to account for this in waveform inversion by using an appropriate source wavelet.

Our synthetic seismograms are the elastic response of the ground to an idealized point force. In the experiment, however, the hammer's target plate is of finite extent and the ground definitely undergoes plastic deformation below it. For the moment it is unclear whether our idealized model is physically appropriate to explain the observed excitation. But, since the same force time function of the source is contained in each seismogram, we can at least derive an optimal source wavelet to fit the data.

Source Wavelets

Figs. 3a and 3b (top panels) show the source wavelets that were used to calculate the synthetic seismograms in Figs. 2a and 2b, respectively. They are derived from the data by linear regression independently for each Fourier component (Forbriger, 2003). As they should, they are compact in time and shortly follow the hammer impact. These are properties we expect for reasonable estimates. Now, can we derive the true force time-function from them?

The wavelets still contain all filter responses of the recording system, in particular the geophone response to ground velocity rather than displacement. By deconvolution we can remove some of these effects and widen the bandwidth of the signal. But we cannot restore components at low frequencies that got lost due to the filters. In particular the DC-component will remain missing.

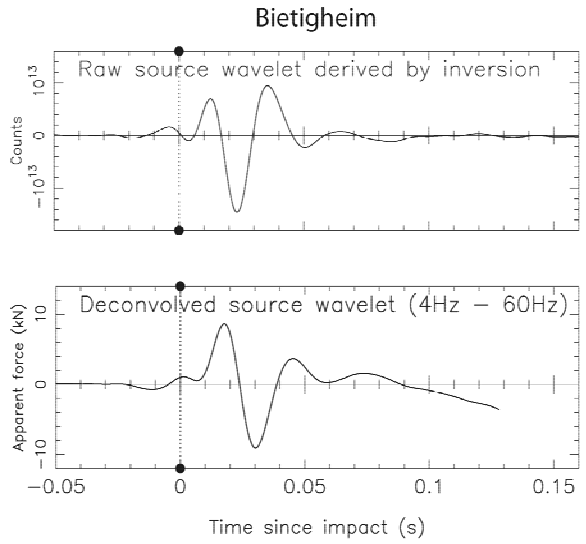

HP 4 Hz, 2 poles	geophones (after deconvolution)
HP 4 Hz, 2poles	data recorder
LP 60 Hz, 4 poles	signal processing
LP 250 Hz, 4 poles	data recorder (anti–aliasing)

a)

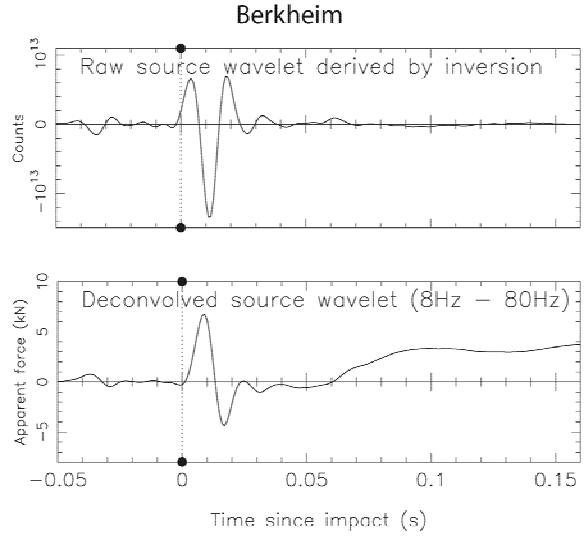

HP 4 Hz, 2 poles	geophones (after deconvolution)
HP 8 Hz, 2poles	data recorder
LP 80 Hz, 4 poles	signal processing
LP 500 Hz, 4 poles	data recorder (anti–aliasing)

b)

Figure 3: The top panels show source wavelets used for the synthetic seismograms for cases BIETIGHEIM (a) and BERKHEIM (b). The wavelets still contain the full geophone response and filters of the recording system. A deconvolved version of each wavelet is given in the bottom panels. The remaining filter responses are specified in the table beneath each graph. All have a Butterworth characteristic.

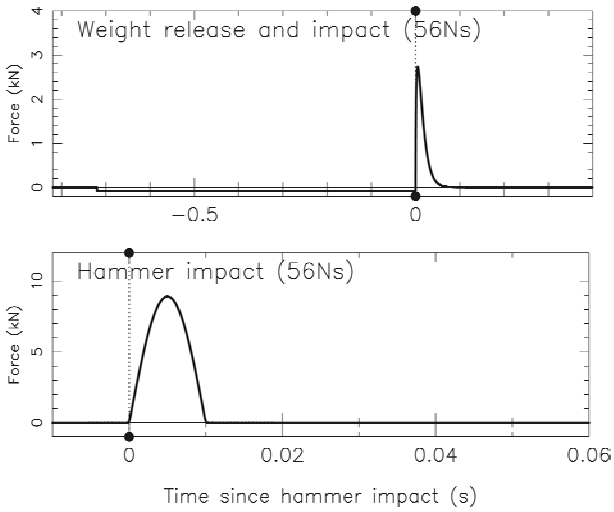

Figure 4: The top panel shows a hypothetical force time function containing a release phase during the acceleration of the hammer. The bottom panel gives the force exerted by an elastically reflected mass.

In the bottom panels of Figs. 3a and 3b the deconvolved wavelets are given already in units of apparent force. The tables beneath the graphs list the remaining filter effects. The signal is positive for a force directed downwards into the ground. The hammer impact only transfers momentum in one direction. We would therefore expect an entirely positive force function. The deconvolved wavelets are, however, definitely two-sided. The remaining high-pass filters remove the average of the input signal, but they have time constants of 125 ms and 250 ms respectively, much longer than the extent of the wavelets. Do these wavelets indicate an inappropriate physical concept for modeling the excitation of the observed wavefield? At this point, Gerhard gave the advice to answer this question in a scientific way, rather than discussing arbitrary philosophical arguments. He proposed to model the wavelets by a hypothetical force time-function.

In several studies he proved interest in source dynamics during his career. In Fig. 4 (top) I show a function that he once used to model seismograms excited by a world-wide recorded rock burst near Völkershausen (Müller, 1989) and which he proposed for modeling a landslide in the Veltlin (Baumann, 1991). This function could also resemble a shallow seismic hammer source. It contains a release phase during the acceleration of the hammer preceding the actual impact. It is

mean free because the hammer first collects exactly the momentum that it transfers to the ground during the impact. Thus the negative and the positive area cancel each other. But in the case of a hammer the release force is small in comparison to the short impact and a high-pass filter will leave only a small wiggle some hundred milliseconds prior to the main onset.

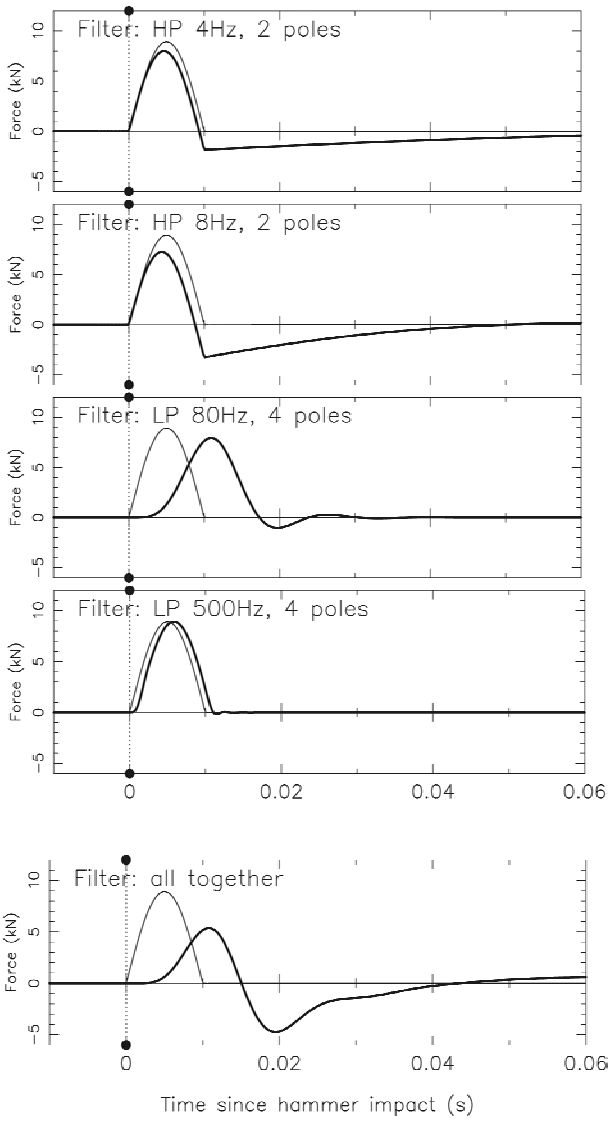

Figure 5: Filtered versions (thick lines) of the hypothetical force time-function (thin line). All filter stages together produce a two-sided wavelet from a purely positive trial function.

Therefore we do not expect to observe the release. We rather concentrate on the impact. The bottom curve in Fig. 4 is the force exerted by an elastically reflected mass. It is actually half a period of a sine function.

Now, how do the remaining filters distort this curve? None of the filter stages alone may explain the wavelet that we obtained from the data. But all of them together produce approximately the two-sided impulse we want to reproduce, as can be seen in Fig. 5.

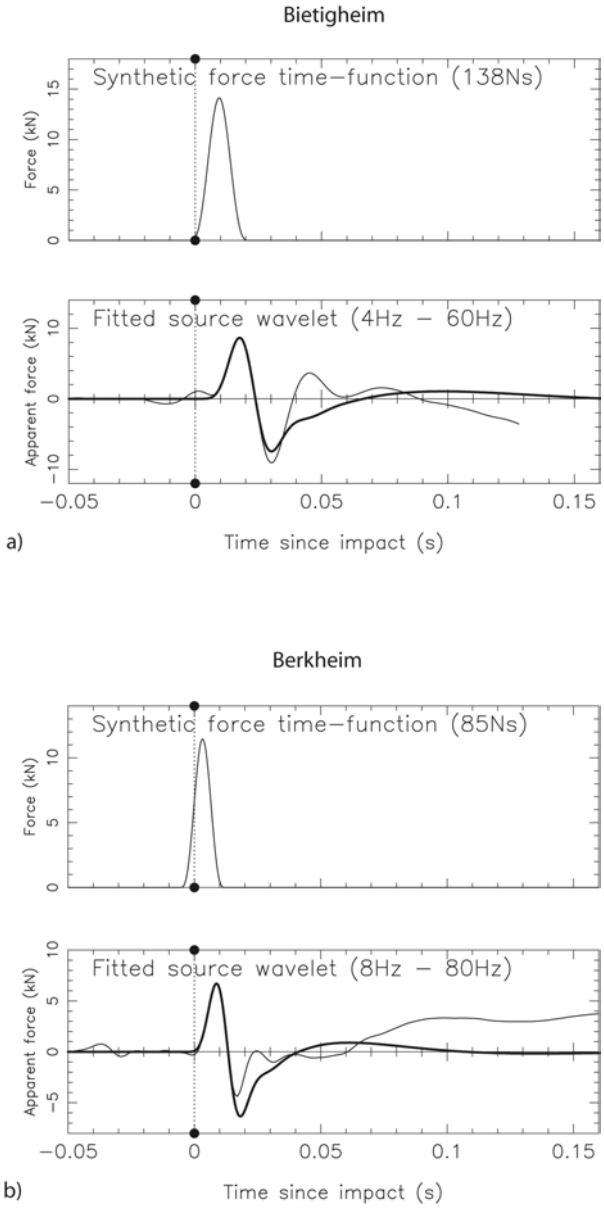

Figure 6: Fitting the source wavelets: The top panels show the trial functions that fit the source wavelets in the case of BIETIGHEIM (a) and BERKHEIM (b). The bottom panels show the fit to the deconvolved source wavelets (thin line) obtained for filtered versions of the trial function (thick line).

The Force Time-Function of a Hammer Blow

A filtered version of the trial function now can be used to fit the deconvolved wavelets obtained from the data. The trial functions and

the fit are shown in Figs. 6a and 6b for both datasets. The result is quite satisfactory.
Although the DC component is not present in the data, we can estimate it when assuming the half-period sine function for the exerted force. We then derive a transferred momentum of 85 Ns in the case of BERKHEIM and of 138 Ns in the case of BIETIGHEIM. Both are larger than 56 Ns, which is the momentum of an 8 kg weight being dropped from 2.5 m height. This is reasonable, because the hammer was accelerated manually in addition to gravity and in some cases was weakly reflected by the ground.
Similar results can be obtained from other datasets. However, a large scatter of the derived momentum for the same hammer blow (in the case of BERKHEIM from 84 Ns to 154 Ns) depending on the subsurface model and the actual fit criterion reminds us, that we should not put too much emphasis on these numbers. But from this study we have clearly learned, that a force time-function defined by three parameters only — which are amplitude, onset time, and duration — can be successful in waveform fitting. This will be a great aid in the task of inverting full shallow seismic seismograms.

Acknowledgements

I am deeply indebted to Gerhard Müller for all good advice and friendship he gave to me. The time I could share with him was too short.
I am grateful to Wolfgang Friederich who contributed remarkably efficient code for the calculation of partial derivatives of full seismograms. Without such code waveform inversion would not be feasible.
I thank Walter Zürn for helpful comments on the manuscript.
Further I thank Ingrid Hörnchen for touching up the figures and typesetting the manuscript with a Wordprocessor I'm too ignorant to use.

References

Baumann, M., 1991. Analyse seismischer Signale des Veltlin-Bergrutsches vom 28. 7. 1987. Diplomarbeit, Geophysikalisches Institut, Universität Karlsruhe.

Forbriger, T., 2001. Inversion flachseismischer Wellenfeldspektren. Dissertation, Universität Stuttgart, 237 pp. (URL: http://elib.uni-stuttgart.de/opus/volltexte/2001/861/).

Forbriger, T., 2003. Inversion of shallow-seismic wavefields. II. Inferring subsurface properties from wavefield transforms, Geophys. J. Int. 153, 735-752.

Müller, G., 1989. Herdvorgang des Gebirgsschlags bei Völkershausen vom 13. 3. 1989. In: Protokoll der Sitzung der Arbeitsgruppe Gräfenberg, 28. – 29. 4. 1989.

Structure and Dynamics of the Dead Sea Transform in the Middle East

Michael Weber, GFZ Potsdam
Zvi Ben-Avraham, Tel Aviv
Khalil Abu-Ayyash, Amman
Radwan El-Kelani, Nablus
Desert Group

Despite numerous efforts to study large transform systems, especially at the San Andreas Fault (SAF) system, the processes responsible for large continental-scale shear zones, one of the key elements of plate tectonics, and their relation and interaction with the crust and upper mantle are still not fully understood. The Dead Sea Transform (DST), at the border between Israel and Jordan, has for a long time been considered a prime site to examine large shear zones, but due to the political situation in this area no geoscientific profile has crossed the DST. Moreover, studies of historical earthquakes of the past few thousand years, paleoseismic studies and instrumental earthquake studies demonstrate that a number of damaging earthquakes have occurred along the DST. The DST therefore poses a considerable seismic hazard to Israel, Jordan, and the Palestine Authority.

Geophysical profiles crossing the DST, the boundary between the African and Arabian plates in the Middle East, and the border between Israel and Jordan, have been performed starting 2000 (Fig. 1). High-resolution seismic tomography and magnetotelluric sounding of the shallow crust show drastic lateral changes in material properties within a narrow zone around the DST. The seismic basement is offset by 3 – 5 km under the DST, and strong lower-crustal reflectors are imaged east of the DST. The seismic velocity sections show a steady increase in the depth of the crust-mantle transition (Moho) from the Mediterranean to the Jordan highlands, but only small topography of the Moho under the DST. These observations can be linked to the left-lateral movement of the two plates of 105 km in the last 17 Ma accompanied by strong deformation within a 20 – 30 km wide zone cutting through the entire crust. Sub-horizontal lower-crustal reflectors and deep reaching deformation zones occur in the DST (originating in a relatively homogeneous cold and stable lithosphere; slow relative plate motion of ca. 0.5 cm) and also in the San Andreas Fault system (originating in a strongly hetero-geneous, hot lithosphere; fast relative plate motion of ca. 3.5 cm). The fact that lower-crustal reflectors and deep deformation zones are observed in transform systems of such different origin could suggest that these structures are fundamental features of large transform plate boundaries.

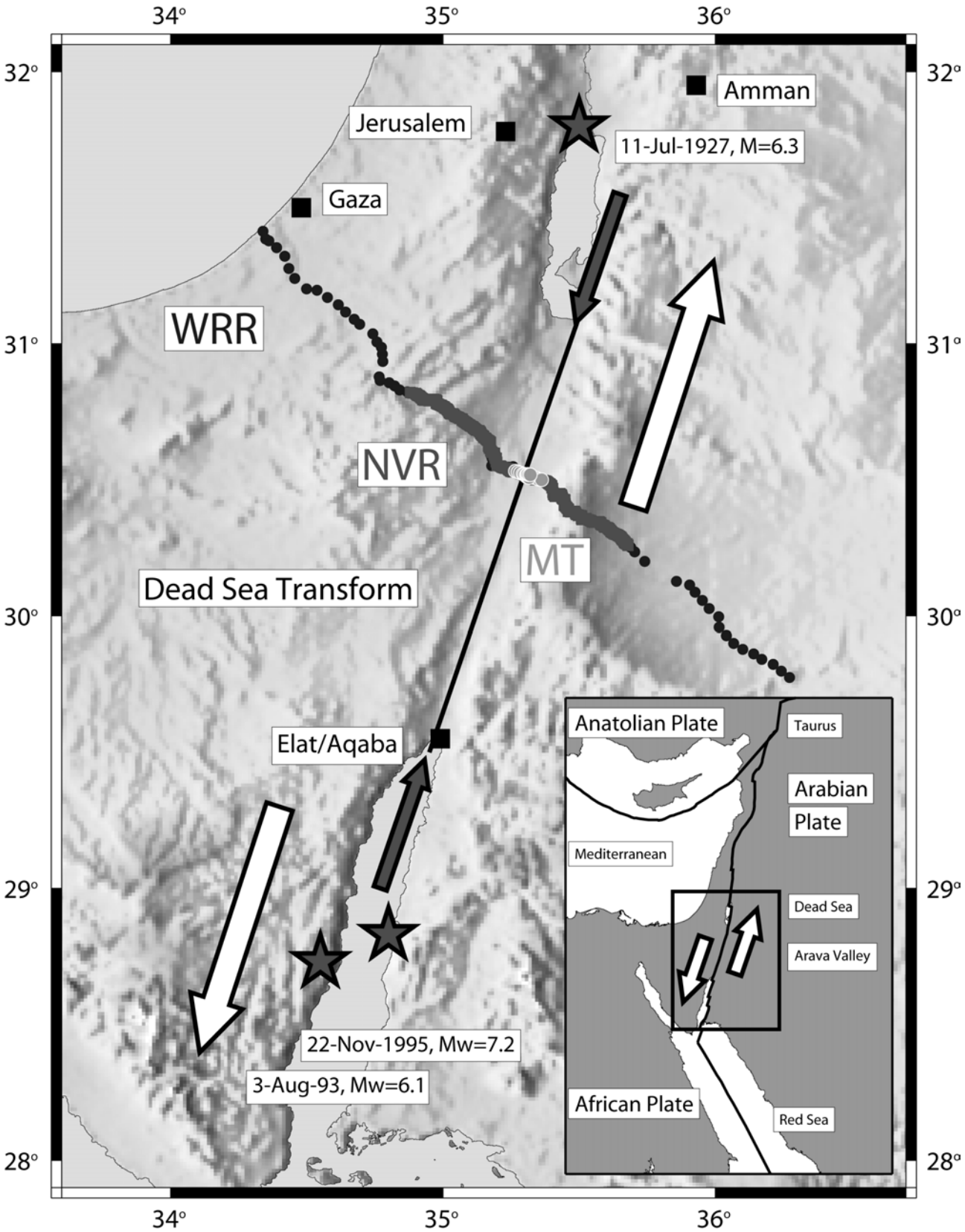

Figure 1: The wide-angle reflection / refraction profile (WRR, dark dots) crosses the Palestine Territories, Israel and Jordan. The near-vertical seismic reflection profile (NVR, gray dots) coincides with the inner 100 km of the WRR. The 10 km long magnetotelluric experiment (MT, white dots) is centered on the Arava Fault. A black line and two dark arrows indicate the Dead Sea Transform (DST) between the Dead Sea and the Red Sea. The white arrows indicate the left-lateral motion between the African and Arabian plates. Stars mark large earthquakes. (Inset) Tectonic setting of the DST.

Cooling Features in Icelandic Lavas and Gerhard Müller's Kitchen Experiments

Wolfgang Jacoby, Mainz

Abstract

The great variety of cooling features in Icelandic basalt includes the well-known columns and many less well-known interactions of lava with water. This note considers both.

(1) Preliminary observation-based statistics of column diameter d and lava body dimension D suggests $d \approx 0.1\ D^{1/2}$. This leads to the Müller constant $\chi \approx ¼$ in $d \approx D^{\chi}$; $0 < \chi << 1$ predicted by Müller (1998a) where d is controlled by the temperature gradient in a solidified cooling lava, in combination with the speed of the cooling front (characteristic time constant $\tau \approx D^2 / \kappa$).

(2) Lava flowing over wet ground generates steam that, if temporarily stored, can break through in steam eruptions leaving characteristic "chimneys" or holes (*e.g.*, the "Selfoss holes" and the "Dettifoss chimney") in the lava layer and to pseudocraters. Typical striae and tear cracks in the inner surfaces can be explained by shear and stress in the meanwhile plastic lava with small cohesion. This is demonstrated by a simple kitchen experiment with flour where the surface is straightened by moving a surface or edge *e.g.*, of a knife across it.

Introduction

Patterns are intriguing aesthetically and intellectually. They can reveal deeper laws of nature and connections between apparently remote phenomena. Cases in point are mud cracks, basalt columns and Gerhard Müller's kitchen experiments with starch. They motivated me to combine his deductions with my observations in Iceland. Beside columns, many other, most varied cooling features occur in basalt. A comprehensive review of Iceland's geology and volcanism is given by Sæmundsson (1979). This note presents (1) a combination of Müller's (1998a) theory with scaling of basalt columns and (2) "new" observations and a kitchen experiment to explain them by cooling with steam.

The origin of basalt columns has been discussed in the literature; of the references quoted by Müller (1998a) the most important are probably Lachenbruch (1962), Spry (1962), Peck & Minakami (1968), Grossenbacher & McDuffie (1995), but Müller (1998a) seems to be the most revealing work; however, he did not scale his theory to basalt columns quantitatively.

Basalt Columns

Laboratory experiments are inspiring and useful for checking ideas. They "give new insights and help to clarify scientific issues ... and ... they are of tutorial value." (Müller, 1998a, p. 15239). G. Müller did kitchen experiments with starch-water mixtures to model the generation of columns and he reinforced this with theoretical considerations. This induced me to re-collect many observations and photographs of columns in Icelandic lavas, to deduce a semi-quantitative relation between column diameter d and Lava body dimension D, and to exploit it to numerically constrain the constant χ in the d-D relationship; Müller (1998a, p. 15247, eq. 15, notation changed: D replaced by d, here, and z by D, here) suspected that determination from basalt columns could be difficult". Indeed, relating eq. 15 (in the present notation and with $z \cong D$):

$$d \sim (T/z)^{-\chi} \sim D^{\chi}\ ;\ 0 < \chi << 1, \qquad (1)$$

to basalt columns requires some "theoretical acrobatics" to be presented below. The above "Müller relationship" is, however, plausible as

thermal stress relaxation in space and time, after a crack has formed or advanced, depends on the temperature gradient and the distance of the crack tip to the hot and soft "interior"; the distance is short at the beginning of cooling and grows until the whole body is sufficiently "solid". After that the cracks will mainly "self-extend". This seems to happen in "jerks" indicated by the cross pattern of basalt column surfaces (Fig. 1)

Figure 1: Cross patterns on basalt columns.

To get some order into the relation between column diameter and lava dimension and, moreover, into the multitude of cooling phenomena in basalt lavas, it is useful to loosely classify them into flood basalts (exposed especially well in the eastern and western fjords), flows from volcanic shields (well exposed *e.g.*, in Ásbyrgi, northern Iceland, and Allmannagjá, southern Iceland) and flows in river beds or into water or ice and interacting with water (exposed well in gorges and at waterfalls). In addition, small bodies as dykes are considered.

Typical dimensions of lavas and columns are "observed", mostly in flood basalt, further in shield basalt, stock-like intrusions, dykes and pillows from all lava types. No real data set is collected by measurements; rather in this preliminary stage, only few examples have been measured or scaled from photographs and the scatter is guessed essentially from memory. Even "exact" measurements would be imprecise by about ±10 %, because of the irregular shapes, and the estimation procedure may add ±20 %, so that ±25 % uncertainty is plausible. The variability of dimensions of d and D, assumed to be ±30 % (or ± half order of magnitude) may be estimated with an uncertainty of ±50 %. Plotting the d-D pairs for the different lava types (Tab. 1) in double logarithmic scale (Fig. 2) derives a preliminary relation between d and D. Though only semi-quantitative, the present findings are worth reporting.

Table 1: Dimensions of basalt lava bodies and column diameter (orders of magnitude) in [m].

Lava Type	**Body Dimension D**	**Column Diameter d**	**Temperature Gradient [K/m]**
Basalt Floods	$10^{1\pm0.5}$	$10^{-0.5\pm0.5}$	$10^{2\pm0.5}$
River Basalts	$10^{1\pm0.5+}$	$10^{-0.5\pm0.5}$	$10^{2\pm0.5}$
Stocks*)	$10^{0\pm0.5}$	$10^{-1\pm0.3}$	$10^{3\pm0.5}$
Pillows	$10^{-0.2\pm0.2}$	$10^{-1.3\pm0.2}$	$10^{3.5\pm0.2}$
Dykes	$10^{-1\pm0.5+}$	$10^{-1.5\pm0.5}$	$10^{3.7\pm0.5}$

*) Intrusions into tuff (Hljóðarklettar), shield lavas.

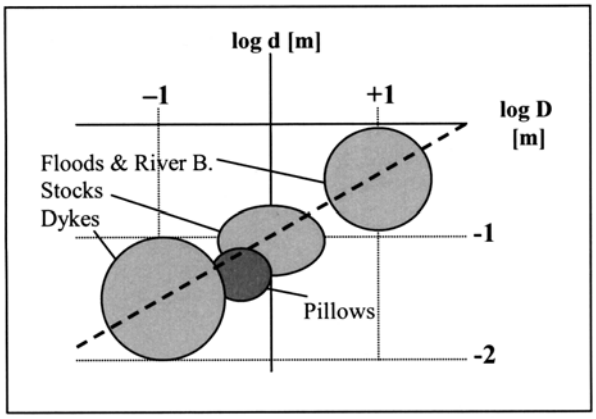

Figure 2: Double logarithmic plot of column diameter d (in m) vs. lava body dimension D, both estimated for classes of lavas as explained in text.

As shown in Fig. 2, an approximate linear relation in the log-log scale is suggested by the numbers of Tab. 1, expressed by

$$\log d \approx ½ \log D - 1 \qquad (2)$$

or

$$d \approx 0.1 \sqrt{D} \qquad (d \text{ and } D \text{ in [m]}) \qquad (3)$$

This approximate relationship has certainly only a limited range of applicability; I know of no jointed dykes thinner than in the order of 1 cm = 0.01 m (for which (2) and (3) give d = D). And there is probably an upper limit of perhaps 30 – 50 m. I suspect that the column dimensions tend toward some upper limit, which would imply a smaller slope in Fig. 2.
Müller disagrees (p. 15246) with the view of Grossenbacher & McDuffie (1995) that the "column diameter is controlled by the cooling rate $\partial T/\partial t$ at the crack front". But taking into account that the local temperature gradient and the instantaneous cooling rate or heat flux, $q \approx -\lambda (\partial T/\partial z)$, are linearly related, $d \sim (\partial T/\partial t)^{-\alpha}$, $0 < \alpha < 1$ is suggested, *i.e.*,

$$|\partial T/\partial t| \sim |\partial T/\partial z| \text{ , and } \alpha / \chi \approx 1. \qquad (4)$$

This allows us to relate the thermal relaxation time τ

$$\tau \approx D^2 / \kappa \text{ or } \tau \sim D^2 \qquad (5)$$

by one-dimensional conduction through a layer of thickness D to the speed of temperature change, and hence through the gradient to eq. (1) (or eq. 15 of Müller). From (5), $d \sim D^{1/2}$, and we get:

$$d \sim \tau^{1/4} \quad \text{and} \quad \alpha, \chi \approx 0.25 \qquad (6)$$

If, as suggested above, the slope in Fig. 2 is smaller than 1/2, $\chi < 0.25$ would be implied.
According to Müller, the initial cooling conditions are unimportant. The temperature gradient changes with time and determines the rate of cooling, which at first is fast and later very slow. This explains that often columns are thin near a lava surface and thicker in the interior. The highly variable initial temperature contrast ΔT and the boundary conditions (type of confinement laterally and vertically, cooling from above or from both sides; heat transfer conditions) plausibly explain the large scatter of the observations and limit the present treatment to this very gross analysis. Nevertheless, the Müller relationship can be combined with data from Iceland and a first determination of the value of the Müller constant has been attempted suggesting that $\chi \leq 0.25$.

Cooling of Lava Flows Passing Over wet Ground (Rivers)

In many cases heat transport by water plays a key role in cooling lava. The phenomena are most varied and range from pillows to steam vents and pseudo craters. Water percolates in columnar joints; its influence will not be discussed, except mentioning that it certainly widens the scatter in the diameter distribution and, moreover, adds many fascinating variations, especially in the "river basalts".
In this section first observations are reported of lava cooling features by steam, then a corresponding kitchen experiment will illustrate the suggested process. The observations are "steam holes" in lava surfaces and a vertical cross section of a "steam chimney". The kitchen experiment is extremely simple.
The "Selfoss holes" occur in a clean surface of a postglacial lava flow close to Ölfusá rapids

which when flooding had removed all loose material (Fig. 3) near the town of Selfoss, South Iceland. There seems to be no report in the literature although nearly every geologist, Icelandic or visitor, must have passed over them on the Ölfusá bridge, but few people stop to have a look.
More than 10 holes are well preserved. They have meter dimensions and in plan are circular to elliptical, sometimes two or three joined together. They are somewhat trumpet-shaped in section, opening up toward the lava surface, which is often marginally warped up. Their "inner" surfaces show striae and tear cracks.

Figure 3: "Selfoss holes"; openings of steam chimneys in lava flow near Selfoss; the rapids have cleaned away all loose material. Striae and tears are clearly displayed.

These features clearly identify the holes: they cannot be mill holes of the nearby rapids, but must have been generated, when the lava was still plastic, by shear flow of steam. Similar surface texture can also be seen in lava extrusions through solidified crust (example in Hekla lava). It can also be seen at the surface of kneaded dough and can be modelled even more simply by applying shear to low-cohesion material as powder, *e.g.*, flour: such a kitchen experiment is presented below.
First, some more field observations from other regions must be brought into the context in order to complete the picture of steam cooling. Best known are the accompanying so-called pseudocraters (*e.g.*, in Mýrdalssandur, South Iceland), which have long been interpreted as the result of steam eruptions from heated water under lava flows. They require that steam could collect beforehand in "bubbles" or reservoirs at the bottom of a lava reservoir. Such phenomena have been found in Iceland and the Faeroe Islands (near the village Kvivik).

Figure 4: Steam chimney near Dettifoss, North Iceland

Recently I discovered the entire phenomenon (reservoir, steam channels, chimney or vent) displayed fully in cross section in a lava cliff near Dettifoss, North Iceland (Fig. 4). Only floods of the river Jökulsá á Fjöllum had long removed the pseudocrater on top. The hole is not completely "empty", but filled by debris of welded coarse solid lava blocks. The "bubbles" where steam collected are domed-up open volumes, from where it escaped upward through narrow "meandering" channels. Where they merge, the trumpet shaped chimney develops; obviously it needed the combined force of enough steam to break through the solidifying lava layer.

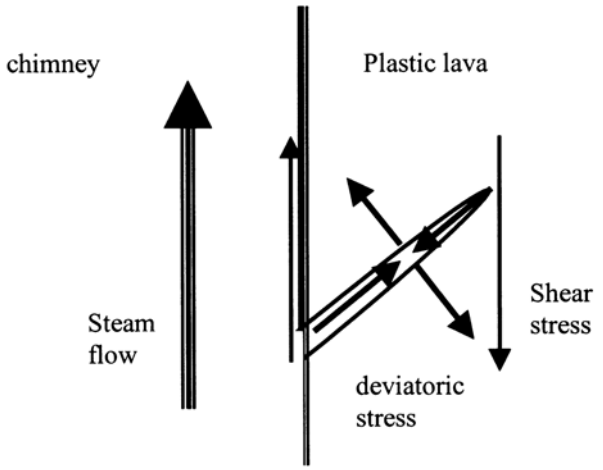

Figure 5: Shear flow along wall of plastic lava and stress field inside.

While in the Selfoss holes the crack orientation inside the lava is difficult to see, the Dettifoss chimney clearly exhibits them to

ascend into the lava, some 10 cm deep. The interpretation is sketched in Fig. 5. Steam flow and debris exert shear on the lava surface. It is transmitted into the still hot soft "plastic" lava. The deviatoric stress situation is as sketched: maximum tension and compression pointing ~45^{o} relative to the surface. Cracks form parallel to maximum compression, *i.e.*, they ascend into the lava away from the wall. This is exactly as observed.

In order to demonstrate this situation an extremely simple kitchen experiment is done with flour. It is nearly too simple to be presented here, certainly not comparable with Gerhard Müller's experiments. Everybody who kneads dough unintentionally can observe the effect, as dough behaviour is also "plastic". The essential material property is weak cohesion or small tensional strength.

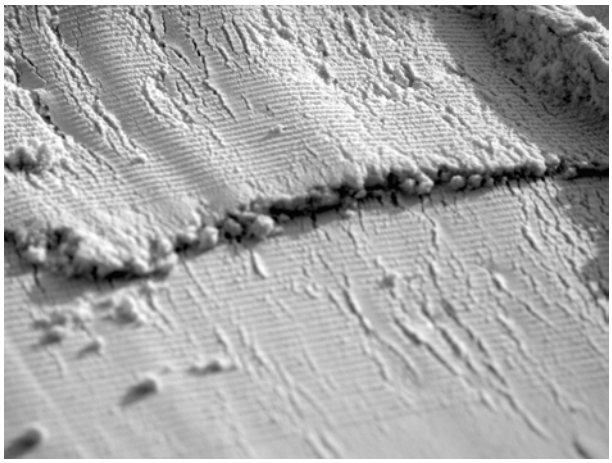

Figure 6: Surface of sheared flour.

Here is the recipe: take a flat dish or something like it and pour a pound of flour on it. Then move a knife over it to flatten the surface; it does not matter if you scrape the flour with the edge or if the blade glides over the surface. Nearly every time the flour surface shows, beside the striae, tears approximately perpendicular to them (Fig. 6). Close examination shows that the cracks always point "forward" into the flour as shown in Fig. 5, and that the crack edges show some "drag deformation. The experiment confirms that surface shear can generate the features observed in lava.

Returning to lava, note that the plastic, low-cohesion state lasts only some limited time during cooling. This places constraints on the timing of the chimney formation. It must be – accidentally? – compatible with the time it takes to heat the subjacent wet ground to boil enough water and generate sufficient steam overpressure in a reservoir where it can be stored in sufficiently large volumes below the lava flow (as seen at Dettifoss and also at Kvivik, Faeroe Islands). To hold back the steam, the lava must also have reached a plastic state with sufficient strength. Otherwise steam bubbles will move up and generate lava fountains (Fig.7).

Figure 7: Lava fountain from steam; lava is still hot and highly fluid.

No attempt is made here to quantify the various aspects of the process. Systematic variations of some parameters (cohesion or tensile strength, grain size, packing of powder or confining pressure, thickness of powder layer, shear stress) may lead to further insights.

Conclusion

Cooling by steam seems perhaps surprising as steam is mostly used for heating, but all that is relative. But many questions are left open. One is how cracks stop, *e.g.*, where their diameters should become wider. Similar circumstances exist near the surfaces of basalt flows from volcanic shields. Maybe these flow are frequently reheated by "the next hot flow" interrupting the cooling process. Lava cooling has many more facets, as lava towers, multi-floored structures and bizarre forms with and without columns. Iceland offers opportunities to a host of observations, which should be

studied systematically, but that is a task for the future.

The open human mind observes many apparently disconnected phenomena and relates them to each other: columns, pseudo craters, holes in lava, ... Gerhard Müller did this and opened new insights. They inspired the above considerations. Aesthetics also come into play (Fig. 7). The ultimate criterion for insight into nature may be the beauty of it, as great scientists have confessed.

Acknowledgements

I owe new insights to Gerhard Müller who posthumously inspired me to think about basalt cooling, put together my many photographs of Icelandic lava and to do a little kitchen experiment demonstrating a mechanism of a little known lava deformation.

References

Grossenbacher, K. A. & S. M. McDuffie, 1995. Conductive cooling of lava: columnar joint diameter and striae width as functions of cooling rate and gradient. J. Volcanol, Geotherm. Res. **69**, 95-103.

Lachenbruch A. H., 1962. Mechanics of thermal contraction cracks and ice-wedge polygons in permafrost. Geol. Soc. Am., Special Papers **70**, 69 pp.

Peck, D. L. & T. Minakami, 1968. The formation of columnar joints in the upper part of Kilauea lava lakes, Hawaii. Geol. Soc. Am. Bull. **79**, 1151-1166.

Sæmundsson K., 1979. Outline of the geology of Iceland. Jokull **29**, 7-28.

Spry, A., 1962. The origin of columnar jointing, particularly in basalt flows. J. Geol. Soc. Austr. **5**, 191-216.

Gerhard Müller – the Bibliography

1964

G. Müller, 1964. Elastische Kugelwellen und ihre Reflexion und Brechung an der ebenen Trennfläche zwischen zwei homogenen, isotropen Halbräumen. Dipl. Arbeit, Universität Mainz.

1966

Ehrisman, W., G. Müller, O. Rosenbach, & N. Sperlich, 1966. Topographic reduction of gravity measurements by the aid of digital computers. Boll. Geof. Teor. Appl. **8**, 3-20.

1967

Müller, G., 1967. Theoretische Seismogramme für Punktquellen in geschichteten Medien. Technische Hochschule Clausthal, Fakultät für Natur- und Geisteswissenschaften, Dissertation vom 3. Juli 1967, 136 pp.

Burkhardt, H., F. Keller, G. Müller, O. Rosenbach & R. Vees, 1967. Bemerkungen zur Einsatzmöglichkeit der Magnetband-Refraktionsapperaturen MARS 66 in großen Registrierentfernungen. Z. Geophys. **33**, 455-457.

1968

Müller, G., 1968a. Theoretical seismograms for some types of point-sources in layered media, Part I: Theory. Z. Geophys. **34**, 15-35.

Müller, G., 1968b. Theoretical seismograms for some types of point-sources in layered media, Part II: Numerical calculations. Z. Geophys. **34**, 147-162.

1969

Müller, G., 1969. Theoretical seismograms for some types of point-sources in layered media, Part III: Single force and dipole sources of arbitrary orientation. Z. Geophys. **35**, 347-371.

1970

Müller, G., 1970. Exact ray theory and its application to the reflection of elastic waves from vertically inhomogeneous media. Geophys. J. R. astr. Soc. **21**, 261-283.

1971

Müller, G., 1971a. Approximate treatment of elastic body waves in media with spherical symmetry. Geophys. J. R. astr. Soc. **23**, 435-449.

Müller, G., 1971b. Direct inversion of seismic observations. Z. Geophys. **37**, 225-235.

Müller, G. & D. Mayer-Rosa, 1971. Theoretical seismograms for models of the upper mantle in Europe. In: Proceedings of the XIIth General Assembly of the European Seismological Commission at Luxembourg, 64-70.

Fuchs, K. & G. Müller, 1971. Computation of synthetic seismograms with the reflectivity method and comparison with observations. Geophys. J. R. astr. Soc. **23**, 417-433.

1973

Müller, G., 1973a. Seismic moment and long-period radiation of underground nuclear explosions. Bull. Seism. Soc. Am. **63**, 847-857.
Also published on August 24, 1972 as IBM Research RC 4003 (#18023), 24 pp.

Müller, G., 1973b. Amplitude studies of core phases. J. Geophys. Res. **78**, 3469-3490. Also published on January 5, 1973 as IBM Research RC 4175 (#187222), 68 pp. For a correction see Müller, 1977d.

Müller, G., 1973c. Theoretical body wave seismograms for media with spherical symmetry – discussion and comparison of approximate methods. Z. Geophys. **39**, 229-246.

1974

Müller, G. & L. E. Alsop, 1974. Partial derivatives of travel times. Geophys. J. R. astr. Soc. **36**, 239-243.

1975

Müller,G., 1975a. Further evidence against discontinuities in the outer core. Phys. Earth Planet. Int. **10**, 70-73.

Müller, G., 1975b. Aufbau und Zustand des Erdkerns. Physikalische Blätter **31**, 246-256, 309-315.

Müller, G., 1975c. A simple model of the Earth's core. Akadademie der Wissenschaften der DDR, Veröffentlichungen des Zentralinstitutes Physik der Erde **31**, 311-321.

Kind, R. & G. Müller, 1975. Computations of SV waves in realistic Earth models. J. Geophys. **41**, 149-172.

1976

Müller, G. & K. Fuchs, 1976. Inversion of seismic records with the aid of synthetic seismograms. In: Giese, P., C. Prodehl, & A. Stein (editors): Explosion seismology in Central Europe, Springer Verlag, Berlin, ISBN 3-540-07764-2, 178-188.

Müller, G. & R. Kind, 1976. Observed and computed seismogram sections for the whole earth. Geophys. J. R. astr. Soc. **44**, 699-716.

1977

Müller, G., 1977a. Fault-plane solution of the earthquake in Northern Italy, 6 May 1976, and implications for the tectonics of the Eastern Alps. J. Geophys. **42**, 343-349.

Müller, G., 1977b. Earth-flattening approximation for body waves derived from geometric ray theory - improvements, corrections and range of applicability. J. Geophys. **42**, 429-436.

Müller, G., 1977c. Thermoelastic deformations of a half-space – a Green's function approach. J. Geophys. **43**, 761-769.

Müller, G., 1977d. Correction. J. Geophys. Res. **82**, 1541-1542.

Müller, G., A. H. Mula & S. Gregersen, 1977. Amplitudes of long-period PcP and the core-mantle boundary. Phys. Earth Planet. Int. **14**, 30-40.

Kind, R. & G. Müller, 1977. The structure of the outer core from SKS amplitudes and traveltimes. Bull. Seism. Soc. Am. **67**, 1541-1554.

1978

Müller, G., K.-P. Bonjer, H. Stöckl & D. Enescu, 1978. The Romanian earthquake of March 4, 1977: I. Rupture process inferred from fault-plane solution and multiple-event analysis. J. Geophys. **44**, 203-218.

Fertig, J. & G. Müller, 1978. Computation of synthetic seismograms for coal seams with the reflectivity method. Geoph. Prospecting **26**, 868-883.

Gebrande, H., H. Häge, H. Miller, G. Müller & E. Schmedes, 1978. Aftershock investigations and fault-plane solutions of the Friuli earthquakes 1976. In: Closs, H., D. H. Roeder & K. Schmidt (editors): Alps, Apennines, Hellenides, E. Schweizerbart'sche Verlagsbuchhandlung, Stuttgart, ISBN 3-510-65083-2, 173-177.

1979

Müller, G. & H. Häge, 1979. Comments on 'The gravitationally powered dynamo' by D. E. Loper. Geoph. J. R. astr. Soc. **58**, 509-514.

Müller, G. & S. Mueller, 1979. Traveltime and amplitude interpretation of crustal phases on the refraction profile Delta-W, Utah. Bull. Seism. Soc. Am. **69**, 1121-1132.

Fertig, J. & G. Müller, 1979. Approximate diffraction theory for transparent half-planes with application to seismic-wave diffraction at coal seams. J. Geophys. **46**, 349-367.

Häge, H. & G. Müller, 1979. Changes in dimensions, stresses and gravitational energy of the Earth due to crystallization at the inner-core boundary under isochemical conditions. Geoph. J. R. astr. Soc. **58**, 495-508.

1980

Choy, G. L., V. F. Cormier, R. Kind, G. Müller & P. G. Richards, 1980a. A comparison of synthetic seismograms for core phases generated by the full wave theory and by the reflectivity method. Geoph. J. R. astr. Soc. **61**, 21-39.

Choy, G. L., V. F. Cormier, R. Kind, G. Müller & P. G. Richards, 1980b. Corrigendum, Geoph. J. R. astr. Soc. **62**, 733-735, 1980.

Faber, S. & G. Müller, 1980. Sp phases from the transition zone between upper and lower mantle. Bull. Seism. Soc. Am. **70**, 487-508.

Mula, A.H. & G. Müller, 1980. Ray parameters of diffracted long period P and S waves and the velocities at the base of the mantle. Pure Appl. Geophys. **118**, 1272-1292.

1981

Müller, G & W. Schott, 1981. Some recent extensions of the reflectivity method. In: Husebye, E. S. & S. Mykkeltveit (editors) Identification of Seismic Sources – Earthquake or Underground Explosion, D. Reidel Publ. Comp., Dordrecht, ISBN 90-277-1320-0, 347-371.

Cerveny, V., K. Fuchs, G. Müller & J. Zahradnik, 1981. Theoretical seismograms for inhomogeneous elastic media. In: Petrashen, G. I. (editor) Special Volume Voprosy dinamicheskoy teorii rasprostraneniya seismicheskikh voln **20**, 84-109, (in Russian).

1982

Räkers, E. & G. Müller, 1982. The Romanian earthquake of March 4, 1977. III. Improved focal model and moment determination. J. Geophys. **50**, 143-150.

Temme, P., G. Müller, 1982. Numerical simulation to vertical seismic profiling. J. Geophys. **50**, 177-188.

1983

Müller, G., 1983. Rheological properties and velocity dispersion of a medium with power law dependence of Q on frequency. J. Geophys. **54**, 20-29.

Brüstle, W. & G. Müller, 1983. Moment and duration of shallow earthquakes from Love-wave modelling for regional distances. Phys. Earth. Planet. Int. **32**, 312-324.

Korn, M., G. Müller, 1983. Comparison of the Alekseev-Mikhailenko method and the reflectivity method. Geophys. J. R. astr. Soc. **73**, 541-556.

1984

Müller, G., 1984. Efficient calculation of Gaussian-beam seismograms for two-dimensional inhomogeneous media. Geophys. J. R. astr. Soc. **79**, 153-166.

Müller, G. & W. Zürn, 1984. Seismic waves and free oscillations. In: Fuchs, K. & H. Soffel (editors) Landolt-Börnstein – Zahlenwerte und Funktionen aus Naturwissenschaften und Technik, Neue Serie, Gruppe 5 Geophysik und Weltraumforschung, Bd. 2: Geophysik der festen Erde, des Mondes und der Planeten, Teilband a **(Bd. V/2a)**, Springer, Heidelberg, ISBN 3-540-12209-5, 61-83.

Faber, S. & G. Müller, 1984. Converted phases from the mantle transition zone observed at European stations. J. Geophys. **54**, 183-194.

1985

Müller, G., 1985. The reflectivity method: a tutorial. J. Geophys. **58**, 153-174.

Harjes, H.-P., M. Henger, G. Müller & H. Wilhelm, 1985. A system design for the gradual improvement of the seismic monitoring and verification capabilities for a Comprehensive Nuclear Test Ban. Conference on Disarmament, **CD/624**, 26 July 1985, 65 pp.

Schlittenhardt, J., J. Schweitzer & G. Müller, 1985. Evidence against a discontinuity at the top of D". Geophys. J. R. astr. Soc. **81**, 295-306.

1986

Müller, G., 1986a. Generalized Maxwell bodies and estimates of mantle viscosity. Geophys. J. R. astr. Soc. **87**, 1113-1141.

Müller, G., 1986b. Die seismologische Erforschung des Erdinnern. Jahresbericht des Physikalischen Vereins zu Frankfurt am Main 1984. 179-204.

Müller, G. & W. Brüstle, 1986. Untersuchung von Herdvorgängen mit Gräfenberg-Daten. In: DFG Deutsche Forschungsgemeinschaft: Zehn Jahre Gräfenberg-Array – Schrittmacher der Breitband Seismologie. Mitteilung XV der Senatskommission für Geowissenschaftliche Gemeinschaftsforschung, VCH-Verlagsgesellschaft, Weinheim, ISBN 3-527-27351-4, 73-79.

Publication in English: Müller, G. & W. Brüstle, 1986. Investigation of source processes with the Gäfenberg Array. In: B. Buttkus (editor): Ten years of the Gräfenberg Array – Defining the frontiers of broadband seismology. Geologisches Jahrbuch **E-35**, Hannover, ISSN 0341-6437, 60-64.

Müller, G., S. Faber & J. Schlittenhardt, 1986. Untersuchung konvertierter Phasen und der Reflexion PcP an der Kern-Mantel-Grenze. In: DFG Deutsche Forschungsgemeinschaft. Zehn Jahre Gräfenberg-Array – Schrittmacher der Breitband Seismologie. Mitteilung XV der Senatskommission für Geowissenschaftliche Gemeinschaftsforschung, VCH-Verlagsgesellschaft, Weinheim, ISBN 3-527-27351-4, 111-120.

Publication in English: Müller, G., S. Faber & J. Schlittenhardt, 1986. Investigation of converted phases and the reflection PcP at the core-mantle boundary. In: B. Buttkus (editor): Ten years of the Gräfenberg Array – Defining the frontiers of broadband seismology. Geologisches Jahrbuch **E-35**, Hannover, ISSN 0341-6437, 88-95.

Schmidt, Th. & G. Müller, 1986. Seismic signal velocity in absorbing media. J. Geophys. **60**, 199-203.

Schweitzer, J. & G. Müller, 1986. Anomalous difference traveltimes and amplitude ratios of SKS and SKKS from Tonga-Fiji events. Geophys. Res. Lett. **13**, 1529-1532.

Temme, P. & G. Müller, 1986. Fast plane-wave and single shot migration by Fourier transform. J. Geophys. **60**, 19-27.

1987

Müller, G., 1987. Geschwindigkeiten seismischer Wellen – Definition und Bedeutung. In: Proceedings, 7th Mintrop Seminar, Seismische Geschwindigkeiten, May 1987, 13-31.

Müller, G. & P. Temme, 1987. Fast frequency-wavenumber migration for depth-dependent velocity. Geophysics **52**, 1483-1491.

Brüstle, W. & G. Müller, 1987. Stopping phases in seismograms and the spatio-temporal extent of earthquakes. Bull. Seism. Soc. Am. **77**, 47-68.

Görich, U. & G. Müller, 1987. Apparent and intrinsic Q: the one-dimensional case. J. Geophys, **61**, 46-54.

1988

Müller, G., W. Zürn & K. Lindner, 1988. Ein gravimetrisches Experiment zur Suche nach Abweichungen vom Newton'schen Gravitationsgesetz. Mitteilungen der Deutschen Geophysikalischen Gesellschaft **1988 (2)**, 12-13.

1989

Müller, G., 1989. Ein Schwerkraftexperiment zur Suche nach der fünften Kraft. Forschung Frankfurt **1989 (4)**, 58-64.

Müller, G., W. Zürn, K. Lindner & N. Rösch, 1989. Determination of the gravitational constant by an experiment at a pumped-storage reservoir. Phys. Rev. Lett. **63**, 2621-2624.

Kampfmann, W. & G. Müller, 1989. PcP amplitude calculations for a core-mantle boundary with topography. Geophys. Res. Lett. **16**, 653-656.

Körnig, M. & G. Müller, 1989. Rheological models and interpretation of postglacial uplift. Geoph. J. Int. **98**, 243-253.

Schenk, Th. & G. Müller & W. Brüstle, 1989. Long-period precursors to pP from deep-focus earthquakes: the Moho underside reflection pMP. Geoph. J. Int. **98**, 317-327.

1990

Müller, G., W. Zürn, K. Lindner & N. Rösch, 1990. Search for non-Newtonian gravitation - a gravimetric experiment in a hydroelectric lake. Geoph. J. Int. **101**, 329-344.

1991

Fang, Y. & G. Müller, 1991. Seismic-wave attenuation operators for arbitrary Q. Geophys. J. Int. **106**, 703-707.

Zürn, W., D. Ollinger, E. Bäuerle & G. Müller, 1991. Eigenschwingungen eines künstlichen Stausees als Funktion der Stauhöhe. Mitteilungen der Deutschen Geophysikalischen Gesellschaft **1991 (4)**, 3-6.

1992

Müller, G., M. Roth & M. Korn, 1992. Seismic-wave traveltimes in random media. Geophys. J. Int. **110**, 29-41.

1993

Emmerich, H., J. Zwielich & G. Müller, 1993. Migration of synthetic seismograms for crustal structures with random heterogeneities. Geophys. J. Int. **113**, 225-238.

Roth, M., G. Müller & R. Snieder, 1993. Velocity shift in random media. Geoph. J. Int. **115**, 552-563.

1996

Witte, O., M. Roth & G. Müller, 1996. Ray tracing in random media. Geoph. J. Int. **124**, 159-169.

Fang, Y. & G. Müller, 1996. Attenuation operators and complex wave velocities for scattering in random media. Pure Appl. Geophys. **148**, 269-285.

1997

Müller, G., 1997. Trocknungsexperimente zur Simulation von Basaltsäulen. Mitteilungen der Deutschen Geophysikalischen Gesellschaft **1997 (4)**, 2-10.

Hock, S., Roth, M. & G. Müller, 1997. Long-period ray parameters of the core diffraction Pdiff and mantle heterogeneity. J. Geophys. Res. **102**, 17843-17856.

1998

Müller, G., 1998a. Starch columns: analog model for basalt columns. J. Geophys. Res. **103**, 15239-15253.

Müller, G., 1998b. Experimental simulation of basalt columns. J. Volcanol. Geotherm. Res. **86**, 93-96.

1999

Müller, G., 1999. Trocknungsrisse in Stärke. Phys. Blätter **55**, 35-37.

2000

Müller, G. & T. Dahm, 2000. Fracture morphology of tensile cracks and rupture velocity. J. Geophys. Res. **105**, 723-738.

2001

Müller, G., 2001a. Volume change of seismic sources from moment tensors. Bull. Seism. Soc. Am. **91**, 880-884.

Müller, G., 2001b: Experimental simulation of joint morphology. J. Struct. Geol. **23**, 45-49, 2001.

2002

Müller, G. & M. Zillmer, 2002. Reflexion seismischer Wellen an der FL-Verwerfung. Mitteilungen der Deutschen Geophysikalischen Gesellschaft **2002 (2)**, 13-19.

Zillmer, M., G. Müller & M. Stiller, 2002. Seismic reflections from the crystalline crust below the Continental Deep Drilling Site KTB – modeling and inference on reflector properties. J. Geophys. Res. **107 (B9)**, 2180, ESE 2, (DOI 10.1029/2001JB000843).

Lecture Notes

University Karlsruhe

Müller, G., 1971 – 1973. Theorie elastischer Wellen. Institut für Geophysik, Universität Karlsruhe, 213 pp.

Müller, G. early 1970s. Grundzüge der Geophysik. Universität Karlsruhe, 125 pp.

Müller, G., ~1975. Einführung in die angewandte Geophysik. Institut für Geophysik, Universität Karlsruhe, 94 pp.

Müller, G., 1978. Seismologie. Institut für Geophysik, Universität Karlsruhe, 188 pp.

University Frankfurt

Müller, G., 1980 – 1999. Digitale Signalverarbeitung. Institut für Meteorologie und Geophysik, Universität Franfurt, 182 pp.

Müller, G., 1981 – 1997. Inversionstheorie geophysikalischer Beobachtungen. Institut für Meteorologie und Geophysik, Universität Franfurt, 134 pp.

Müller, G., 1981 – 1994. Theorie elastischer Wellen. Institut für Meteorologie und Geophysik, Universität Franfurt, 238 pp.

Müller, G., 1982 – 1990. Grundlagen der mathematischen Geophysik (first title: Mathematische Grundlagen der Geophysik). Institut für Meteorologie und Geophysik, Universität Franfurt, 135 pp.

Müller, G., 1986 – 1997. Rekonstruktion von Strukturen aus Wellenfeldern (first title: Migration seismischer Wellenfelder), Institut für Meteorologie und Geophysik, Universität Franfurt, 150 pp.

Müller, G., 1994. Seismologie. Institut für Meteorologie und Geophysik, Universität Frankfurt, 197 pp. + Appendix A (18 pp.), B (4 pp), C (6 pp.) and D (35 pp), Appendixes A and D are by T. Dahm.

The lecture notes had been always under change and were constantly improved by Gerhard Müller over the years. The dates given here are the first and the last publication year of the lecture notes; page numbers are from the last issue.


ZOOM 40